

Copyright

by

James Patrick Sutton

2007

**Evaluating the Redundancy of Steel Bridges: Effect of a Bridge Haunch
on the Strength and Behavior of Shear Studs under Tensile Loading**

by

James Patrick Sutton, B.S.C.E.

Thesis

Presented to the Faculty of the Graduate School of

The University of Texas at Austin

in Partial Fulfillment

of the Requirements

for the Degree of

Master of Science in Engineering

The University of Texas at Austin

May 2007

**Evaluating the Redundancy of Steel Bridges: Effect of a Bridge Haunch
on the Strength and Behavior of Shear Studs under Tensile Loading**

**APPROVED BY
SUPERVISING COMMITTEE:**

Karl H. Frank

Eric B. Williamson

Dedication

To Mom and Dad for your endless love and support in everything that I do

To Molly for loving and supporting me throughout my time in Texas

To Erin, Patrick, and Mary Beth for making growing up in the Sutton house so much fun

Acknowledgements

First, I would like to thank Dr. Karl H. Frank for all of his help and guidance over the course of the two years that I have been at the University of Texas. I enjoyed learning from him and am very thankful to have had the opportunity to work with him on this project. Also, thanks to Dr. Eric B. Williamson for his help as the co-supervisor of this project and as the second reader of this thesis. Thanks to all the members of the faculty, who were always willing to offer advice and help.

I would like to acknowledge my research partners, Tim Barnard, Catherine Hovell, and Joshua Mouras. Particular thanks to Josh for the many hours that he spent helping me with the construction, instrumentation, and testing of my specimens. I would like to thank Omar Espinoza and Lewis Agnew as well for their help during the casting of my test specimens. I would also like to thank all of the other graduate students that worked at the lab over the past two years for always being around to help with homework or research problems and for being great friends.

I would like to thank Blake Stasney, Dennis Phillip and Greg Harris for all of their help while I worked at the lab. I would like to thank Eric Schell and Mike Wason for their help with the setup and trouble-shooting of the data acquisition system. Finally, I would like to thank Ella Schwartz and Barbara Howard for all their help with the ordering of materials and supplies.

Last, but certainly not least, thanks to the people at the Texas Department of Transportation for funding this project and for showing a genuine interest in the results of the research.

May 4, 2007

Abstract

Evaluating the Redundancy of Steel Bridges: Effect of a Bridge Haunch on the Strength and Behavior of Shear Studs under Tensile Loading

James Patrick Sutton, M.S.E.

The University of Texas at Austin, 2007

Supervisor: Karl H. Frank

AASHTO defines a fracture critical member (FCM) as a component in tension whose failure is expected to result in the collapse of the bridge. Bridges with FCMs must be inspected more frequently for this reason, which can lead to greater cost during the life of the bridge and a general reluctance to design new bridges with FCMs. However, evidence has shown that certain bridges with FCMs have redundant load paths and can withstand a fracture to an FCM.

There are many twin steel box girder bridges across the state of Texas, all of which are considered to be fracture critical because it is assumed that a fracture in one girder will initiate a total bridge collapse. In order to prevent collapse after the fracture of one box girder, the load that had been resisted by that girder must be transferred to the intact girder. The fractured girder will deflect so that the shear studs are loaded in tension and the deck slab is bending in double curvature. The shear studs and deck slab must both have the capacity to transfer the force over to the other girder.

The governing failure mode for the studs loaded in tension is a concrete breakout failure. This is a brittle failure in which the studs pull out with a large prism of concrete. When making these calculations, it was discovered that the bridge haunch may greatly reduce the concrete breakout strength of a single row of studs because it creates an edge effect. In order to determine the exact effect that the bridge haunch has on the tensile capacity of the shear studs, a series of laboratory tests were performed on bridge deck sections with and without a haunch.

The results of the laboratory tests showed that the bridge haunch greatly reduces the capacity of a row of studs grouped transversely across the top flange. More importantly the specimens with a haunch exhibited no ductility at failure, which may prevent redistribution of load during a fracture event. The specimens without a haunch did not suffer a reduction in strength when multiple studs were grouped across the flange width because there was no edge effect. In addition these specimens exhibited some ductility at failure because the studs extended into the bottom reinforcement mat, which forced the reinforcement bars to intersect the breakout failure plane.

The haunch is a necessary part of bridge construction, and despite the negative effects it has on the tensile behavior of the studs, it cannot be eliminated. With this in mind a series of techniques to improve the tensile behavior of the studs are recommended. These techniques include using haunch reinforcement bars, spacing studs longitudinally rather than grouping the studs transversely across the flange width, using longer studs, and developing a reduced diameter shear stud that will make yielding of the studs the governing failure mode. Yielding of the studs is the ideal failure mode because it would allow for the most redistribution of load during a fracture event.

Table of Contents

List of Tables	xii
List of Figures	xiii
CHAPTER 1	1
Introduction and Background	1
1.1 Fracture Critical Bridges.....	1
1.2 FSEL Fracture Critical Bridge Test	3
1.3 Analysis of Bridge Components	5
1.3.1 Introduction.....	5
1.3.2 Load Path	5
1.3.3 Analysis of Shear Studs	7
1.3.4 Analysis of Deck Slab.....	7
1.3.5 Analysis of Composite Section.....	10
1.3.6 Summary	11
CHAPTER 2	12
Strength of Concrete Anchors under Tensile Loading	12
2.1 Introduction.....	12
2.2 Tensile Strength of Concrete Anchors.....	12
2.2.1 Overview: ACI 318 Appendix D – Anchoring to Concrete	12
2.2.2 Steel Strength.....	14
2.2.3 Concrete Breakout Strength.....	14
2.2.4 Pullout Strength	20
2.2.5 Concrete Side-Face Blowout Strength.....	20
2.3 Capacity of a Row of Studs on the FSEL Test Bridge	21
2.4 Summary	25

CHAPTER 3	26
Testing Program.....	26
3.1 Introduction.....	26
3.2 Test Specimens	27
3.2.1 Specimen Details	27
3.2.2 Stud Welding	33
3.2.3 Formwork.....	33
3.2.4 Concrete Mix	34
3.3 Test Setup.....	35
3.4 Instrumentation	36
3.4.1 Shear Studs.....	36
3.4.2 Reinforcing Steel	37
3.4.3 Load and Displacement.....	39
3.5 Testing Procedure	40
CHAPTER 4	42
Test Results.....	42
4.1 General Comments.....	42
4.2 Capacity	43
4.3 Behavior at Failure.....	44
4.3.1 Specimens with a Haunch	44
4.3.2 Specimens with No Haunch.....	47
4.4 Stud Gage Data	49
4.4.1 Analysis of Data.....	49
4.4.2 Specimens with a Haunch.....	50
4.4.3 Specimens with No Haunch.....	53
4.5 Reinforcing Steel Gage Data	56
4.5.1 Concrete Slab – Cracking, Yielding, and Ultimate Loads.....	56
4.5.2 Specimens with a Haunch.....	60
4.5.3 Specimens with No Haunch.....	63
4.6 Slab Deflection.....	66

4.7 Concrete Cylinder Tests.....	68
CHAPTER 5	69
Analysis and Discussion of Test Results	69
5.1 Predicted Capacities versus Test Results.....	69
5.2 Evaluation of Current Shear Connector Detail	77
5.2.1 Introduction.....	77
5.2.2 Capacity	77
5.2.3 Ductility	77
5.2.4 Efficiency.....	79
5.2.5 Summary	80
5.3 Possible Techniques to Improve Shear Connector Detail.....	81
5.3.1 General Comments.....	81
5.3.2 Haunch Reinforcement	81
5.3.3 Longitudinal Spacing of Studs.....	83
5.3.4 Longer Studs	85
5.3.5 Combination of Longer Studs and Longitudinal Spacing.....	87
5.3.6 Reduction of Stud Diameter.....	89
5.3.7 Summary	93
CHAPTER 6	94
Conclusions and Recommendations	94
6.1 Summary of Objectives.....	94
6.2 Conclusions.....	94
6.3 Recommendations and Future Work	97

APPENDIX A	99
Analysis of Bridge Components	99
APPENDIX B	109
FSEL Bridge Deck Details and TxDOT Stud Detail	109
APPENDIX C	113
Complete Test Specimen Details	113
APPENDIX D	119
Test Specimens – Cracking, Yield and Ultimate Load.....	119
APPENDIX E	124
Predicted Tensile Capacity of Test Specimens.....	124
APPENDIX F	131
Mill Test Report for Studs used in Test Specimens.....	131
REFERENCES	132
VITA	133

List of Tables

Table 2.1: Estimated tensile capacities for a single stud and a row of three studs on the FSEL test bridge ($f_c' = 4,000$ psi; 7/8-in. diameter x 5-in. long studs; $f_{uta} = 60,000$ psi).....	24
Table 3.1: Specimen identification and details	30
Table 4.1: Testing order	42
Table 4.2: Maximum load resisted by each specimen	43
Table 4.3: Stud gage data at maximum load for specimens with a 3-in. haunch...50	
Table 4.4: Stud gage data at maximum load for specimens with no haunch.....54	
Table 4.5: Concrete cylinder compression tests	68
Table 5.1: Calculation of predicted capacities ($f_c' = 6,000$ psi).....	72
Table 5.2: Experimental results versus nominal capacity from ACI design equations	73
Table 5.3: Percent difference assuming no cracking in specimens with a 3-in. haunch	74
Table 5.4: Cross-over point for a single 7/8-in. diameter stud with no edge or group effects in various concrete compressive strengths	89

List of Figures

Figure 1.1: Collapse of Silver Bridge (Connor, Dexter, and Mahmoud, 2005)	1
Figure 1.2: Full-depth fracture of the I-79 two girder bridge at Neville Island in Pittsburgh, PA (Connor, Dexter, and Mahmoud, 2005)	2
Figure 1.3: Cross-section of FSEL test bridge.....	4
Figure 1.4: Assumed deflected shape at point of girder fracture.....	6
Figure 1.5: Bending moment in deck slab at ultimate state.....	8
Figure 1.6: Composite section of non-fractured girder.....	10
Figure 2.1: FSEL test bridge shear stud – 7/8-in. diameter x 5-in. long.....	13
Figure 2.2: Failure modes for anchors loaded in tension (ACI 318-05).....	13
Figure 2.3: Tensile breakout shape as idealized by: (a) CCD method (b) 45° cone method (Shirvani, Klingner, and Graves III, 2004).....	15
Figure 2.4: Multiple studs behaving as a group – (a) projected failure area (b) section through failure prism; multiple studs behaving independently – (c) projected failure areas (d) section through failure prisms	18
Figure 2.5: Edge reduction ($c < 1.5h_{ef}$) – (a) section through failure prism (b) projected failure area.....	19
Figure 2.6: Shear stud detail for FSEL test bridge.....	22
Figure 2.7: Concrete breakout prism following 35° angle.....	23
Figure 3.1: Bridge slab in double curvature.....	27
Figure 3.2: Transverse and longitudinal directions of test specimens	28
Figure 3.3: Details for specimens with no haunch.....	31
Figure 3.4: Details for specimens with 3-in. haunch	32
Figure 3.5: (a) Stud welding; (b) bend over test	33

Figure 3.6: Formwork for specimens with (a) no haunch (b) 3-in. haunch	34
Figure 3.7: Test setup.....	35
Figure 3.8: (a) Stud gage installation.....	36
Figure 3.8 (cont.): (b) shear stud after gage installation; (c) drawing of typical stud gage placement.....	37
Figure 3.9: Instrumentation of reinforcing steel	38
Figure 3.10: Labeling of gages on steel reinforcing bars.....	38
Figure 3.11: Attachment of load cell	39
Figure 3.12: Linear potentiometer measuring separation between the slab and WT.	40
Figure 3.13: Test setup, hydraulic setup and data acquisition system.....	41
Figure 4.1: Specimen 3-1b – Applied load versus stud pullout deflection.....	45
Figure 4.2: Initial cracking in specimen with a 3-in. haunch.....	46
Figure 4.3: Specimens with a 3-in. haunch – (a) Center crack at failure; (b) horizontal cracking across top of haunch; (c) complete separation of haunch ..	47
Figure 4.4: Specimen 0-3b – Applied load versus stud pullout deflection.....	48
Figure 4.5: Specimens with no haunch – (a) Increased flexural cracking; (b) breakout prism cracking as seen from underside of specimen; (c) formation of breakout prism	49
Figure 4.6: Tensile resistance provided by shear stud	51
Figure 4.7: Specimen 3-2b – Applied load versus calculated force in the shear studs	52
Figure 4.8: Specimen 3-3b – Applied load versus calculated force in the shear studs	53

Figure 4.9: Applied load versus calculated force in the shear studs – (a) Specimen 0-3a; (b) Specimen 0-3b.....	55
Figure 4.10: Assumed location of neutral axis at yield of bottom reinforcement	58
Figure 4.11: Strain and stress profiles at point of yield	59
Figure 4.12: Strain and stress profile at ultimate	60
Figure 4.13: Specimen 3-2b – Reinforcing steel load versus strain at the (a) mid-span location (b) quarter-span location	62
Figure 4.14: Specimen 0-2a – Mid-span reinforcing steel load versus strain.....	64
Figure 4.15: Specimen 0-3a – Mid-span reinforcing steel load versus strain.....	65
Figure 4.16: Specimen 0-3a – Quarter-span reinforcing steel load versus strain ..	66
Figure 4.17: Specimen 3-3a – Typical load versus top of slab deflection plot.....	67
Figure 5.1: Assumed projected concrete failure area of studs for specimens with a 3-in. haunch and (a) one stud, (b) two studs, and (c) three studs.....	71
Figure 5.2: Assumed projected concrete failure area of studs for specimens with no haunch and (a) one stud, (b) two studs, and (c) three studs.....	72
Figure 5.3: Specimen with 3-in. haunch – no flexural cracking in haunch	74
Figure 5.4: Deck transverse direction – (a) assumed breakout failure; (b) actual breakout failure	75
Figure 5.5: Deck longitudinal direction – (a) assumed breakout failure; (b) actual breakout failure	75
Figure 5.6: (a) Assumed projected failure area; (b) actual failure area	76
Figure 5.7: Complete haunch separation as seen from (a) the side view and (b) underneath the specimen.....	78

Figure 5.8: (a) Drawing and (b) photograph showing the center transverse bars running through the concrete failure prism for a specimen with no haunch	79
Figure 5.9: Haunch reinforcement to improve ductility (a) cross-section (b) plan view	82
Figure 5.10: Load versus stud pullout for (a) current detail and (b) reinforced haunch detail.....	83
Figure 5.11: Longitudinal spacing of shear studs	84
Figure 5.12: (a) 5-in. long studs with no haunch; (b) 8-in. long studs with 3-in. haunch	86
Figure 5.13: Potential concrete breakout failure prism for longer studs.....	86
Figure 5.14: Tensile capacity versus effective height for a single 7/8-in. diameter stud embedded in 4,000 psi concrete.....	88
Figure 5.15: Reduced diameter shear stud.....	92
Figure 5.16: Stud under shear and bending	92
Figure A.1: Truck load distribution, shear diagram, and moment diagram.....	100
Figure A.2: Deck slab – 1-ft wide section	102
Figure A.3: Strain and stress profiles at positive moment capacity.....	102
Figure A.4: Strain and stress profiles at negative moment capacity.....	103
Figure A.5: Assumed bending moment in deck slab at ultimate state.....	105
Figure A.6: Composite section	106
Figure A.7: Plastic neutral axis location	107
Figure B.1: FSEL bridge deck – typical transverse section.....	109
Figure B.2: FSEL bridge deck – plan view.....	110
Figure B.3: Notes for FSEL bridge deck drawings (Fig. B.1-B.2).....	111

Figure B.4: TxDOT typical stud connector detail for three studs (TxDOT Bridge Standard Drawings: Miscellaneous Details (Steel Girders and Beams), 2006)	112
Figure C.1: Specimen 0-1 (a,b).....	113
Figure C.2: Specimen 0-2 (a,b).....	114
Figure C.3: Specimen 0-3 (a,b).....	115
Figure C.4: Specimen 3-1 (a,b).....	116
Figure C.5: Specimen 3-2 (a,b).....	117
Figure C.6: Specimen 3-3 (a,b)	118
Figure D.1: Test specimen – slab cross section	119
Figure D.2: Assumed location of neutral axis at yield load.....	120
Figure D.3: Assumed strain and stress profile at yielding	121
Figure D.4: Assumed strain and stress profiles at ultimate moment capacity	122
Figure E.1: Stud details for specimens with no haunch.....	124
Figure E.2: Concrete breakout – projected failure areas for specimens with no haunch (A_{Nc})	125
Figure E.3: Stud details for specimens with a 3 in. haunch.....	128
Figure E.4: Concrete breakout – projected failure areas for specimens with a 3 in. haunch (A_{Nc}).....	128
Figure F.1: Shear stud mill test report	131

CHAPTER 1

Introduction and Background

1.1 FRACTURE CRITICAL BRIDGES

In 1967 the Silver Bridge in Point Pleasant, West Virginia collapsed due to the brittle fracture of a non-redundant eyebar chain that supported the main span (Figure 1.1). This collapse initiated a series of changes in the design, material specifications, and inspection of steel bridges. In 1978 special provisions were developed for bridges with fracture critical members (FCM) (Connor, Dexter, and Mahmoud, 2005). An FCM is defined by the American Association of State Highway Transportation Officials (AASHTO) as a “component in tension whose failure is expected to result in the collapse of the bridge or the inability of the bridge to perform its function” (AASHTO, 2004).



Figure 1.1: Collapse of Silver Bridge (Connor, Dexter, and Mahmoud, 2005)

Fracture critical bridges (FCB), or bridges with an FCM, are required to be inspected more frequently than a bridge that is considered non-fracture critical. The cost of inspection during the life of an FCB can typically be two to five times greater than a bridge without FCMs (Connor, Dexter, and Mahmoud, 2005). The increased cost associated with FCBs has led to fewer new FCBs being designed even in situations when an FCB may be a more effective solution.

There has been evidence that certain FCB types have redundant load paths and can withstand a fracture to an FCM. AASHTO classifies all two girder steel bridges as fracture critical, but experience has shown that two girder bridges do not collapse due to a fracture in one girder and can even continue to remain in service (Daniels, Kim, and Wilson, 1989). For example, in 1977 a two girder bridge at Neville Island in Pittsburgh, Pennsylvania suffered a full-depth crack in one girder and continued to carry traffic until a boat captain passing underneath the bridge spotted the crack (Figure 1.2).



Figure 1.2: Full-depth fracture of the I-79 two girder bridge at Neville Island in Pittsburgh, PA (Connor, Dexter, and Mahmoud, 2005)

Current bridge specifications assume that two girder bridges are fracture critical because they assume that the structural components of a bridge behave independently, but in reality these components interact with each other to form one structural system (Ghosn and Moses, 1998). In the case of two girder bridges, other components such as the deck slab can provide a redundant load path and prevent collapse when one girder experiences a fracture (Connor, Dexter, and Mahmoud, 2005).

1.2 FSEL FRACTURE CRITICAL BRIDGE TEST

The opportunity to perform a full-scale fracture test arose when the Texas Department of Transportation (TxDOT) was removing a 120-ft simple span twin steel trapezoidal box girder bridge segment along Interstate Highway 10 in Houston. There are many twin steel box girder bridges in the state of Texas, all of which are considered to be FCBs. The inspection of box girder bridges is particularly difficult and expensive because it requires the inspector to be inside of the box girder. The goal of this fracture test was to learn about the load transfer that takes place during a fracture event and to use that information to help calibrate an analytical model that can predict the behavior of twin girder FCBs in a fracture event.

Initially the bridge was to be tested in place, but, due to safety concerns, the bridge girders were removed and transported to the Phil M. Ferguson Structural Engineering Laboratory (FSEL) at the University of Texas at Austin. Once the girders arrived at FSEL, a contractor was hired to reconstruct the bridge deck and traffic rails. A cross-section of the FSEL test bridge, including the T501 rails, is shown in Figure 1.3.

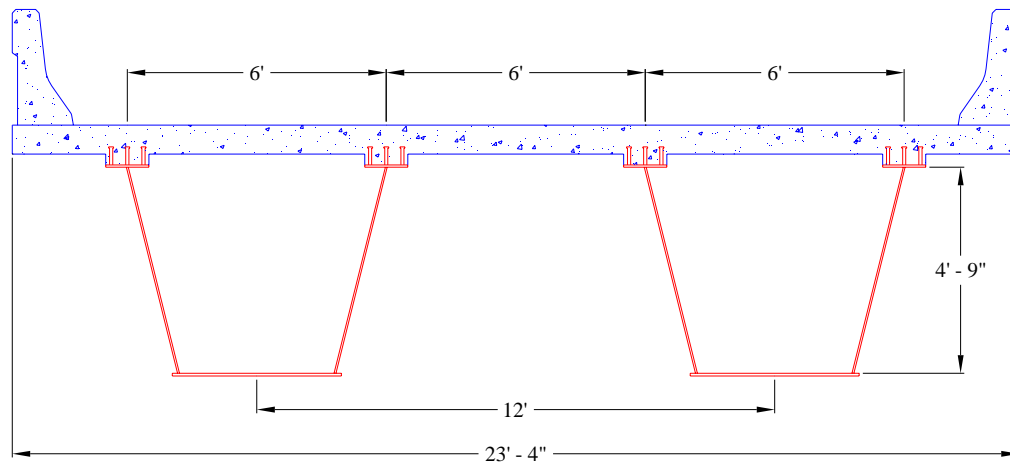


Figure 1.3: Cross-section of FSEL test bridge

After the bridge had been reconstructed in accordance with TxDOT standard practices, a fracture test was performed on the bridge. During the test, the bridge was loaded with the equivalent of a 76-kip truck. The fracture was simulated by cutting the bottom flange of the exterior girder at the mid-span location. A linear-shaped charge was used to cut the flange to simulate the dynamic fracture of the flange. The charge cut completely through the tension flange of the girder, but the fracture did not propagate up the girder webs. The bridge behaved extremely well during the test, and the fractured girder deflected only an additional 1/4 in. after the fracture of the flange.

Unfortunately, there was not much evidence of load transfer to the other girder because the load carried by the fractured flange was simply resisted by the webs in the area of the fracture. A future test is planned to propagate the existing crack up the webs in order to determine how the load is transferred from the fractured girder to the non-fractured girder and to determine if the bridge can withstand a full depth fracture without collapse.

1.3 ANALYSIS OF BRIDGE COMPONENTS

1.3.1 Introduction

Currently, the best way to model system behavior is through the use of detailed analytical models such as finite element programs. While these models may produce the most accurate results, they also require a substantial amount of work and time to be developed and to be run. It would be beneficial for designers or bridge owners to have a simple set of analytical procedures that can be checked before developing a complex finite element model. If these simple analyses show that a bridge might have adequate redundancy, a more detailed analysis can then be developed to confirm that the system can withstand a fracture to an FCM. However, if the simple analyses show that the bridge cannot withstand a fracture to an FCM, then the time and money that would have been spent on a more detailed model can be saved.

A set of simple calculations was developed to predict the behavior of the FSEL test bridge during the fracture test. These analyses focused on the individual components of the bridge that would be required to provide an alternate load path after the fracture of one girder – namely the shear studs, deck slab, and remaining girder. In each case specific assumptions were made in order to simplify the analysis. Therefore, these analyses do not capture the exact behavior of the system during a fracture event. Rather, they are meant to be used as an initial check prior to making the decision to develop a detailed finite element model.

1.3.2 Load Path

After a fracture occurs in the tension flange of one of the girders and propagates up the webs, it is assumed that the girder will no longer be able to resist load. The fracture at mid-span can be compared to placing a hinge in the girder. A simply

supported beam cannot carry load by flexure with a hinge at the mid-span; therefore, in order to prevent a total bridge collapse, the load that had been resisted by the fractured girder must be transferred to the other girder. The fractured girder will drop down and deflect as shown in Figure 1.4. When this happens, the shear studs will be loaded in tension and must be able to transfer the load into the deck slab. The deck slab must have enough capacity to transfer the load over to the other girder. Finally, the other girder must have enough moment capacity to support the entire weight of the bridge and any live load on the bridge at the time of fracture.

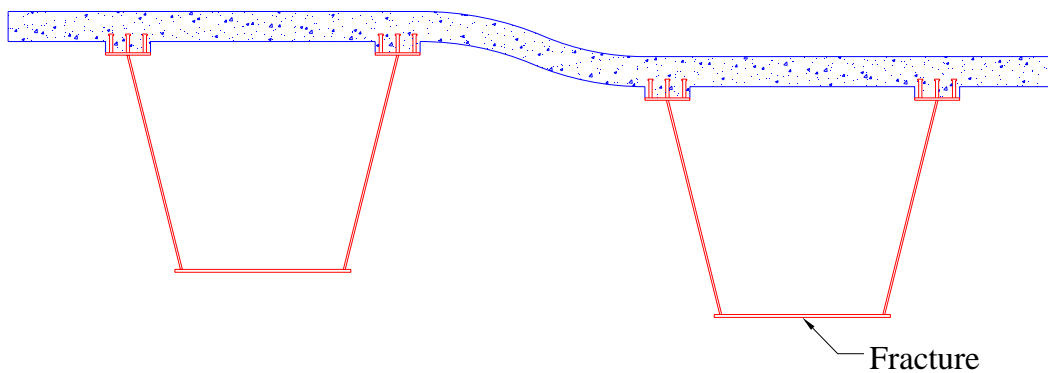


Figure 1.4: Assumed deflected shape at point of girder fracture

For these calculations it was assumed that the required load the studs and slab needed to redistribute was equal to half of the total weight on the bridge. This includes the weight of the fractured girder, half of the slab, one railing, and half of the simulated truck load. This load was multiplied by a factor of two to account for the dynamic effect. It is important to note that the dynamic amplification factor of 2.0 is an upper bound and is expected to be lower for the actual response. For the FSEL test bridge, half the weight of the bridge plus half the weight of a 76-kip truck was calculated to be about 277 kips, or 554 kips after doubling the load for the dynamic effect. Strength reduction factors (ϕ)

were not applied to any of these calculations. Refer to Appendix A for the calculation details. The concepts used to make these calculations are presented here.

1.3.3 Analysis of Shear Studs

The first components of the bridge system that must be able to transfer the load from the fractured girder to the intact girder are the shear studs that connect the girder to the deck slab. In order to simplify the calculations, it was assumed that the studs would be under tension only. The equations from Appendix D of the ACI 318 Building Code were used to calculate the tensile capacity of a single row of studs. After the capacity of a single row of three studs was calculated, the number of rows needed to resist the 554-kip force was determined. This calculation assumes that the studs can perform in a ductile manner and redistribute the force along the length of the girder.

The calculation of the tensile capacity of anchors in concrete, the predicted tensile capacity of a row of shear studs on the FSEL test bridge, and the percentage of the span length required to distribute the 554-kip force are discussed in detail in Chapter 2.

1.3.4 Analysis of Deck Slab

Assuming that the shear studs are able to transfer load into the deck slab, the deck slab must then be able to transfer the load across to the other box girder. In this analysis two criteria were checked for the deck slab. The first was the flexural capacity of the slab, and the second was the shear capacity of the slab. In each case the capacity of a 1-ft wide section of the deck slab was calculated. Then the percentage of the total span length needed to distribute the required force during a fracture event was determined. Refer to Appendix A for all calculations associated with the deck slab capacity and distribution of the 554-kip force.

To calculate the bending capacity of the deck slab, it was assumed that the slab would be in double curvature after the fracture and that the bending moment diagram at the ultimate state would be as shown in Figure 1.5. The positive and negative moment capacities were calculated assuming that the ultimate concrete compressive strain was equal to 0.003 in./in. and that the concrete stress distribution could be estimated as a rectangular stress block with magnitude equal to $0.85f_c'$ (ACI 318-05). The concrete compressive strength (f_c') was assumed to be 4,000 psi. This value is the required minimum strength of TxDOT Class “S” concrete, which was used in the deck slab of the FSEL test bridge.

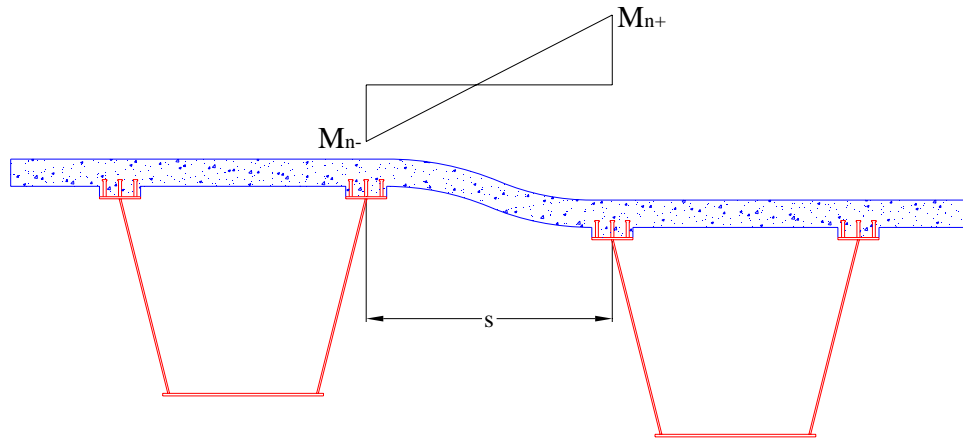


Figure 1.5: Bending moment in deck slab at ultimate state

The positive moment capacity and the negative moment capacity were calculated to be 20.5 kip-ft and 16.6 kip-ft, respectively, for a 1-ft wide section of the deck. After calculating the ultimate positive and negative moment capacity of the deck slab, the shear across the slab can be determined from the following equation:

$$V = \frac{M_n^+ + M_n^-}{s} \quad \text{Equation 1.1}$$

where: V = shear in slab at ultimate moment state (kip)

M_n^+ = nominal positive moment capacity (kip-ft)

M_n^- = nominal negative moment capacity (kip-ft)

s = spacing between top flanges (= 6 ft)

Using Equation 1.1, the shear in the slab at the ultimate moment state is calculated to be 6.2 kips for a 1-ft wide deck section. Therefore, approximately 90 ft of the deck slab, or 76% of the span length, is required to resist the 554-kip force. This result indicates that the slab has the flexural capacity to transfer the force to the other girder provided that the slab can behave in a ductile manner and distribute the force along the length of the girder.

The second criteria checked for the deck slab was the shear capacity. There is no shear reinforcement in the deck slab; therefore, the shear capacity of the slab is based solely on the shear resistance of the concrete. The shear capacity of the slab was calculated using the following equation from the ACI 318 Building Code:

$$V_c = 2\sqrt{f'_c}bd \quad \text{Equation 1.2}$$

where: V_c = nominal shear strength provided by concrete (lb)
 f'_c = specified compressive strength of concrete (= 4,000 psi)
 b = width of section (= 12 in.)
 d = distance from extreme compression fiber to centroid of tension reinforcement (= 4.375 in.)

The shear capacity calculated from Equation 1.2 was 6.6 kips for a 1-ft wide deck section. Therefore, approximately 84 ft of the deck slab, or 71% of the span length, is required to resist the 554-kip force. This result indicates that the shear capacity is adequate and that the flexural capacity will govern the deck strength.

1.3.5 Analysis of Composite Section

Provided that both the shear studs and the deck slab can resist the required load, the remaining box girder must then have enough moment capacity to resist the entire load on the bridge. This includes all of the dead load in addition to the live load that is placed on the bridge at the time of fracture. In order to simplify the calculations, the girder was assumed to be straight – the FSEL girders are actually slightly curved – and the effect of torsion was neglected. The plastic moment capacity of the composite section of the non-fractured girder (Figure 1.6) was calculated assuming that the concrete strength was 4 ksi and that the yield strength of the steel girder was 50 ksi. Refer to Appendix A for this calculation and the calculation of the maximum moment on the bridge at the time of the fracture test.

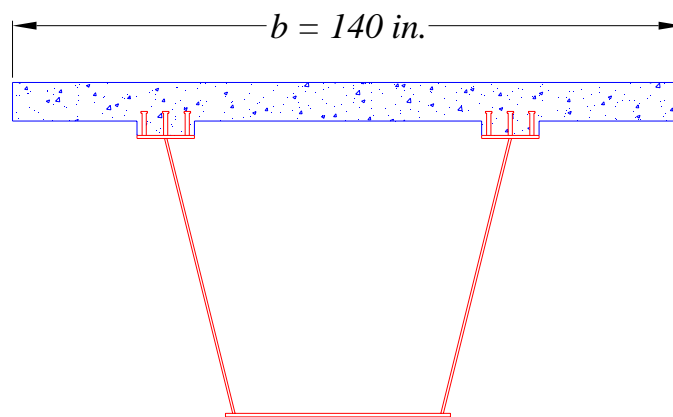


Figure 1.6: Composite section of non-fractured girder

The effective width of the concrete slab was equal to half of the total slab width. The plastic neutral axis was found to be in the web of the steel girder, and the plastic moment capacity was calculated to be 17,840 kip-ft. The maximum moment on the bridge at the time of the fracture was calculated to be 8,950 kip-ft. This calculation indicates that the composite section of a single box girder can withstand a moment that is approximately twice the moment on the bridge at the time of failure. If the applied

moment is multiplied by two for the dynamic effect, then the remaining girder has exactly enough reserve capacity to support the entire weight of the bridge. Recall that the dynamic amplification factor of 2.0 is an upper bound and is expected to be lower for the actual response.

1.3.6 Summary

The simple analysis techniques presented in this chapter have shown that the deck slab and the remaining box girder may be able to provide a redundant load path when one of the box girders experiences a full-depth fracture. The third component that must be able to provide a redundant load path is the shear studs. As is discussed in Chapter 2, the tensile capacity of the studs can be estimated using Appendix D in the ACI 318 Building Code, but the bridge haunch and the grouping of studs across the flange width create some uncertainty in this calculation. A series of laboratory tests were conducted in order to determine the effect that the bridge haunch has on both the tensile capacity and the behavior of the studs. The remainder of this thesis, beginning with Chapter 3, discusses these laboratory tests.

CHAPTER 2

Strength of Concrete Anchors under Tensile Loading

2.1 INTRODUCTION

In Chapter 1, the simple analysis techniques used to determine if the FSEL test bridge might have the redundancy to withstand a full-depth fracture to one of the box girders were discussed. The three components of the bridge that need to resist the load in the fractured girder were identified as the shear studs, the deck slab, and the remaining girder. These calculations showed that the deck slab and remaining box girder may have the ability to resist the additional load. This chapter will discuss the strength of concrete anchors loaded in tension and will use that information to determine if the shear studs on the FSEL test bridge can resist the required load during a fracture event.

2.2 TENSILE STRENGTH OF CONCRETE ANCHORS

2.2.1 Overview: ACI 318 Appendix D – Anchoring to Concrete

In order to calculate the tensile capacity of the shear studs, Appendix D of the ACI 318 Building Code was referenced. This appendix provides requirements for concrete anchors loaded in tension, shear, or a combination of tension and shear. It covers a wide range of both cast-in-place anchors and post-installed anchors. Cast-in-place anchors include headed bolts, headed studs, and hooked bolts. Post-installed anchors include expansion anchors and undercut anchors. The shear studs used on a bridge are an example of cast-in-place headed stud anchors; thus, the remainder of this discussion will deal with the strength of headed stud anchors in tension. A drawing of the headed stud used on the FSEL test bridge is shown in Figure 2.1. Dimensions for

various stud sizes and the required minimum yield and tensile strengths are governed by Section 7.3 of the AASHTO/AWS D1.5 Bridge Welding Code.

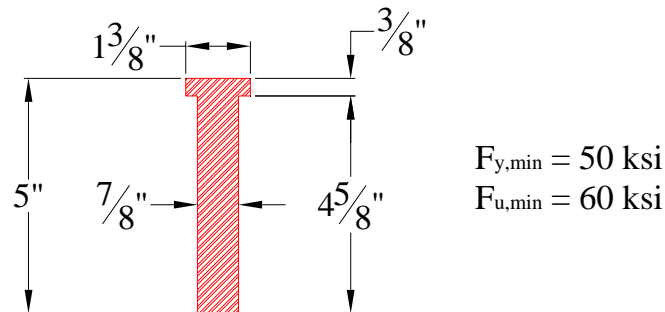


Figure 2.1: FSEL test bridge shear stud – 7/8-in. diameter x 5-in. long

A headed stud anchor loaded in tension must be checked for four different failure modes. These four failure modes are steel failure, concrete breakout failure, pullout failure, and concrete side-face blowout failure. Each of these failure modes is shown in Figure 2.2. Spacing, edge distance, and thickness requirements must also be satisfied in order to prevent a concrete splitting failure, which is also shown in Figure 2.2.

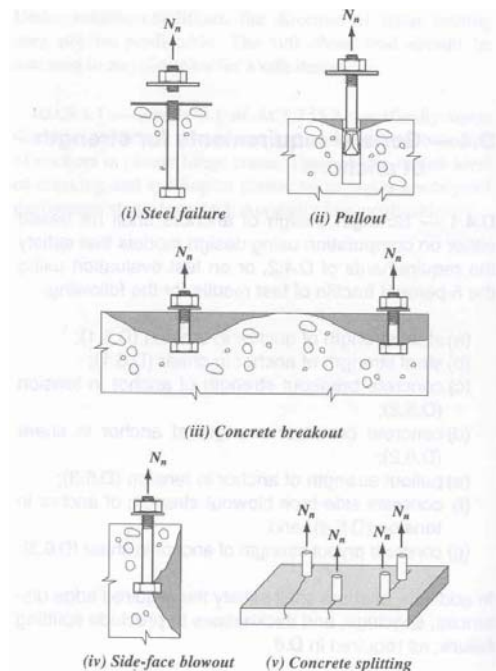


Figure 2.2: Failure modes for anchors loaded in tension (ACI 318-05)

2.2.2 Steel Strength

A steel failure will only occur if the ultimate strength of the steel can be reached prior to a concrete failure. If this can occur, failure of a ductile steel element allows for significant redistribution of anchor forces to other anchors. The equation for the steel strength of an anchor is given as:

$$N_{sa} = nA_{se}f_{uta} \quad \text{Equation 2.1 (ACI 318-05)}$$

where: N_{sa} = nominal strength of an anchor in tension as governed by the steel strength (lb)

n = number of anchors in a group

A_{se} = effective cross-sectional area of anchor (in.²)

f_{uta} = specified tensile strength of anchor steel (psi)

The steel strength of an anchor is based on the ultimate tensile strength rather than the yield strength because a large majority of anchor materials do not exhibit a well defined yield point (ACI 318-05). The strength reduction factor (ϕ) for an anchor governed by the strength of a ductile steel element is 0.75 for tension loads. The Commentary in the ACI 318-05 Code states that this factor may seem low, but it provides the same level of safety as applying a higher factor to the yield strength (ACI 318-05).

2.2.3 Concrete Breakout Strength

A concrete breakout occurs when the stud pulls out with a large prism or cone of concrete as shown in Figure 2.3. It is a failure of the concrete rather than the steel anchor, and therefore can be a very brittle failure if no reinforcement is present to intersect the failure prism. The ACI 318-05 Code equations for concrete breakout strength is based on the concrete capacity design (CCD) approach, which assumes a concrete failure prism with an angle of approximately 35° as shown in Figure 2.3 (a).

The projected failure area of the prism is a square with lengths equal to three times the effective embedment depth of the anchor. Another approach for calculating the concrete breakout capacity is based on an assumed breakout cone with a 45° angle as shown in Figure 2.3 (b).

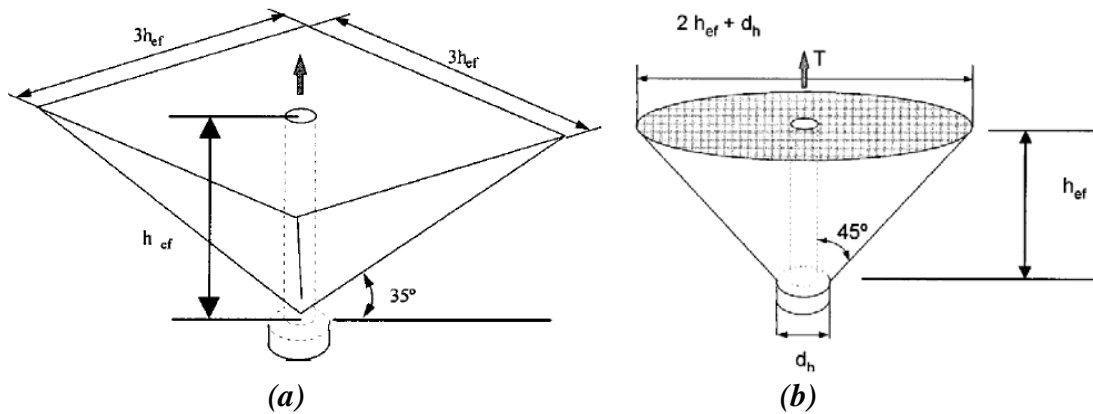


Figure 2.3: Tensile breakout shape as idealized by: (a) CCD method (b) 45° cone method (Shirvani, Klingner, and Graves III, 2004)

A large number of experimental tests performed on anchors in uncracked concrete found that the CCD approach provided an accurate prediction of the tensile capacity while the 45° cone method was less accurate and at times unconservative (Fuchs, Eligehausen, and Breen, 1995). In addition to providing better results, the CCD approach is also more user-friendly for design. Therefore, the CCD method is the approach that has been adopted by the ACI 318 Code.

Additional research has shown that the concrete breakout strength of headed stud anchors is reduced by approximately 25% when the stud is located in a region of a member where there is concrete cracking (Eligehausen and Balogh, 1995). Therefore, the design equations for concrete breakout assume cracked conditions, but they can be adjusted for uncracked conditions through the use of a modification factor. The nominal

concrete breakout strength of an anchor or group of anchors in tension is given by the following equations:

For a single anchor:

$$N_{cb} = \frac{A_{Nc}}{A_{Nco}} \psi_{ed,N} \psi_{c,N} \psi_{cp,N} N_b \quad \text{Equation 2.2 (ACI 318-05)}$$

For a group of anchors:

$$N_{cbg} = \frac{A_{Nc}}{A_{Nco}} \psi_{ec,N} \psi_{ed,N} \psi_{c,N} \psi_{cp,N} N_b \quad \text{Equation 2.3 (ACI 318-05)}$$

- where:
- N_{cb} = nominal concrete breakout strength in tension of a single anchor (lb)
 - N_{cbg} = nominal concrete breakout strength in tension of a group of anchors (lb)
 - A_{Nc} = projected concrete failure area of an anchor or group of anchors loaded in tension (in.²)
 - A_{Nco} = projected concrete failure area of one anchor when not limited by edge distance or spacing ($= 9h_{ef}^2$) (in.²)
 - $\psi_{ec,N}$ = modification factor to account for eccentric loading of groups (<1.0 for eccentric loading, =1.0 for no eccentricity)
 - $\psi_{ed,N}$ = modification factor to account for edge distances smaller than $1.5h_{ef}$ (= 1.0 if edge distance is greater than $1.5h_{ef}$)
 - $\psi_{c,N}$ = modification factor to account for cracking (= 1.25 if analysis indicates no cracking; otherwise = 1.0)
 - $\psi_{cp,N}$ = modification factor applicable only to post-installed anchors (= 1.0 for cast-in anchors)
 - N_b = basic concrete breakout strength in tension of a single anchor in cracked concrete (lb)

The equation for the basic concrete breakout strength of a single anchor in cracked concrete (N_b) is shown in Equation 2.4. The capacity obtained from this equation is adjusted by the design equations (Equation 2.2 and Equation 2.3) to account for other factors such as group effects, edge distances, uncracked members, and eccentric loadings.

$$N_b = k_c \sqrt{f'_c} h_{ef}^{1.5} \quad \text{Equation 2.4 (ACI 318-05)}$$

where: k_c = 24 for cast-in-place anchors
 f'_c = specified compressive strength of concrete (psi)
 h_{ef} = effective anchor embedment depth – distance from base of stud to underside of the head (= 4-5/8 in. for a 5-in. stud)

To calculate the capacity of multiple studs in a group, the capacity of a single stud cannot simply be multiplied by the number of studs in the group. When the distance between studs becomes less than $3h_{ef}$, there is a group effect because the projected failure areas of the studs overlap. Thus, the projected failure area of a group with n studs becomes less than n times the projected failure area of a single stud. The concrete breakout strength equation (Equation 2.3) accounts for multiple anchors in a group by multiplying the basic breakout strength of a single anchor by the projected failure area of the group over the projected failure area of a single stud (A_{Ng}/A_{Nco}). Examples of projected failure areas for multiple studs behaving both independently and as a group are shown in Figure 2.4. This figure shows that closely spacing three studs results in a projected failure area that can be much less than the projected failure area of three studs behaving independently. Thus, those three studs will have a tensile capacity that is much less than the tensile capacity of three studs behaving independently.

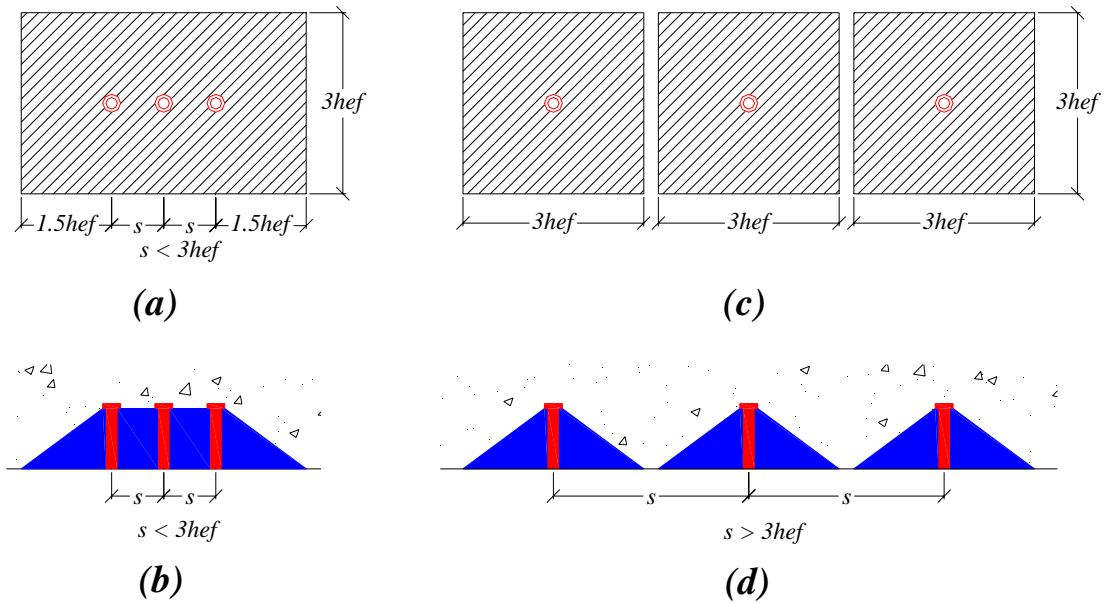


Figure 2.4: Multiple studs behaving as a group – (a) projected failure area (b) section through failure prism; multiple studs behaving independently – (c) projected failure areas (d) section through failure prisms

The concrete breakout strength of an anchor or group of anchors must also be reduced if a stud is located near an edge. When an anchor is located less than a distance of $1.5h_{ef}$ away from an edge, the full breakout prism cannot develop. The concrete breakout equation (Equation 2.3) accounts for this effect in both the calculation of the projected failure area and the edge modification factor. An example of an anchor located near an edge and its projected failure area is shown in Figure 2.5. This figure shows that the projected failure area, and thus capacity, can be significantly less when a stud is located near an edge.

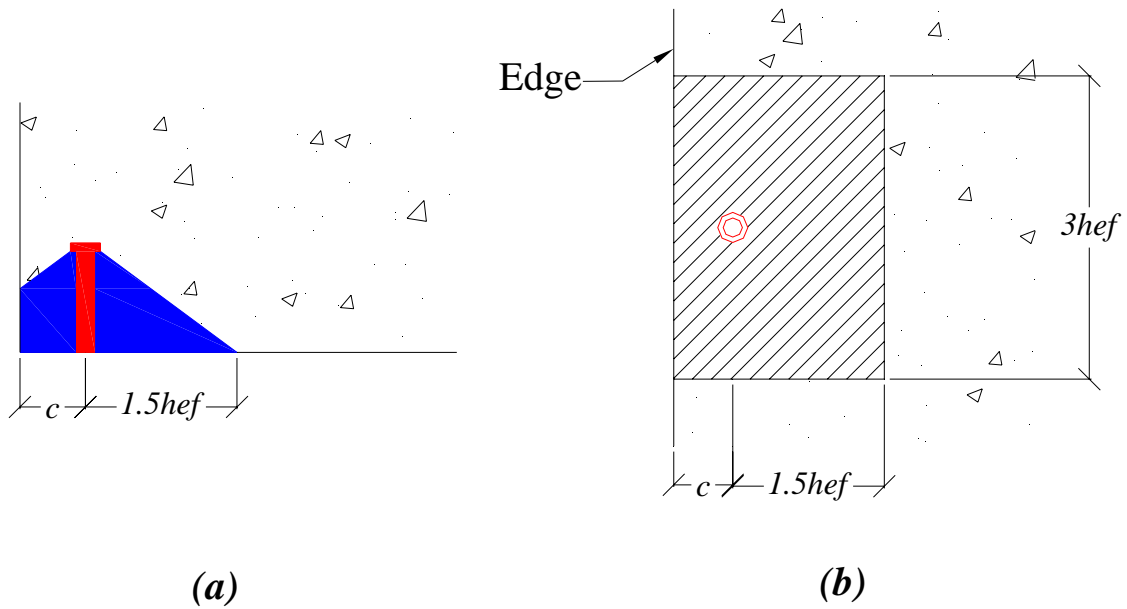


Figure 2.5: Edge reduction ($c < 1.5h_{ef}$) – (a) section through failure prism (b) projected failure area

The capacity of anchors located near an edge is further reduced by the modification factor for edge effects, $\psi_{ed,N}$. If the edge distance is greater than $1.5h_{ef}$, this factor is taken as 1.0. However, when the edge distance is less than $1.5h_{ef}$, the modification factor is reduced to a value less than 1.0. As the edge distance becomes very small, this factor approaches 0.7. Therefore, specimens with very small edge distances can experience as much as a 30% decrease in capacity. The equation used to calculate the edge distance modification factor is as follows:

$$\psi_{ed,N} = 0.7 + 0.3 \frac{c_{a,min}}{1.5h_{ef}} \quad \text{Equation 2.5 (ACI 318-05)}$$

where: $c_{a,min}$ = smallest edge distance measured from center of an anchor shaft to the edge of concrete (in.)

2.2.4 Pullout Strength

A pullout failure differs from a concrete breakout failure in that the stud pulls out only the small volume of concrete directly under the stud head rather than a large prism or cone of concrete. The equation for the pullout strength of an anchor loaded in tension is given as:

$$N_{pn} = \psi_{c,P} 8A_{brg} f'_c \quad \text{Equation 2.6 (ACI 318-05)}$$

where: N_{pn} = pullout strength in tension of a single anchor (lb)
 $\psi_{c,P}$ = modification factor for cracking (= 1.4 if analysis indicates no cracking; otherwise = 1.0)
 A_{brg} = bearing area of the head of the stud (in.²)

This equation is a function of the compressive strength of the concrete and the bearing area of the stud head, but not the effective embedment depth. This is because the equation corresponds to the load at which the concrete under the anchor head begins to crush, not the load which will completely pull the anchor out of the concrete. However, local crushing under the head greatly reduces the stiffness of the connection and is usually the beginning of a pullout failure (ACI 318-05).

2.2.5 Concrete Side-Face Blowout Strength

A concrete side-face blowout failure can occur when an anchor with deep embedment is located close to an edge. A concrete side-face blowout failure differs from a concrete breakout failure because the stud does not actually pull out with a large volume of concrete. Rather the side concrete between the stud and the edge breaks off (Figure 2.2). If a single headed anchor is located a distance less than $0.4h_{ef}$ away from an edge, the following equation must be checked:

$$N_{sb} = 160c_{a1} \sqrt{A_{brg}} \sqrt{f'_c} \quad \text{Equation 2.7 (ACI 318-05)}$$

where: N_{sb} = side-face blowout strength of a single anchor (lb)
 c_{a1} = distance from center of anchor shaft to the edge (in.)

When multiple studs with deep embedment are located close to an edge ($c_{a1} < 0.4h_{ef}$), the nominal concrete side-face blowout capacity is given as:

$$N_{sbg} = \left(1 + \frac{s}{6c_{a1}} \right) N_{sb} \quad \text{Equation 2.8 (ACI 318-05)}$$

where: N_{sbg} = side-face blowout strength of a group of anchors (lb)
 s = spacing of the outer anchors along the edge (in.)

2.3 CAPACITY OF A ROW OF STUDS ON THE FSEL TEST BRIDGE

The shear studs on the FSEL test bridge are grouped transversely across the width of the top flanges in rows of three. These rows are spaced longitudinally along the length of the girder at approximately 22 in. The FSEL test bridge also has a haunch, which is a standard detail in composite bridges. The height of this haunch is 3 in., which is the maximum allowable haunch height that can be used on a bridge with 5-in. long studs. This detail is based on both AASHTO and TxDOT specifications that require the studs to extend a minimum of 2 in. above the haunch into the deck slab. The details of the haunch and the rows of studs are shown in Figure 2.6. The deck reinforcement is not shown in this figure.

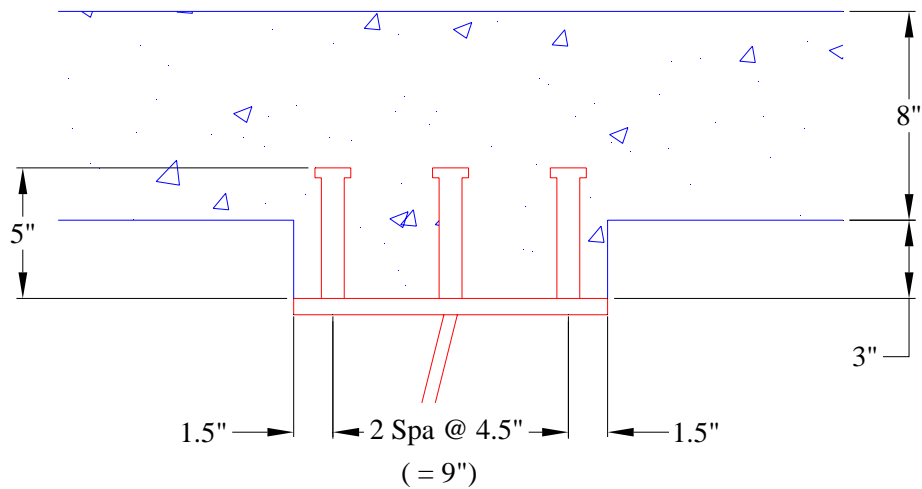


Figure 2.6: Shear stud detail for FSEL test bridge

The haunch produces a pseudo-edge effect. Clearly, the full breakout prism cannot develop, but the edge is not a true edge. The edge is only 3 in. high, and above that point the concrete extends well beyond $1.5h_{ef}$. The concrete breakout strength for this detail is bracketed by the lower bound strength, which assumes that there is an edge 1.5 in. away from the outer studs, and the upper bound strength, which assumes that the breakout strength is not reduced by any edge effect. If the concrete breakout prism forms at the same 35° angle, the prism would intersect the bottom of the slab only slightly past the haunch edge as shown in Figure 2.7. Based on this fact, the concrete breakout strength will most likely be closer to the lower bound strength calculated assuming that the haunch represents an edge.

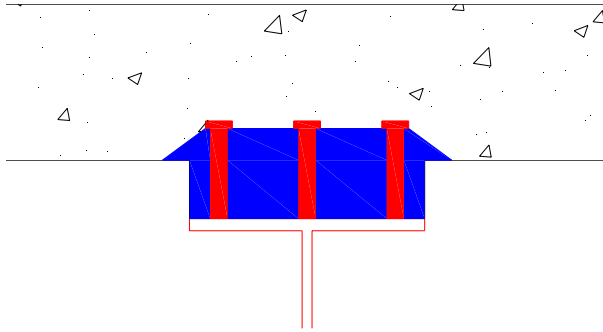


Figure 2.7: Concrete breakout prism following 35° angle

The tensile capacity for the different failure modes was calculated for a single row of studs on the FSEL test bridge. The steel strength of the studs was based on the minimum required tensile strength set forth by the AASHTO/AWS D1.5 Bridge Welding Code. The concrete breakout capacity was calculated assuming that the haunch was an edge. Concrete side-face blowout was not calculated because it was assumed that this failure could not occur due to the fact that the edge does not extend above the height of the stud. The result of these calculations is shown in the following equations:

Steel Strength:

$$N_{sa} = nA_{se}f_{uta} = 3\frac{\pi}{4}(0.875in.)^2(60,000psi) = \mathbf{108,240\ lb}$$

Concrete Breakout:

$$N_b = k_c\sqrt{f'_c}h_{ef}^{1.5} = (24)\sqrt{4000psi}(4.625in.)^{1.5} = 15,100lb$$

$$A_{Nc} = (c_a + s + s + c_a)(3h_{ef}) = [2(1.5in.) + 2(4.5in.)](3)(4.625in.) = 166.5in.^2$$

$$A_{Nco} = 9h_{ef}^2 = 9(4.625in.)^2 = 192.5in.^2$$

$$\psi_{ed,N} = 0.7 + 0.3\frac{c_{a,\min}}{1.5h_{ef}} = 0.7 + 0.3\frac{(1.5in.)}{1.5(4.625in.)} = 0.765$$

$$N_{cbg} = \frac{A_{Nc}}{A_{Nco}} \psi_{ec,N} \psi_{ed,N} \psi_{c,N} N_b = \frac{(166.5in.^2)}{(192.5in.^2)} (1.0)(0.765)(1.0)(15,100lb) = \mathbf{9,990 lb}$$

Pullout (of 1 stud):

$$N_{pn} = \psi_{c,p} 8A_{brg} f_c' = (1.0)(8) \frac{\pi}{4} ((1.375in.)^2 - (0.875in.)^2)(4,000 psi) = \mathbf{28,270 lb}$$

These calculations show that concrete breakout is clearly the governing failure mode. Even if it was assumed that the haunch had no effect, concrete breakout would still be the governing failure mode. The estimated breakout capacity of a row of studs (N_{cbg}) on the FSEL test bridge was rounded to 10 kips. The modification factor for eccentric loading ($\psi_{ec,N}$) was taken as 1.0 because the load is not applied eccentrically, and the modification factor for cracking ($\psi_{c,N}$) was taken as 1.0 because it was assumed that the deck slab will be cracked after the fracture.

A summary of the estimated tensile capacities is shown in Table 2.1. The effect of slab cracking is demonstrated by comparing the estimated capacities in cracked concrete to those in uncracked concrete. The effect of the bridge haunch is demonstrated by comparing the capacity of a single stud with a row of studs on the FSEL test bridge both with and without the haunch.

Table 2.1: Estimated tensile capacities for a single stud and a row of three studs on the FSEL test bridge ($f_c' = 4,000 psi$; 7/8-in. diameter x 5-in. long studs; $f_{uta} = 60,000 psi$)

Failure Mode		Number of Studs	Estimated Tensile Capacity (kip)	
			Cracked Concrete	Uncracked Concrete
Concrete Breakout	No Haunch	Single	15.1	18.9
		Row of 3	24.9	31.1
	3" Haunch	Single	12.5	15.7
		Row of 3	10.0	12.5
Stud Pullout		Single	28.3	39.6
		Row of 3	84.8	118.7
Stud Fracture		Single	36.1	36.1
		Row of 3	108.3	108.3

If a single row of studs can resist 10 kips, then 56 rows of studs are required to resist the 554-kip force from the fractured girder. The stud rows are spaced at 22 in.; therefore, 103 ft, or 87% of the span length, is required to resist the 554-kip force. Spreading the force among 56 rows assumes that the studs can behave in a ductile manner and redistribute the force along the length of the girder. However, a concrete breakout failure is governed by brittle failure of the concrete. This aspect of the response may prevent the 554-kip force from being distributed among such a large percentage of the span length.

2.4 SUMMARY

The calculations in this chapter have shown that the governing failure mode for a row of shear studs on the FSEL test bridge is a concrete breakout failure. The concrete breakout capacity of a row of three studs is greatly reduced when the studs are located close to an edge. The haunch used in bridge construction produces a pseudo-edge very close to the outer studs in the row. Therefore, it is assumed that the capacity of a row of studs will be reduced, but the magnitude of the reduction can only be estimated using the ACI 318 equations. Furthermore, while the strength of the studs appears to be adequate, the studs may not be able to redistribute forces along the span due to the brittle nature of a concrete breakout failure.

The remainder of this thesis will discuss the laboratory tests that were performed to determine the effect that the bridge haunch has on both the capacity and the behavior of the shear studs loaded in tension. The laboratory tests will also include the effect of slab cracking due to a moment being applied to the deck slab in addition to the tensile force acting on the studs.

CHAPTER 3

Testing Program

3.1 INTRODUCTION

The bridge haunch creates a great deal of uncertainty in the calculation of the tensile capacity of the shear studs. The haunch is assumed to have a detrimental effect because the full volume of the concrete breakout prism cannot be developed. The goal of this testing program is to quantify the effect that the haunch has on the tensile capacity of the shear studs.

Pullout tests were performed on 12 reinforced bridge deck sections. Half of these deck sections were constructed with a haunch, while the other half have no haunch. The number of studs was varied for both the specimens with and without a haunch. For the specimens with a haunch, increasing the number of studs decreases the spacing between the studs and the edge of the haunch. Theoretically, as this edge spacing decreases, the capacity will decrease. For the specimens without a haunch, increasing the number of studs should increase the capacity because the volume of concrete in the breakout failure prism is increased.

When one of the bridge girders fractures, that girder will drop down, loading the studs in tension and also loading the deck slab in bending. This situation is duplicated in the laboratory tests. The studs will be loaded in tension, but the tension force used to load the studs also creates a bending moment in the slab. However, it is important to realize that test setup will not exactly replicate the situation in the bridge. Prior to a fracture, the deck slab of the bridge experiences compressive stresses due to the

longitudinal bending of the composite section. The deck sections tested in the laboratory do not have any initial stresses in the slab due to longitudinal bending.

3.2 TEST SPECIMENS

3.2.1 Specimen Details

Six unique reinforced composite deck sections were tested. A duplicate of each specimen was tested for a total of 12 tests. Half of the specimens were constructed with a 3-in. haunch while the other half was constructed with no haunch. When selecting the dimensions and details to be used in the specimens, every effort was taken to replicate the details built into the full scale test bridge at FSEL, which uses typical TxDOT bridge deck details. Refer to Appendix B for the TxDOT details and the deck slab details of the test bridge at FSEL, from which all of the specimen details were based. Refer to Appendix C for the detailed drawings of all six unique specimens.

When a fracture occurs in one girder, that girder will deflect so that the deck slab is bending in double curvature with the inflection point approximately midway between the girders as shown in Figure 3.1. When this happens, the bending stresses occur in the transverse direction of the deck slab. The test specimens were designed so that the tension force applied to the studs would also create a bending moment in the deck slab transverse direction.

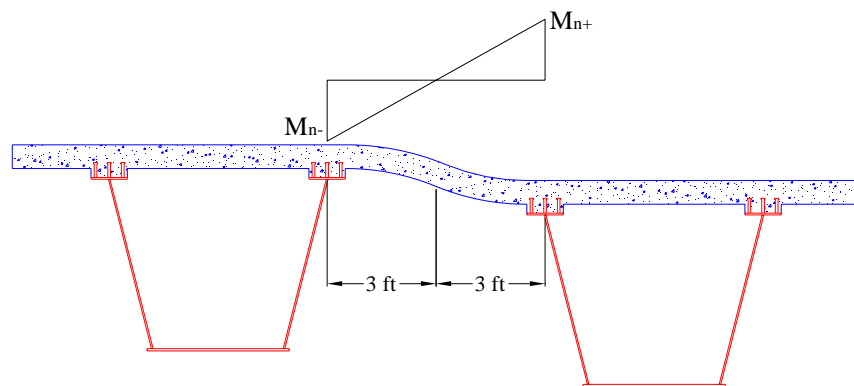


Figure 3.1: Bridge slab in double curvature

The deck sections tested in the laboratory were 7-ft long by 2-ft wide. Although the 7-ft length would typically be considered the longitudinal direction, this length actually corresponds to the transverse direction of the FSEL test bridge. In order to be consistent with the FSEL test bridge, the longitudinal direction of the test specimens will be referred to as the transverse direction, and vice versa, throughout the remainder of this thesis. The naming of the longitudinal and transverse directions is clarified in Figure 3.2.

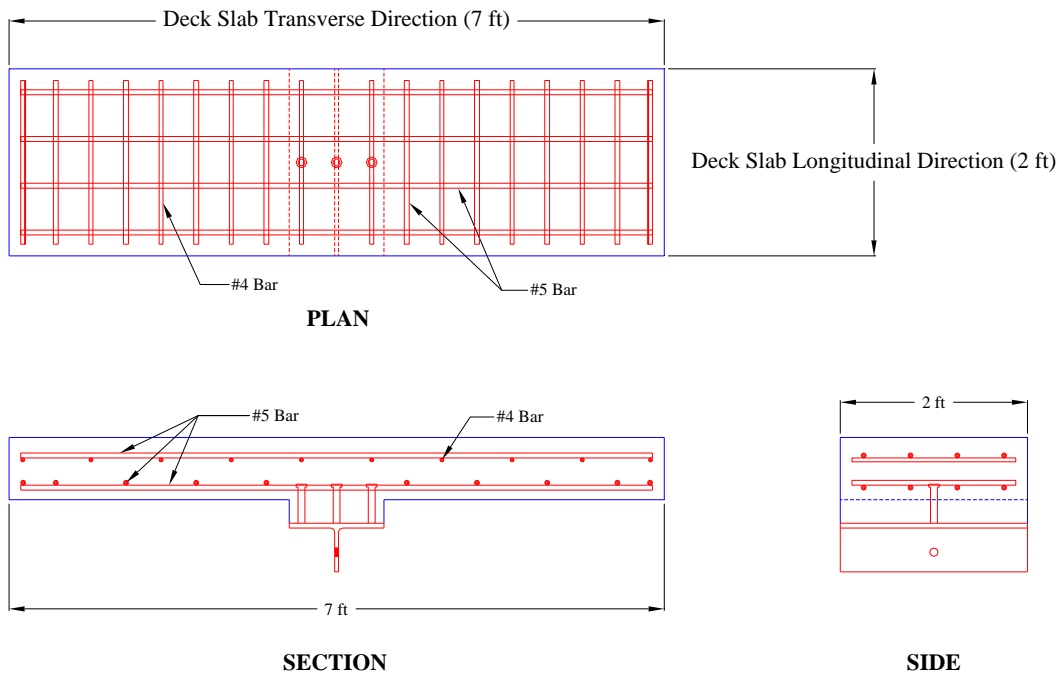


Figure 3.2: Transverse and longitudinal directions of test specimens

The steel sections were cut to a 2-ft length, and the row of studs was welded at the center of this length. The 2-ft length was chosen because the longitudinal spacing of the studs on the FSEL test bridge is approximately 2 ft. This 2-ft length also allows for the full concrete breakout prism to develop in the longitudinal direction for all specimens. The span length was selected based on the deflected shape of the deck slab during the fracture event. As shown in Figure 3.1, when the deck slab bends in double curvature,

the maximum moment in the deck slab occurs at the shear stud connection, and the distance between the inflection point and the studs is approximately 3 ft. The test specimens were tested as simply supported slabs with a tension force loading the studs at the mid-span. This arrangement allowed the maximum moment to occur at the location of the stud connection. The span length of approximately 6 ft was chosen because it corresponds to 3 ft from the point of zero moment to maximum moment as is the case when the deck slab bends in double curvature. The 7-ft overall length was chosen so that an adequate bearing length was available at each end. The 6-ft span is also long enough to assure that an adequate moment is present in the slab, but short enough that a tension failure of the studs will occur before a bending failure of the slab.

The slab thickness was chosen to be 8 in. because it matches the thickness of the deck slab on the FSEL test bridge. The size and spacing of the slab reinforcement was based on the typical TxDOT deck slab details, which are also used in the FSEL test bridge. The reinforcement consisted of a top and bottom mat of reinforcing steel with bars running in both the transverse and longitudinal directions as also shown by Figure 3.2. The top and bottom transverse bars and the bottom longitudinal bars are all #5 bars. The top longitudinal bars are all #4 bars. The transverse bars are spaced at 6 in., and the longitudinal bars are spaced at 9 in. The clear cover was 1.25 in. and 2 in. to the bottom and top reinforcing mat, respectively.

The steel section used for each specimen is a WT6x39.5. This section was selected because the top flange width, top flange thickness, and web thickness of the WT6x39.5 very closely matches the top flange width, top flange thickness, and web thickness of the box girders on the FSEL test bridge.

The studs used in the test specimens had a diameter of 7/8 in. and a length of 5 in. These stud dimensions were selected to match the studs used in the FSEL test bridge.

The 3-in. haunch height, built into half of the specimens, was chosen because it matches the haunch height on the FSEL test bridge and because it is the largest allowed by TxDOT standard details. Standard TxDOT (and AASHTO) details require that the stud extend a minimum of 2 in. above the haunch into the slab. Thus, for 5-in. long studs, the maximum allowable haunch height is 3 in.

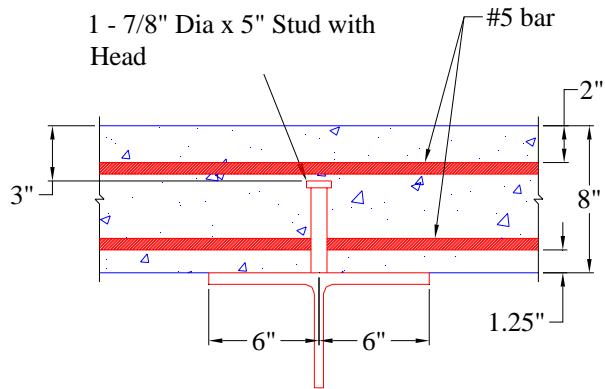
The number of studs was varied between one and three for each haunch height. The studs were grouped transversely across the WT section at the center of the longitudinal (2-ft) length. For the specimens with two studs, the studs were evenly spaced across the width of the top flange. For the specimens with three studs, the typical TxDOT detail was followed. The TxDOT detail for a group of three studs calls for a spacing of 2 in. between the center of the outer studs and the edge of the flange width.

The specimen identification, haunch height, and number of studs for each specimen are given in Table 3.1. Note that, for example, 0-1a and 0-1b refer to the duplicates of the 0-1 specimen, which has a 0-in. haunch height and 1 stud.

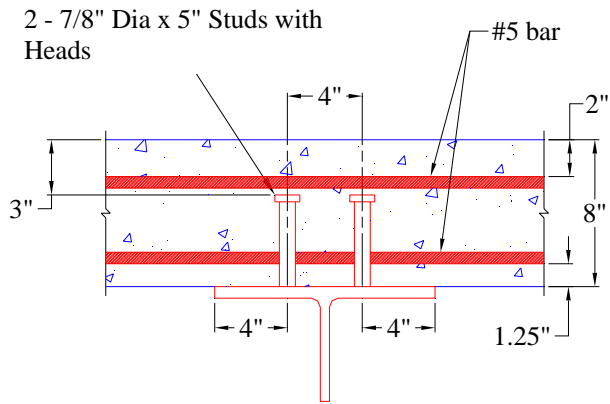
Table 3.1: Specimen identification and details

Specimen ID	Haunch Height (in.)	Number of Studs
0-1 a, b	0	1
0-2 a, b	0	2
0-3 a, b	0	3
3-1 a, b	3	1
3-2 a, b	3	2
3-3 a, b	3	3

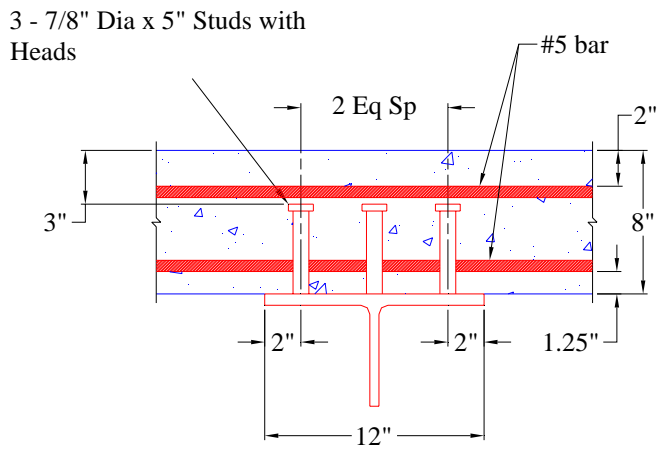
Figures 3.3 and 3.4 show the details of the specimens with no haunch and with a 3-in. haunch, respectively. These drawings show the details at the mid-span of each specimen where the studs connect to the slab. For clarity, these drawings only show the transverse deck reinforcement bars and not the longitudinal deck reinforcement bars.



(a) 0-1 a, b

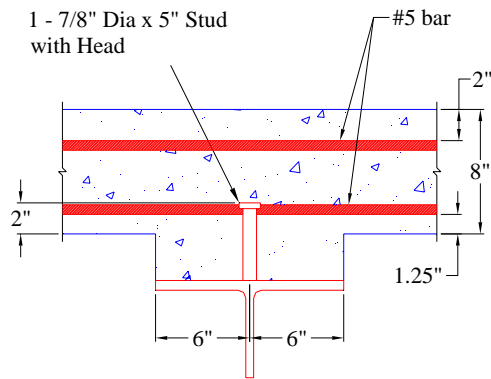


(b) 0-2 a, b

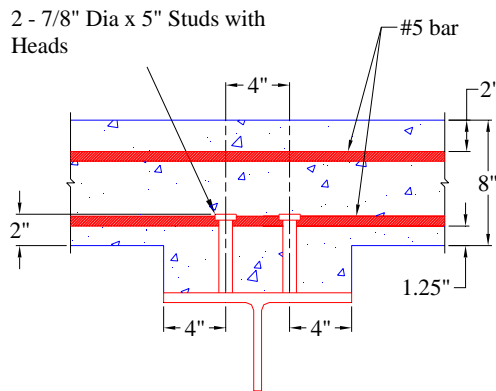


(c) 0-3 a, b

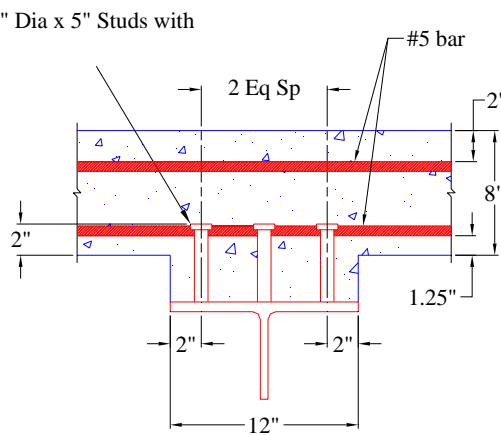
Figure 3.3: Details for specimens with no haunch



(a) 3-1 a, b



(b) 3-2 a, b



(c) 3-3 a, b

Figure 3.4: Details for specimens with 3-in. haunch

3.2.2 Stud Welding

The shear studs were welded to the WT sections using standard stud welding processes as shown in Figure 3.5 (a). This task was sub-contracted to a commercial stud welder in order to assure quality welds. The strength of the weld is required to be stronger than the strength of the stud. A simple way to test that the weld meets this requirement is to use a hammer to bend over the stud as shown in Figure 3.5 (b). If the weld fails before the stud bends over, then the weld is no good. However, if the stud bends over without failing at the weld, then the stud will reach its yield point before the weld will fail. A successful bend over test (Figure 3.5 (b)) was performed on a stud welded to a scrap WT section prior to welding the studs to the actual test specimens.

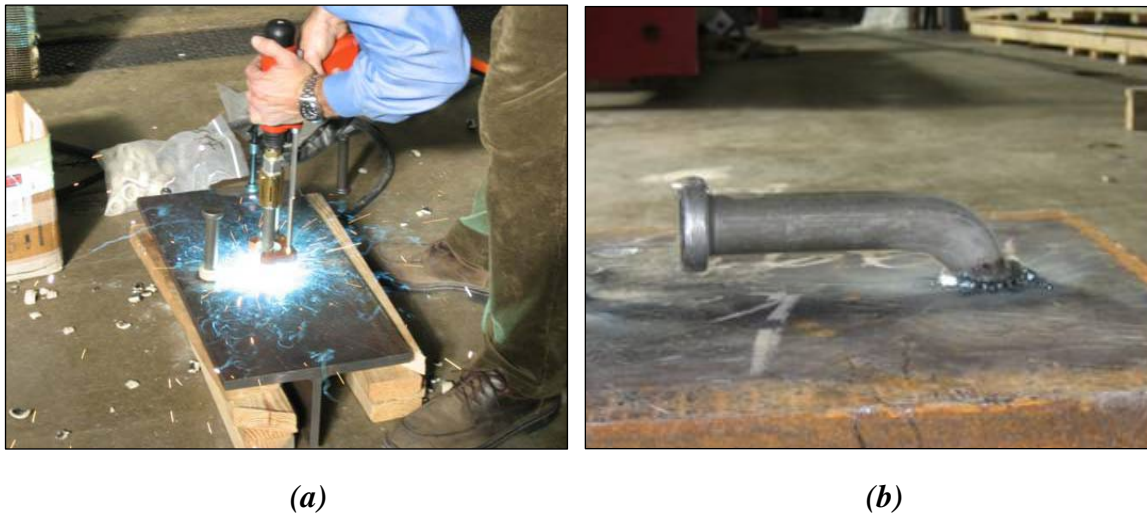


Figure 3.5: (a) Stud welding; (b) bend over test

3.2.3 Formwork

Formwork was constructed so that all 12 specimens could be cast at the same time. Two sets of forms were built, each with the capability of casting six specimens at a time. One set was built to provide a 3-in. haunch while the other set was built for the

specimens with no haunch. Figure 3.6 shows these two sets of forms after the WT sections have been put in place, but prior to the placement of the reinforcement cages.



(a)

(b)

Figure 3.6: Formwork for specimens with (a) no haunch (b) 3-in. haunch

3.2.4 Concrete Mix

The concrete mix used for the test specimens was the equivalent of TxDOT Class “S” Concrete. Class “S” Concrete is required to have a minimum compressive strength of 4,000 psi and a maximum water-to-cement ratio of 0.45. The size of the coarse aggregate in this mix ranges between 3/4 in. and 1-1/2 in.

During the casting of the specimens, concrete cylinders were cast in order to verify the strength of the concrete at various periods throughout the testing program. Testing did not begin until after the concrete had reached its 28-day strength. Cylinders were tested when the testing period began, half-way through the testing period, and after all testing was completed. These three testing dates corresponded to the 38-day strength, 49-day strength, and 59-day strength, respectively.

3.3 TEST SETUP

Each specimen was loaded as a simply supported slab with a point load in the center as shown in Figure 3.7. At each end, 6 in. of the 7-ft total specimen length rested on elastomeric bearing pads. Thus, the distance between the inside edge of the bearing pads was 6 ft. The reaction is assumed to be at the center of the bearing length so the span of each slab was actually 6 ft-6 in., which is 6 in. greater than the span length discussed in the previous section. However, this extra span length does not significantly change the behavior of the test specimens as it only increases the mid-span moment by approximately 8%. The bearing pads were placed 2 in. from the inside edge of the reaction blocks in order to permit as much rotation as possible during the test. A hydraulic ram was anchored to the strong floor directly under the center of the slab. A bolt hole was punched in the center of the web of the steel section of each specimen. Connector plates provided a pin connection between the WT and the clevis attached to the top of the hydraulic ram piston rod.

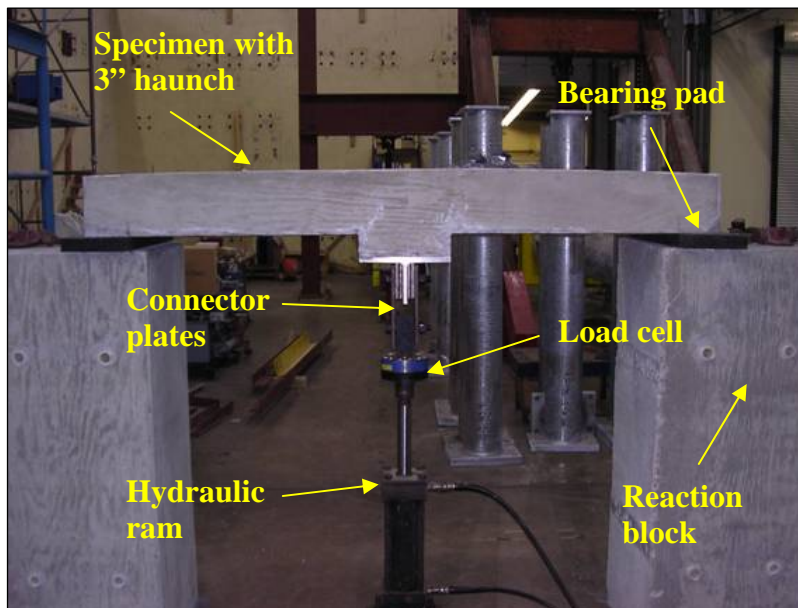


Figure 3.7: Test setup

3.4 INSTRUMENTATION

3.4.1 Shear Studs

Each of the shear studs was instrumented with a special purpose bolt gage. These gages are typically used to measure the tensile strain in a bolt, but in this case they have been installed in the shear studs to serve the same purpose. For the specimens with two or three studs, the results from the stud gages will provide the distribution of the tensile force among the studs.

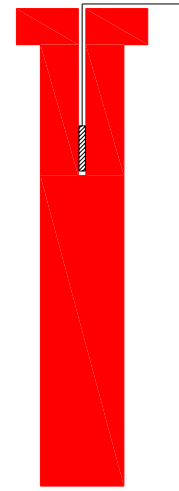
To install the bolt gages, a 2-mm-diameter hole is drilled in the center of the stud head. The hole must extend far enough into the shaft of the stud so that the gage can be placed below the stud head. During installation the drilled hole is filled with a high-strength bonding adhesive. The gage, which has a backing width of 1.7 mm, is then inserted into the hole. The adhesive is allowed to cure at room temperature for a period of 12 hours and then must be raised to an elevated temperature for additional curing. Figure 3.8 shows the installation of a stud gage and the typical placement of the gage in the stud.



Figure 3.8: (a) Stud gage installation



(b)



(c)

Figure 3.8 (cont.): (b) shear stud after gage installation; (c) drawing of typical stud gage placement

3.4.2 Reinforcing Steel

Each transverse reinforcing bar in both the top and bottom mat was instrumented with two general purpose foil gages. The gages were placed so that the location would correspond with the mid-span and the quarter-span of the slab. These gages measured the strain in the reinforcing steel, which can be used to determine the strain profile in the slab. These gages also show if the reinforcing steel in the slab begins to yield prior to a tension failure of the studs. Figure 3.9 shows the reinforcing cage in place in the forms with the gages installed. The yellow wrap around each gage is a protective coating tape that allows the gage to survive the casting of the concrete slabs without any damage.

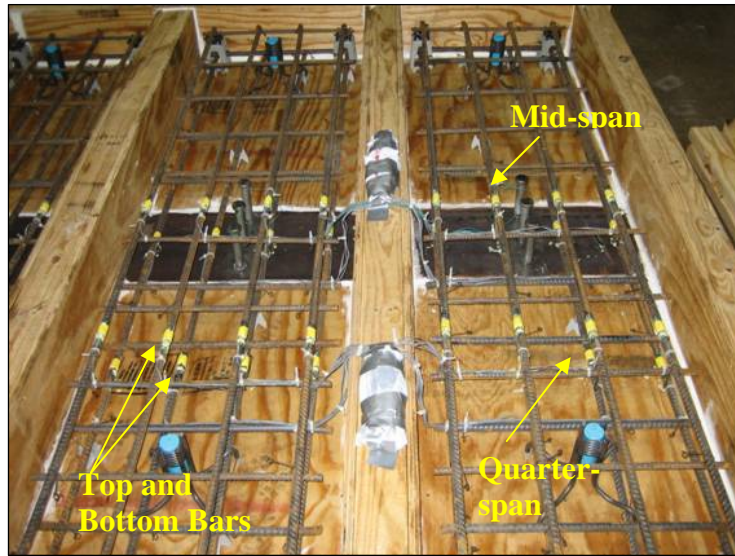


Figure 3.9: Instrumentation of reinforcing steel

Figure 3.10 shows a plan view of a typical slab with the labeling system used for the gages on the reinforcement bars. Gages numbered 1-4 are located at the quarter-span, and gages numbered 5-8 are located at the mid-span. The “T” and “B” suffixes refer to the gage on the top bar and the bottom bar, respectively. Longitudinal reinforcement bars are not shown in this figure.

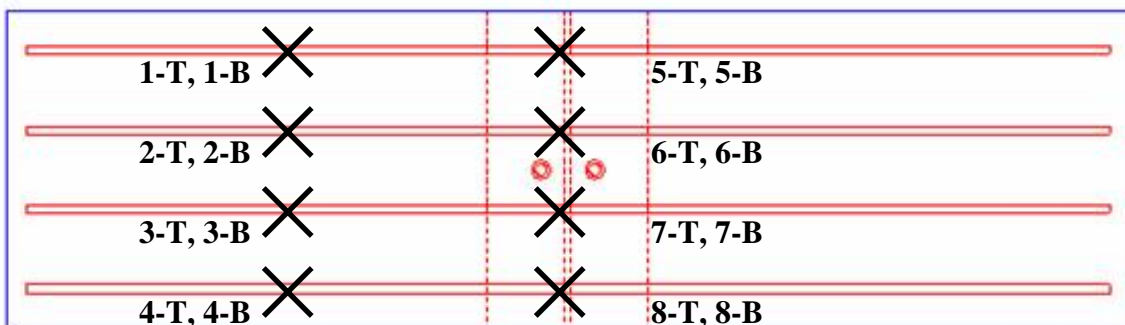


Figure 3.10: Labeling of gages on steel reinforcing bars

3.4.3 Load and Displacement

During each test the applied tensile force was measured with a load cell that was attached to the hydraulic ram. A threaded adaptor connected the piston rod to the bottom side of the load cell, and another threaded adaptor connected the top side of the load cell to the clevis. Figure 3.11 shows a close-up view of the attachment of the load cell to the hydraulic ram. At the other end, the connector plates attach to the hole punched in the web of the WT section.

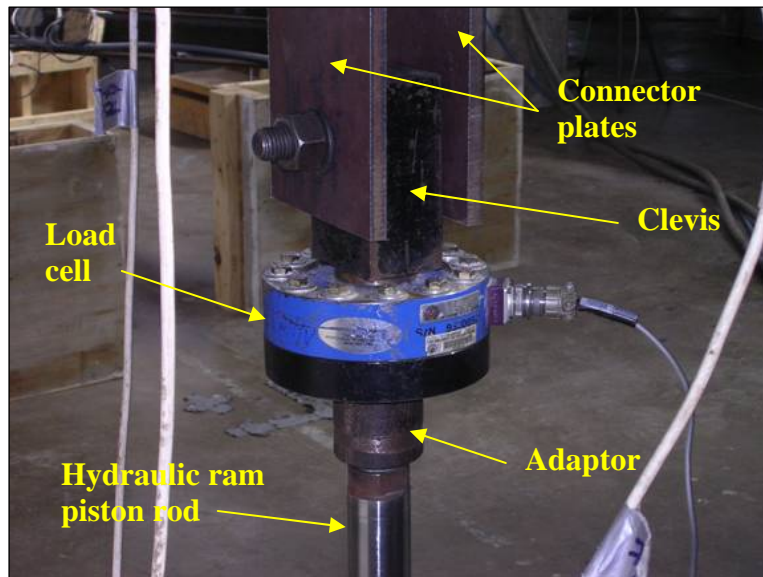


Figure 3.11: Attachment of load cell

Displacements were measured using three linear potentiometers. One linear potentiometer was used to measure the slab deflection at mid-span. Two other linear potentiometers were used to measure the separation of the WT top flange and the bottom of the slab. One was placed on each side of the slab, and the average of the two measured values was taken as the displacement of the stud pulling out of the slab. Figure 3.12 shows one of these linear potentiometers. The linear potentiometer is clamped to the

web of the steel section and it measures the relative displacement of the steel section from the top of the slab. The deformation includes the displacement of the bottom of the concrete relative to the top of the slab.

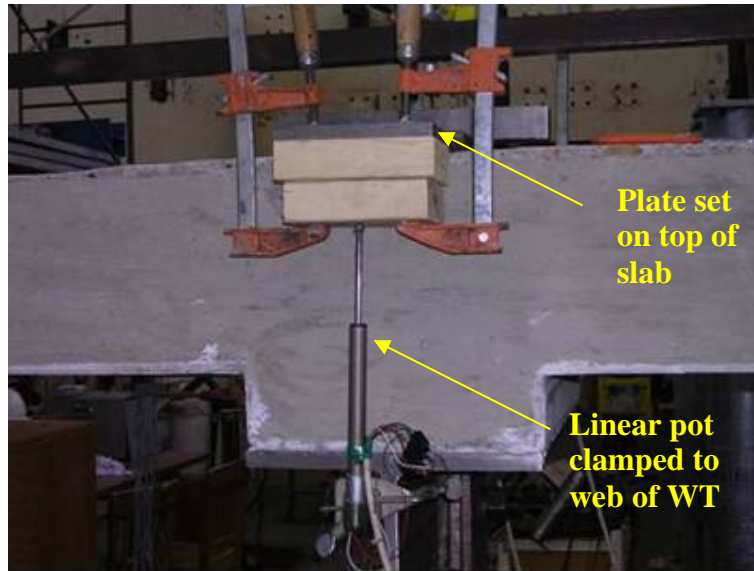


Figure 3.12: Linear potentiometer measuring separation between the slab and WT

3.5 TESTING PROCEDURE

Prior to a test, the hydraulic ram was extended and the connector plates were used to attach the ram to the WT section. At this point, all gages and instruments were zeroed, and the data acquisition system began recording the values measured by the instrumentation. Using an air-powered hydraulic pump to control the loading rate, the ram began to pull down on WT section, loading the studs in tension and creating a bending moment in the slab. Periodically, the loading was stopped to inspect the specimen and to map cracks in the concrete slab. The loading continued until the specimen failed as a result of a tension failure of the studs. Failure was assumed to have taken place when the specimen lost the ability to hold load. The tests did not continue

until the WT and studs completely pulled out of the concrete slab because there was concern that the hydraulic ram and other instrumentation might be damaged by such a failure. However, in general, the tests did not stop until specimens appeared to be very close to complete pullout of the studs. Figure 3.13 shows a picture of the test setup with the hydraulic pump and the data acquisition system visible.

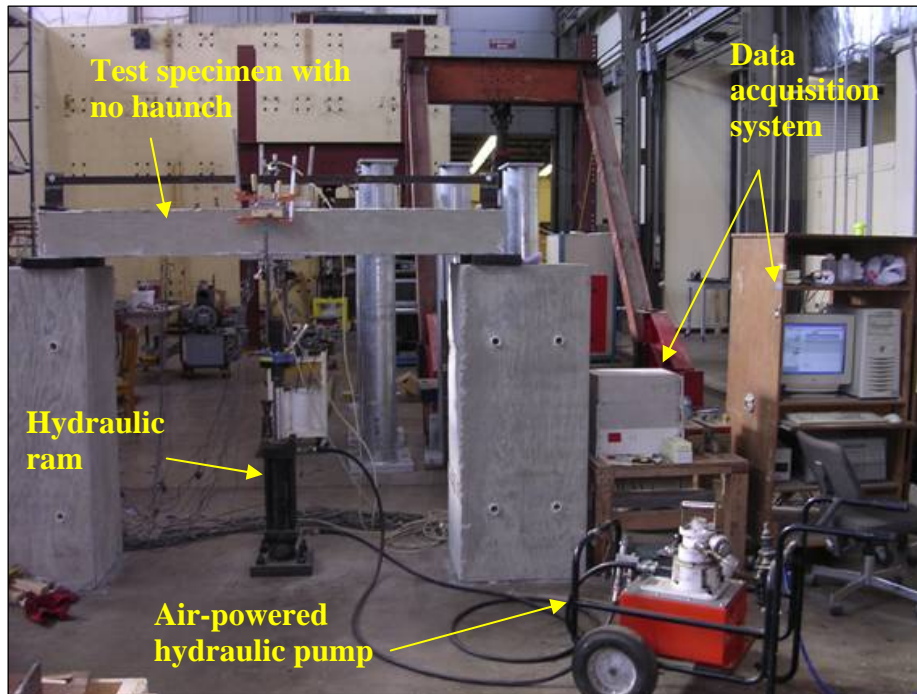


Figure 3.13: Test setup, hydraulic setup and data acquisition system

CHAPTER 4

Test Results

4.1 GENERAL COMMENTS

All specimens experienced a tension failure by concrete breakout. In each test, the slab did not experience much plastic deformation, and thus it can be presumed that there was reserve flexural capacity in the slab remaining at the time of the failure. All of the A-specimens were tested first, and then the B-specimens were tested in the same order. With one exception, the B-specimens reached a slightly higher capacity than the corresponding A-specimens. This outcome is attributed to the fact that the concrete strength increased slightly over the testing period. Table 4.1 shows the testing order and the test date of the specimens.

Table 4.1: Testing order

Specimen	Test Date
3-1 a	25-Jan-07
3-2 a	26-Jan-07
3-3 a	30-Jan-07
0-1 a	30-Jan-07
0-2 a	01-Feb-07
0-3 a	02-Feb-07
3-1 b	06-Feb-07
3-2 b	08-Feb-07
3-3 b	08-Feb-07
0-1 b	13-Feb-07
0-2 b	13-Feb-07
0-3 b	15-Feb-07

4.2 CAPACITY

The maximum load carried by each specimen is shown in Table 4.2. As predicted by the ACI equations, the specimens with a 3-in. haunch lost capacity as the number of studs in the row increased. The reduction of strength is related to the distance of a stud to an edge. The reduction for a stud located very close to an edge is greater than the reduction of a stud located farther away from the edge. The specimens with only one stud resisted the largest load prior to failure because the distance to the edge of the haunch was largest in these specimens. The specimens with three studs had a reduced distance between the outside studs and the edge of the haunch, and so those specimens carried the lowest load.

The specimens with no haunch were able to develop the full volume of the concrete breakout prism and thus did not suffer any reduction in strength. Adding studs increased the volume of the breakout prism, and the specimens experienced an increase in strength as the number of studs in the row increased.

Table 4.2: Maximum load resisted by each specimen

Specimen			Maximum Load (kip)	Average Maximum Load (kip)
3" Haunch	1 stud	A	23.4	22.3
		B	21.2	
	2 studs	A	18.5	19.2
		B	19.9	
	3 studs	A	16.4	17.3
		B	18.2	
No Haunch	1 stud	A	20.4	20.9
		B	21.3	
	2 studs	A	23.8	24.6
		B	25.3	
	3 studs	A	25.6	25.9
		B	26.2	

The results in Table 4.2 show that the presence of a haunch can significantly reduce the tensile capacity of a group of studs. For the specimens with only one stud, the breakout capacity with a haunch and without a haunch is very close. In this case, the specimens with a haunch actually reached slightly higher average maximum load than the specimens without a haunch. However, the strengths of the two-stud and three-stud specimens without a haunch were considerably higher than the two-stud and three-stud specimens with a haunch.

The 3-in. haunch specimens with two and three studs show a large drop in the breakout capacity when compared to the specimens with a haunch and only one stud. The average capacity dropped 14% for the specimens with two studs and 23% for the specimens with three studs. Conversely, the specimens without a haunch showed an increase in strength when the number of studs was increased. However, the increase in tensile strength is small, less than 25% for the three stud test versus the single stud test.

4.3 BEHAVIOR AT FAILURE

4.3.1 Specimens with a Haunch

Each specimen with a 3-in. haunch failed in a very sudden, brittle manner and exhibited very little ductility. These specimens reached a maximum load, failed suddenly, and immediately lost all ability to carry load. Figure 4.1 shows a plot of the applied load versus the stud pullout deflection for a specimen with one stud. The plot shows that the specimen reaches a maximum load and then fails very suddenly with the next data point down near 0 kip. This plot is typical of all of the specimens with a 3-in. haunch.

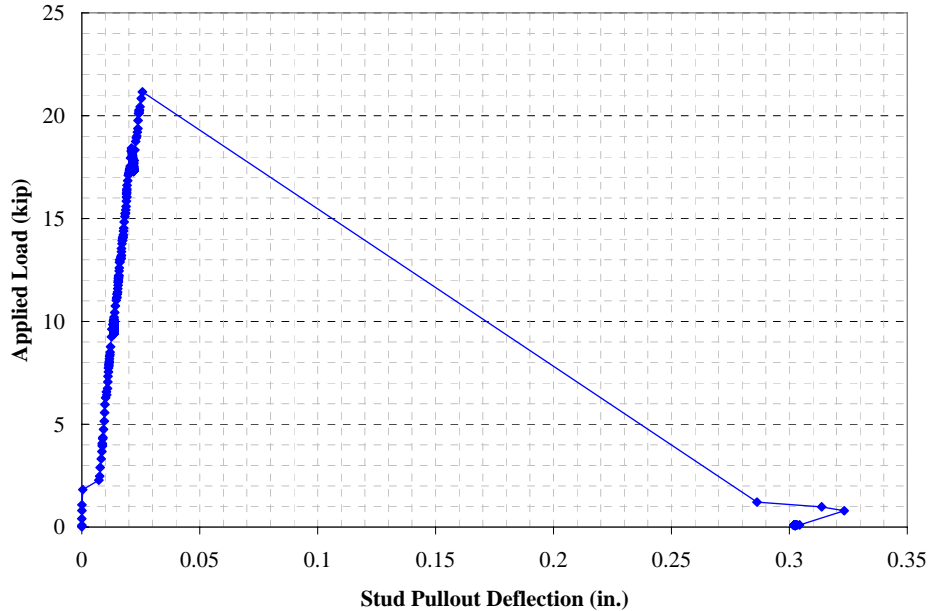


Figure 4.1: Specimen 3-1b – Applied load versus stud pullout deflection

Each of the specimens with a haunch behaved and failed in a very similar manner. Flexural cracking occurred early in each test with the first flexural cracks forming on both sides of the haunch, where the top of the haunch and the bottom of the slab meet as shown in Figure 4.2. The specimens with one stud had the most flexural cracking while the specimens with three studs saw the least amount flexural cracking. This behavior is due to the fact that the specimens with one stud failed at the highest load, while the specimens with three studs failed at the lowest load. Flexural cracks did not occur in the haunch region in any of the specimens with a 3-in. haunch. This result is attributed to the increased slab thickness, and thus moment of inertia, in that area.

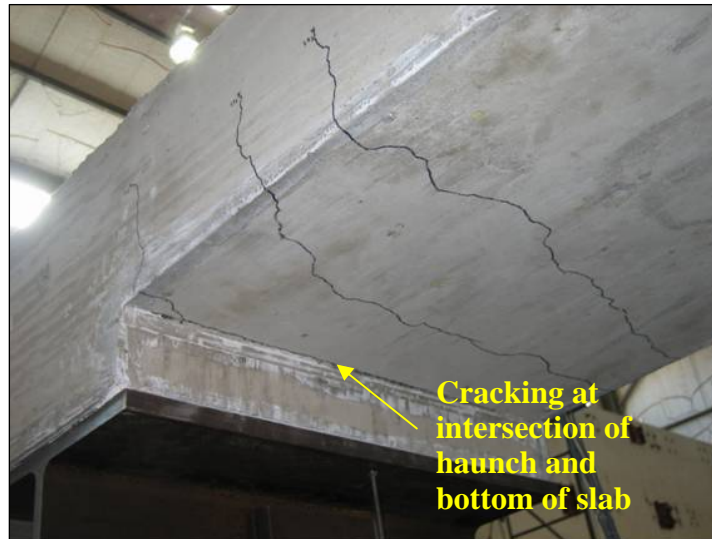
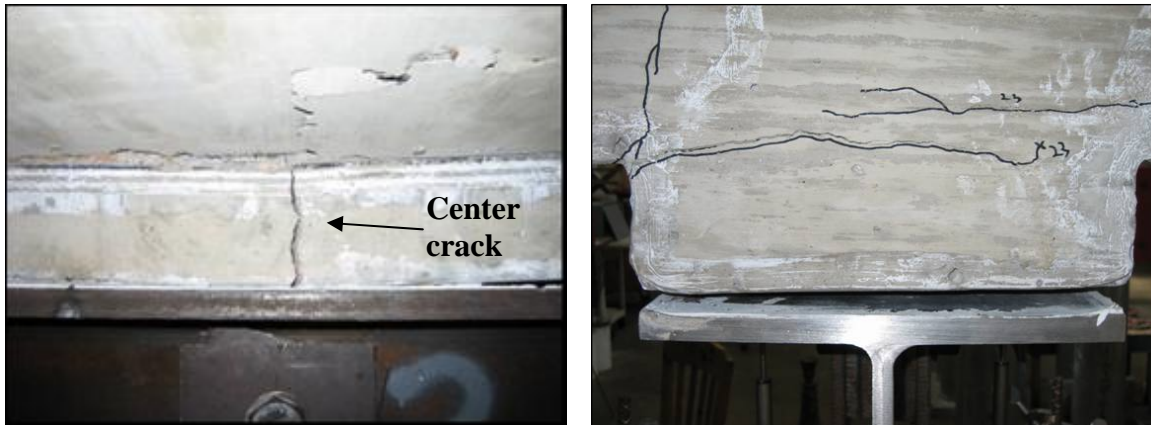


Figure 4.2: Initial cracking in specimen with a 3-in. haunch

At failure, a large crack opened at the center of the haunch, even with the row of studs, and split the haunch in two as shown in Figure 4.3 (a). The two cracks at the intersection of the bottom of the slab and top of the haunch also expanded horizontally, as shown in Figure 4.3 (b). Figure 4.3 (c) shows a specimen with two studs, in which the haunch region and studs completely separated from the bottom of the slab. Notice in this photograph that the haunch concrete is plain concrete. No reinforcing steel runs through the haunch, which is why the failure of the specimens with no haunch is a sudden, brittle failure.



(a)

(b)



(c)

Figure 4.3: Specimens with a 3-in. haunch – (a) Center crack at failure; (b) horizontal cracking across top of haunch; (c) complete separation of haunch

4.3.2 Specimens with No Haunch

The specimens with no haunch experienced some ductility at failure because reinforcing bars run through the concrete breakout prism. Rather than reaching a maximum load and losing all load carrying ability, the specimens with no haunch gradually softened after reaching their maximum load. After the specimens reached the maximum load, the stud slowly began to pull out of the slab. The stud gradually lost load

as the pullout deflection increased. Figure 4.4 demonstrates the gradual loss of load carrying capability for one of the specimens with three studs. This trend was seen in all of the specimens with no haunch.

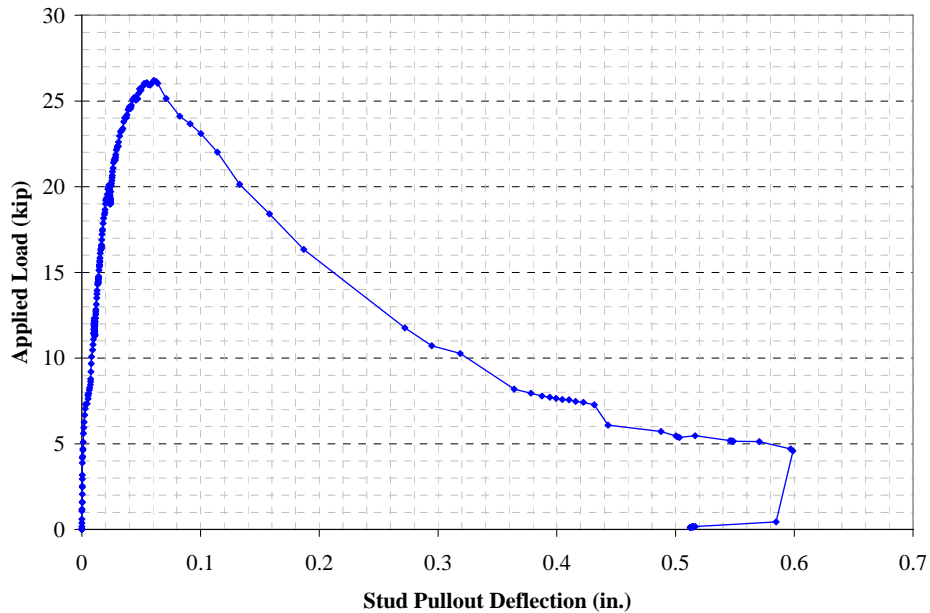
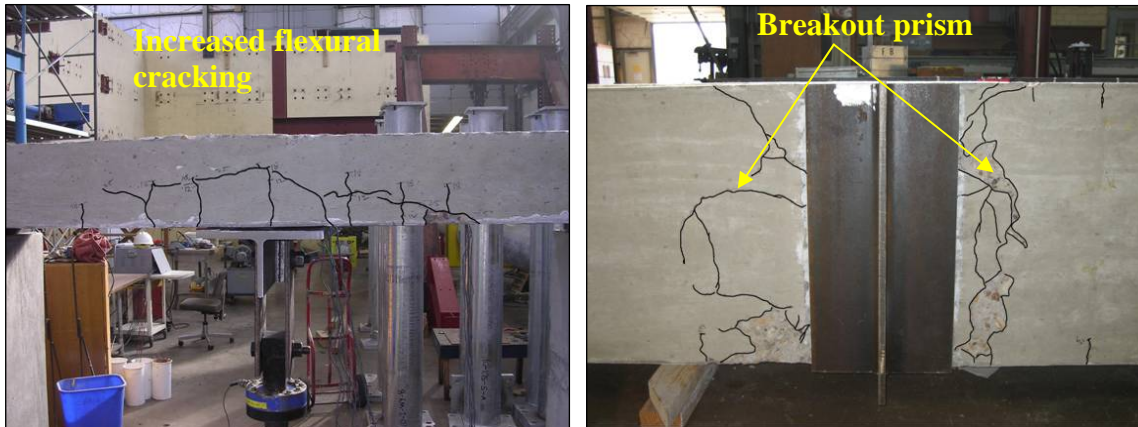


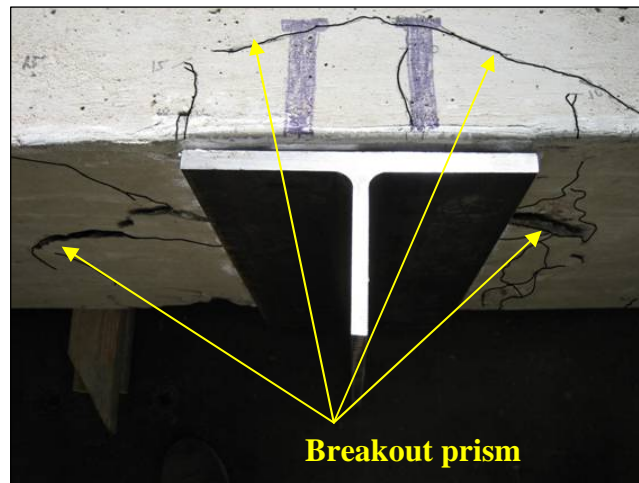
Figure 4.4: Specimen 0-3b – Applied load versus stud pullout deflection

The specimens with no haunch displayed cracking more consistent with the theoretical prism breakout failure mechanism. In addition, flexural cracking in the slab was more prevalent in the specimens with no haunch. The ductility at failure was due to the reinforcement bars providing some confinement as the breakout prism formed. The ductility at failure was not a result of plastic deformations of the deck slab, as there was not much evidence of plastic deformation of the deck slab during any of the tests. The response of the deck slab is discussed further in Section 4.5 and 4.6. Figure 4.5 depicts the increased amount of flexural cracking and the cracking consistent with the breakout failure mechanism.



(a)

(b)



(c)

Figure 4.5: Specimens with no haunch – (a) Increased flexural cracking; (b) breakout prism cracking as seen from underside of specimen; (c) formation of breakout prism

4.4 STUD GAGE DATA

4.4.1 Analysis of Data

The data recorded by the stud gages can be used to show the distribution of the applied tensile force among the shear studs. The specimens with only one stud can be used as a control because in these cases the tension force in the stud should be equal to

the applied tensile force measured by the load cell. In the specimens with multiple studs, the summation of the forces in each stud should be equal to the applied tensile force. In order to determine the stress in each stud, the strain recorded by the stud gage is multiplied by the modulus of elasticity of steel (29,000 ksi). That value of stress is then multiplied by the cross-sectional area of the stud to determine the tensile force present in the stud. Once the force in each stud is determined, the sum of the forces in each of the studs in the row can be obtained. If the gages are measuring the strains accurately, this summation should correspond fairly well to the applied force measured by the load cell.

4.4.2 Specimens with a Haunch

Table 4.3 shows the stud forces calculated at maximum load for the specimens with a 3-in. haunch. Note that the left stud of Specimen 3-2a and the right stud of Specimen 3-3a are shown in bold. These gages did not function properly during their respective tests. The force in these studs was set equal to the symmetrical stud in the specimen. This assumption was based on the symmetrical behavior of the replicate B-specimens.

Table 4.3: Stud gage data at maximum load for specimens with a 3-in. haunch

Specimen	Stud Location	Strain (in/in)	Stress (ksi)	% of Yield Stress	Force (kip)	Sum of Forces (kip)	Actual Force (kip)	% Difference
3-1 a	Center	0.001250	36.3	72.5	21.8	21.8	23.4	-6.8
3-1 b	Center	0.001238	35.9	71.8	21.6	21.6	21.2	1.8
3-2 a	Right	0.000485	14.1	28.1	8.5	16.9	18.5	-8.6
	Left	0.000485	14.1	28.1	8.5			
3-2 b	Right	0.000490	14.2	28.4	8.5	16.7	19.9	-16.3
	Left	0.000465	13.5	27.0	8.1			
3-3 a	Right	0.000214	6.2	12.4	3.7	14.8	16.4	-9.9
	Center	0.000419	12.2	24.3	7.3			
	Left	0.000214	6.2	12.4	3.7			
3-3 b	Right	0.000208	6.0	12.1	3.6	15.9	18.2	-12.7
	Center	0.000466	13.5	27.0	8.1			
	Left	0.000237	6.9	13.7	4.1			

This table shows that the stud forces calculated from the strain gages agreed fairly well with the applied force. With one exception, the sum of the stud forces is less than the total applied force. Recall that the stud gage is located just under the stud head as shown in Figure 4.6. The majority of the tensile force resisted by the stud is due to the stud head bearing on the concrete; however, some force may be resisted by friction between the stud shaft and the concrete as shown in Figure 4.6. The majority of this friction resistance would develop below the location of the gage, which may explain why the summation of the calculated stud forces tended to be slightly lower than the total applied force measured by the load cell.

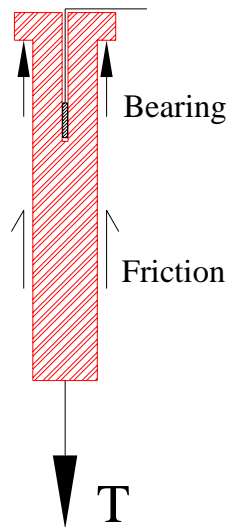


Figure 4.6: Tensile resistance provided by shear stud

In addition, Table 4.3 shows that the studs do not experience large stresses. With the exception of the specimens with only one stud, the stress in the studs was less than 30% of the specified yield stress, 50 ksi. The specimens with one stud experienced stresses that are 70-75% of the yield stress.

The table shows that the specimens with two studs exhibit an even distribution of the tensile force between the studs. Figure 4.7 shows a plot of the total load versus the

calculated force in the studs for Specimen 3-2b, which has a 3-in. haunch and two studs. The force in each of the two studs is nearly identical throughout the entire test up until failure.

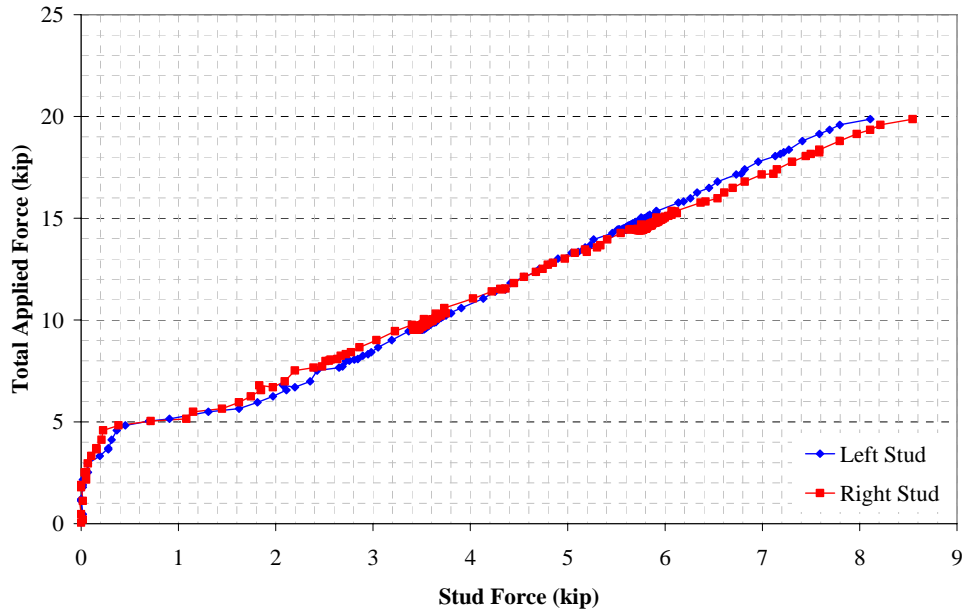


Figure 4.7: Specimen 3-2b – Applied load versus calculated force in the shear studs

The stud gages in the specimens with three studs showed that approximately half of the applied tensile force is resisted by the center stud and that the remaining half is equally distributed between the two outer studs. Figure 4.8 shows a plot of the applied load versus the calculated force in the studs for a specimen with three studs. This plot shows that the force in the three studs is fairly uniform until approximately 7 kips, after which the center stud begins to resist a very large portion of the applied load. This point represents the cracking load of the slab (See Section 4.5.1). The slab cracks first at the haunch edges, which is very close to the outside studs. The slab did not crack inside the haunch region. Therefore, the center stud begins to resist more force after cracking

because the concrete around it has not cracked. The outer studs start resisting less force because cracking has occurred and the breakout prism begins to form near these studs.

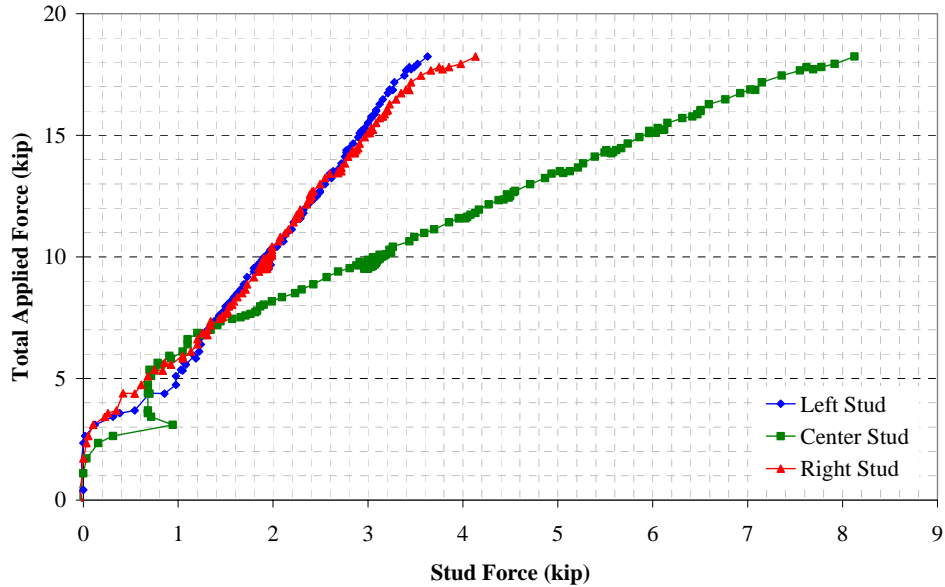


Figure 4.8: Specimen 3-3b – Applied load versus calculated force in the shear studs

4.4.3 Specimens with No Haunch

Table 4.4 shows the calculated stud forces for the specimens with no haunch. This table is additional confirmation that the stud gages are working very well. The percent difference between the sum of the calculated forces in the studs and the actual applied force measured by the load cell is less than 10% for all but one of the specimens. This table also shows that the studs in the specimens with no haunch experience larger stresses. However, the stresses in the studs are still less than 50% of the yield stress for the specimens with two and three studs, and less than 70% of the yield stress for the specimens with one stud.

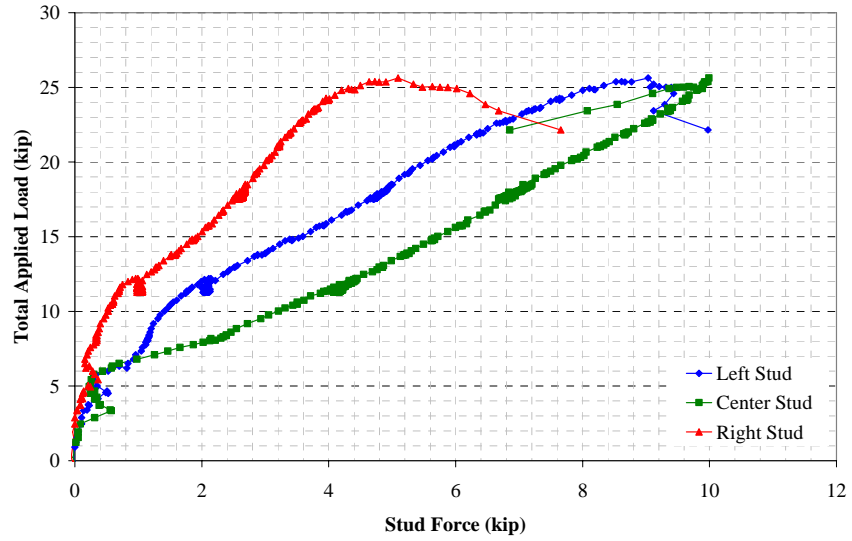
Table 4.4: Stud gage data at maximum load for specimens with no haunch

Specimen	Stud Location	Strain (in/in)	Stress (ksi)	% of Yield Stress	Force (k)	Sum of Forces (k)	Actual Force (k)	% Difference
0-1 a	Center	0.001180	34.2	68.4	20.6	20.6	20.4	0.9
0-1 b	Center	0.001113	32.3	64.6	19.4	19.4	21.3	-8.9
0-2 a	Right	0.000657	19.1	38.1	11.5	26.4	23.8	11.0
	Left	0.000858	24.9	49.8	15.0			
0-2 b	Right	0.000624	18.1	36.2	10.9	23.1	25.3	-8.9
	Left	0.000698	20.2	40.5	12.2			
0-3 a	Right	0.000292	8.5	16.9	5.1	24.1	25.6	-5.8
	Center	0.000573	16.6	33.2	10.0			
	Left	0.000518	15.0	30.0	9.0			
0-3 b	Right	0.000286	8.3	16.6	5.0	24.7	26.2	-5.6
	Center	0.000662	19.2	38.4	11.5			
	Left	0.000471	13.7	27.3	8.2			

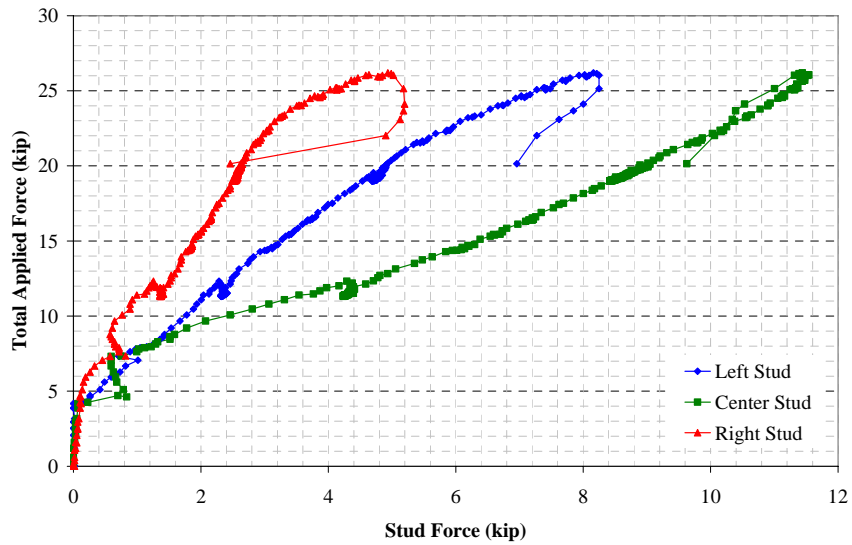
This table also shows that, for the specimens with two studs, the tensile force is fairly equally distributed between the studs as it was in the specimens with two studs and a 3-in. haunch. For the specimens with three studs, slightly less than half of the force is resisted by the center stud. The specimens without a haunch were cracked at the mid-span, which was not the case for the specimens with a 3-in. haunch. However, the center stud still resists the largest portion of the force because the breakout prism begins to develop first around the outer studs. While the largest portion of the force is resisted by the center stud, the remainder of the force does not appear to be evenly distributed between the two outer studs as it was in the specimens with the 3-in. haunch. In both specimens, one of these outer studs resists a larger portion of the force than the other outer stud.

The load versus calculated stud force for the two specimens with no haunch and three studs is shown in Figure 4.9. The figure shows that in both cases the center stud resists the most force. The two outer studs are experiencing an unequal distribution of the remaining force. The unloading part of the curves is cut off at approximately 20 kips

for both plots because the gage wires break as the studs pull out of the concrete. Figure 4.9 (a) shows that the right and left studs pick up additional load as the force in the center stud drops off during the breakout failure.



(a)



(b)

Figure 4.9: Applied load versus calculated force in the shear studs – (a) Specimen 0-3a; (b) Specimen 0-3b

4.5 REINFORCING STEEL GAGE DATA

4.5.1 Concrete Slab – Cracking, Yielding, and Ultimate Loads

The data obtained from the strain gages on the reinforcing steel show how the slab is behaving during each test. The three important stages of each test, in terms of the concrete slab, are the loads that correspond to cracking, yielding, and ultimate. The loads corresponding to each of these points was calculated in order to see if the actual behavior matched the assumed behavior.

Each slab was simply supported, and the ram pulled down on the WT section, loading the studs in tension and the slab in bending. Therefore, it can be assumed that each specimen is a simply supported slab with a point load at mid-span. From simple statics, the moment at the mid-span and the quarter-span is equal to $PL/4$ and $PL/8$, respectively, where P is the applied tensile force and L is the span length of the slab. Using this relationship between applied load and moment, the expected cracking load, yield load, and ultimate load can be determined.

The calculation of the cracking moment, yield moment, and ultimate moment was based on a concrete strength of 6 ksi, steel reinforcement yield strength of 60 ksi, and a slab thickness of 8 in. This concrete strength was used because it corresponds to the strength of the concrete cylinders halfway through the testing period (See Section 4.7). A tension test on a reinforcement bar also confirmed that 60 ksi was an acceptable value to use for the yield strength of the reinforcement. The extra depth in the haunch region was not included in these calculations, and the calculations also assumed that the applied force was uniformly distributed throughout the width of the slab. See Appendix D for actual calculations of each value.

The tensile strength of the concrete in flexure was assumed to be 7.5 times the square root of the compressive strength of the concrete (ACI 318-05). The cracking moment can then be found using the following equation:

$$M_{cr} = \frac{\sigma_{cr} I}{c} = \frac{7.5 \sqrt{f'_c} I}{c} \quad \text{Equation 4.1}$$

where:

- M_{cr} = cracking moment (lb-in.)
- σ_{cr} = tensile strength of concrete (= 581 psi)
- I = gross moment of inertia of the slab (= 1024 in.⁴)
- c = distance from centroidal axis to extreme fibers in tension (= 4 in.)
- f'_c = concrete compressive strength (= 6,000 psi)

Once the cracking moment is determined, the corresponding cracking load can be calculated. The cracking load was calculated to be approximately 7.6 kips for the specimens with no haunch. For the specimens with a 3-in. haunch, it was assumed that the slab would crack first at the edges of the haunch where the slab thickness returns to 8 in. These points are about 6 in. away from the mid-span; therefore, it takes a slightly higher applied force to generate the cracking moment. The cracking load for the specimens with the 3-in. haunch was calculated to be approximately 9 kips.

The next point that was calculated was the moment to cause yielding in the bottom reinforcement bars. Before cracking, the neutral axis is located at the mid-height of the slab, but, after cracking, the neutral axis shifts up. Figure 4.10 shows the assumed position of the neutral axis at the time of yielding. The term kd refers to the depth of the neutral axis. Above this point, the concrete is under compression, and below this point, the steel is assumed to resist all of the tension. Prior to cracking, the top layer of reinforcement was under compression, but after cracking the top layer begins to see tensile forces.

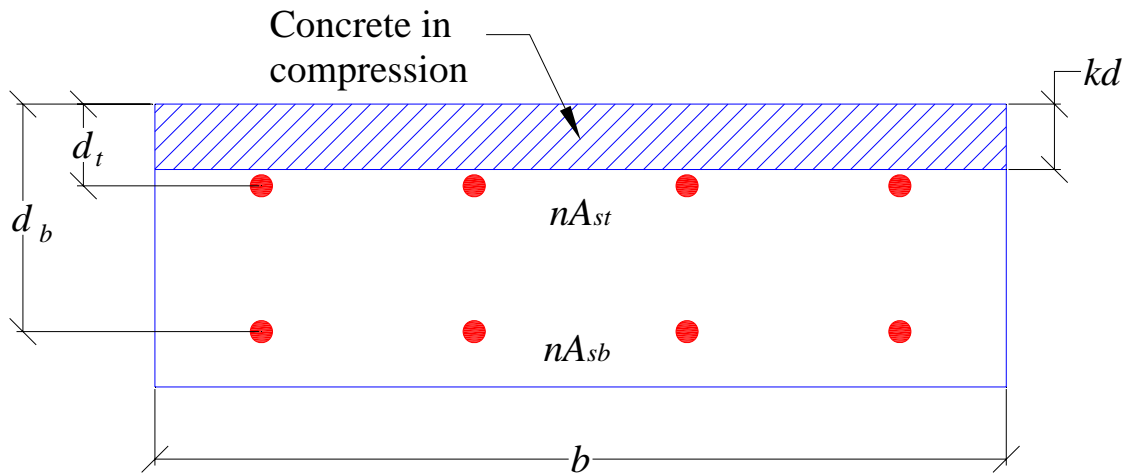


Figure 4.10: Assumed location of neutral axis at yield of bottom reinforcement

By setting the first moment of area of the concrete compression block and the first moment of area of the steel reinforcement equal to each other, the depth of the neutral axis can be determined. The equation below is the result of this technique:

$$b(kd)\left(\frac{kd}{2}\right) = nA_{sb}(d_b - kd) + nA_{st}(d_t - kd) \quad \text{Equation 4.2}$$

- where:
- kd = depth of compressive block (in.)
 - b = width of slab (= 24 in.)
 - n = ratio of steel modulus to concrete modulus (= 6.6)
 - A_{sb} = area of bottom reinforcement steel (= 1.23 in.²)
 - d_b = depth to center of bottom reinforcement steel (= 6.44 in.)
 - A_{st} = area of top reinforcement steel (= 1.23 in.²)
 - d_t = depth to center of top reinforcement steel (= 2.31 in.)

Once the depth of the neutral axis is known, the strain in the top layer of steel and the top concrete strain can be calculated using similar triangles. The strain in the bottom layer of steel is set to the yield strain, which is approximately 0.00207 in./in. for 60 ksi

steel. Using the strain profile, the stress profile can be determined. The concrete stress is assumed to be linear, which will be an acceptable assumption as long as $f_c < 0.7f_c'$. Figure 4.11 shows the assumed strain profile and stress profile at the point of first yielding. At this point, the compressive force and the tensile forces can be calculated, and the yield moment can be determined by taking the summation of moments about the centroid. The yield moment of these specimens was calculated to be approximately 37 kip-ft, which corresponds to an applied force of 23 kips.

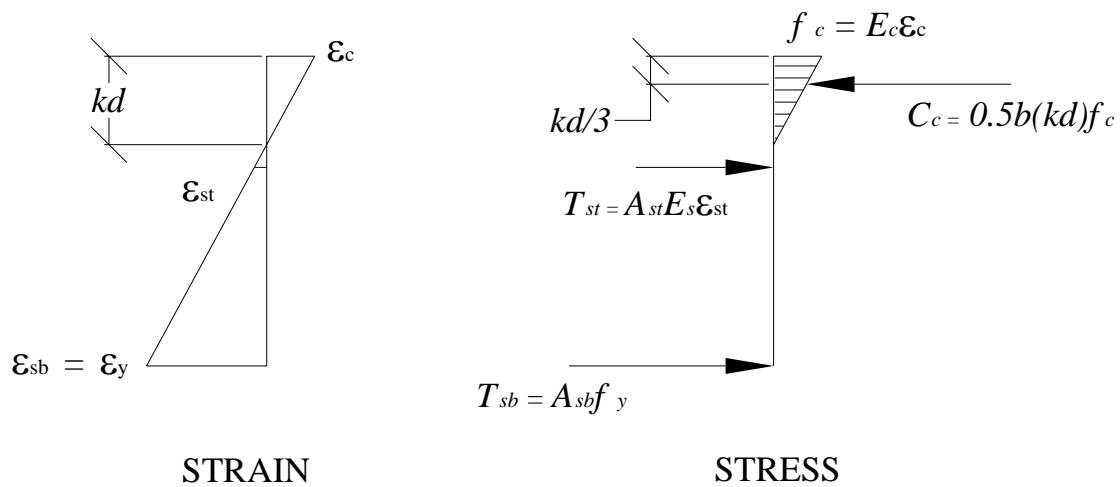


Figure 4.11: Strain and stress profiles at point of yield

Finally, the ultimate moment of the slab was calculated. At ultimate, the strain in the bottom reinforcement is greater than the yield strain and the top concrete strain is assumed to be 0.003 in./in (ACI 318-05). The concrete stress is assumed to be a rectangular stress block with magnitude of $0.85f_c'$ and depth of β_1c (ACI 318-05). Figure 4.12 shows the assumed strain profile and stress profile at the point of ultimate moment. The compressive force is set equal to the sum of the tensile forces, and iterations are performed to solve for the neutral axis depth. Once this depth is calculated, the forces can be calculated, and then the ultimate moment is found by taking the summation of

moments about the centroid. The ultimate moment was found to be approximately 45 kip-ft, which corresponds to an applied force of 28 kips. As mentioned in Section 4.1, all of the specimens experienced a tension failure by concrete breakout prior to reaching the ultimate moment capacity of the deck slab. The largest load that any of the specimens resisted was approximately 26 kips, which is above the yield load but below the predicted ultimate load. It is also important to note that the ultimate moment capacity may actually be greater than 45 kip-ft. The calculations of the ultimate moment assume that concrete crushing will occur at a strain of 0.003 in./in.; however, tests have shown that the crushing strain can be higher than 0.003 in./in. (ACI 318-05). Therefore, the predicted ultimate load is expected to be a conservative prediction.

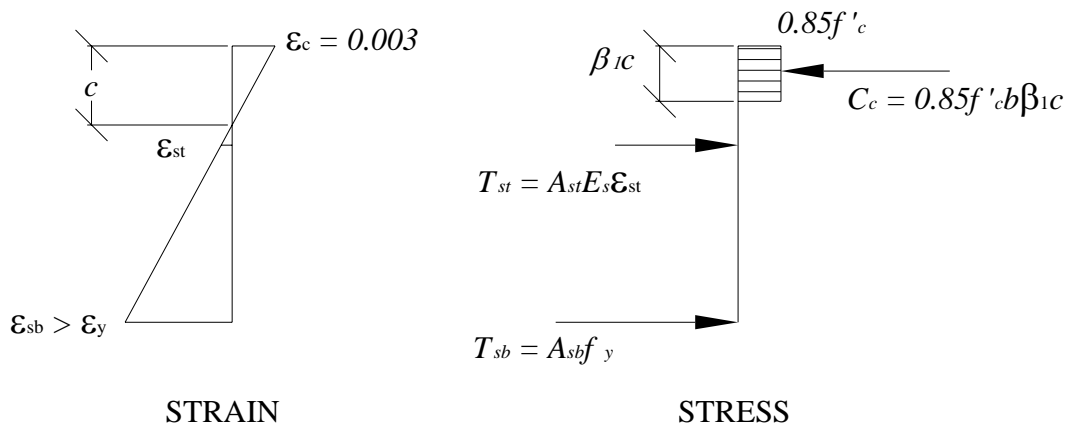


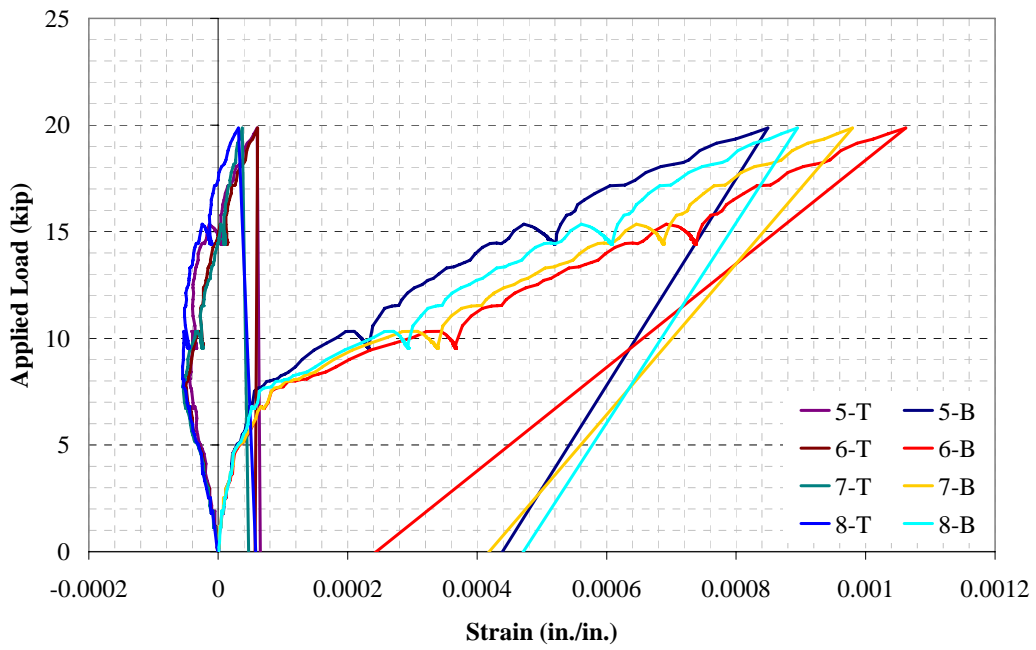
Figure 4.12: Strain and stress profile at ultimate

4.5.2 Specimens with a Haunch

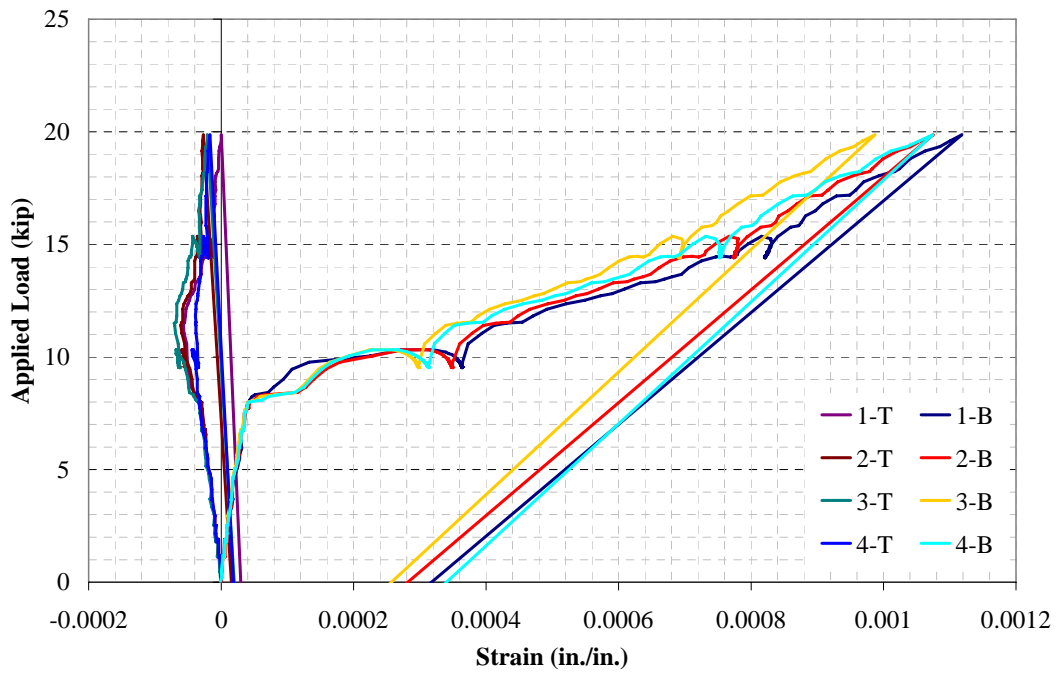
The gages on the slab reinforcement indicated that no yielding took place during any of the tests of the specimens with a 3-in. haunch. The predicted yield load for the slab was 23 kips, and only one of the specimens with a haunch reached that point. Therefore, it is expected that the reinforcement remained elastic. However, the strain in the bottom bars at the mid-span location appears to be lower than expected. The strain

gage data showed that the strain in the bottom bars was about the same at the mid-span and the quarter-span locations in all of the specimens with a haunch as seen in Figure 4.13. This result is not expected because the moment at the quarter-span is only half of the moment at the mid-span. It seems, however, that the increased depth in the haunch region has provided some help and has slightly reduced the strains in the bottom bars at the mid-span.

The strains in the top reinforcing bars are also essentially equal at both locations as shown in Figure 4.13. In each location the strains are very close to zero at the time of failure. At the mid-span location, the top bars are experiencing tensile strains very close to zero at the time of failure. However, at the quarter-span location, the top bars are still under compressive strains at the time of failure, which are also very close to zero. Figure 4.13 shows the load versus strain plots at both the mid-span and quarter-span locations of Specimen 3-2b. These plots are fairly typical of all the specimens with a 3-in. haunch. Recall (from Figure 3.10) that the gages numbered 1-4 are located at the quarter-span, and the gages numbered 5-8 are located at the mid-span. The suffixes “T” and “B” refer to the top and bottom bars, respectively.



(a)



(b)

Figure 4.13: Specimen 3-2b – Reinforcing steel load versus strain at the (a) mid-span location (b) quarter-span location

Initially the slope of the load versus strain curves is very steep, but around 8 kips the slope decreases drastically. This point represents the cracking load, which is very close to the predicted cracking load of 9 kips for the specimens with a haunch. After cracking, the section becomes much less stiff, and the strain increases at a faster rate. These plots also show that the top bars start off in compression (represented by a negative strain), but after cracking they go into tension as the neutral axis shifts upwards.

4.5.3 Specimens with No Haunch

For the specimens with no haunch, the gages on the reinforcement indicated that yielding of the bottom bars at the mid-span occurred in all specimens. The predicted yield load for these specimens was about 23 kips, but, based upon the strain gage readings, all of the bottom reinforcement reached the yield strain even though only four of the six specimens resisted a load greater than 23 kips. However, the strain in these bars was typically just barely above the yield strain at the time of the breakout failure. The strains were not large enough in any of these specimens to produce noticeable plastic deformation of the slab. Figure 4.14 shows a typical load versus strain plot for a specimen with no haunch in which all of the bottom bars have reached the theoretical yield strain of 0.00207 in./in.

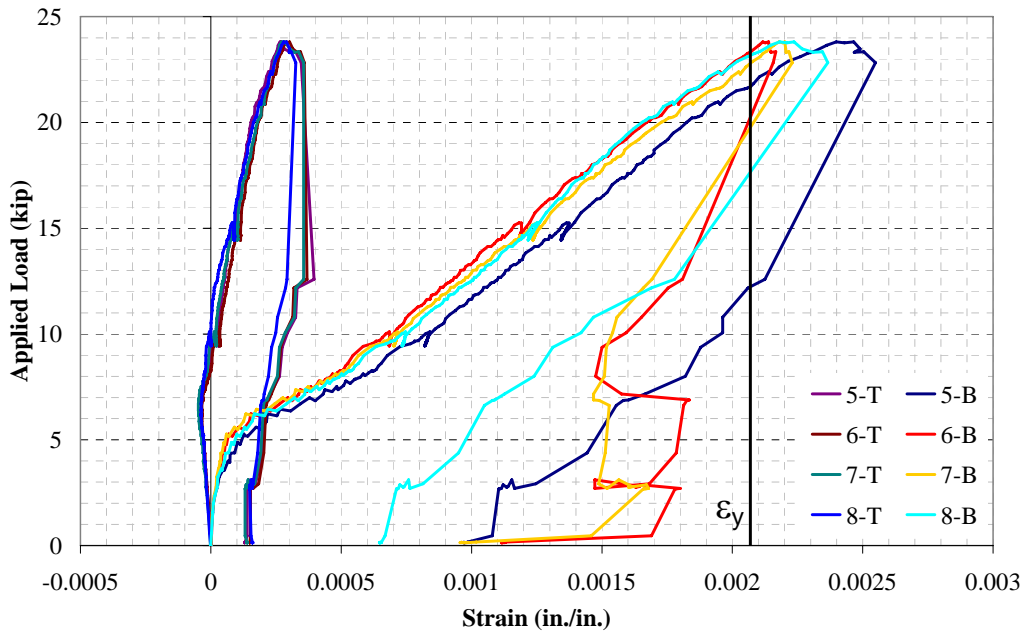


Figure 4.14: Specimen 0-2a – Mid-span reinforcing steel load versus strain

Although the bottom bars have all reached the yield strain, the load continues to increase after this point. This happens because of the presence of the top layer of reinforcement in the slab. The bottom bars have yielded, but the top bars have not, so the slab can continue to resist additional load. The plot also shows that the cracking load is between 5 and 6 kips, which is slightly less than the predicted cracking load of 7.6 kips.

In a couple of the specimens with no haunch, a significant amount of yielding occurred in one or two of the bottom bars at the mid-span. Figure 4.15 shows one of these specimens. The two bars that have yielded significantly are 5-B and 8-B, which correspond to the outer bars. As the breakout prism forms in the center of the slab, and the bond between the middle bars and the concrete is lost, it seems that the strain is redistributed to the outer bars that are not affected by the breakout prism.

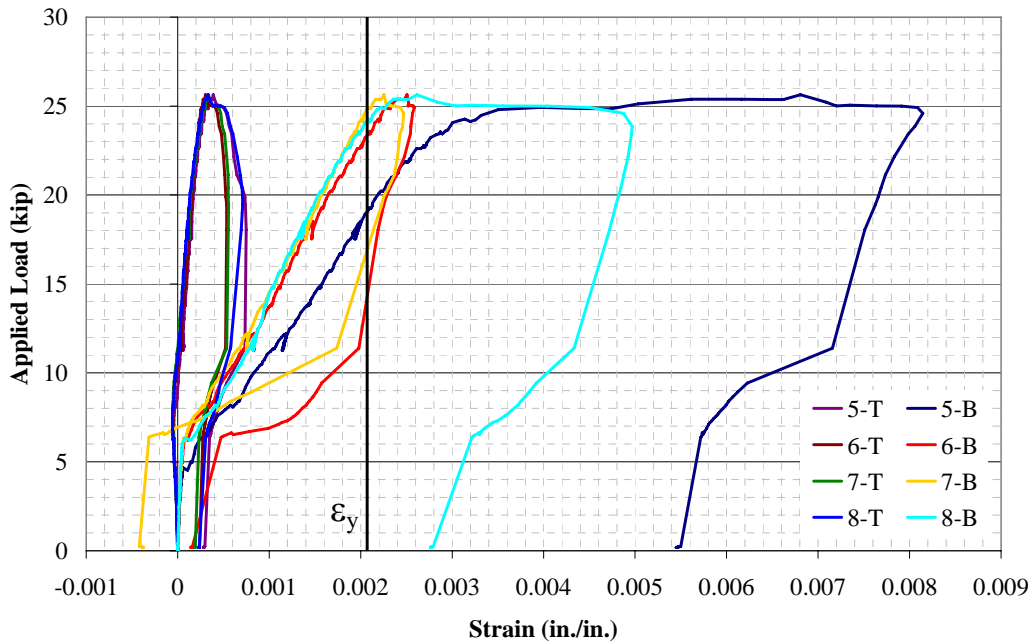


Figure 4.15: Specimen 0-3a – Mid-span reinforcing steel load versus strain

The gages at the quarter-span typically recorded strains that were roughly half of the strains at the mid-span. This is what was expected because the moment at the quarter-span is half of the mid-span moment. In several of the specimens, the gages on the bottom bars recorded large strains at the quarter-span during the pullout of the studs as shown in Figure 4.16. Some of the bars actually reach the yield strain at the quarter-span during the breakout failure. This increase in strain and yielding is due to the effect of the concrete breakout failure rather than the effect of bending stresses.

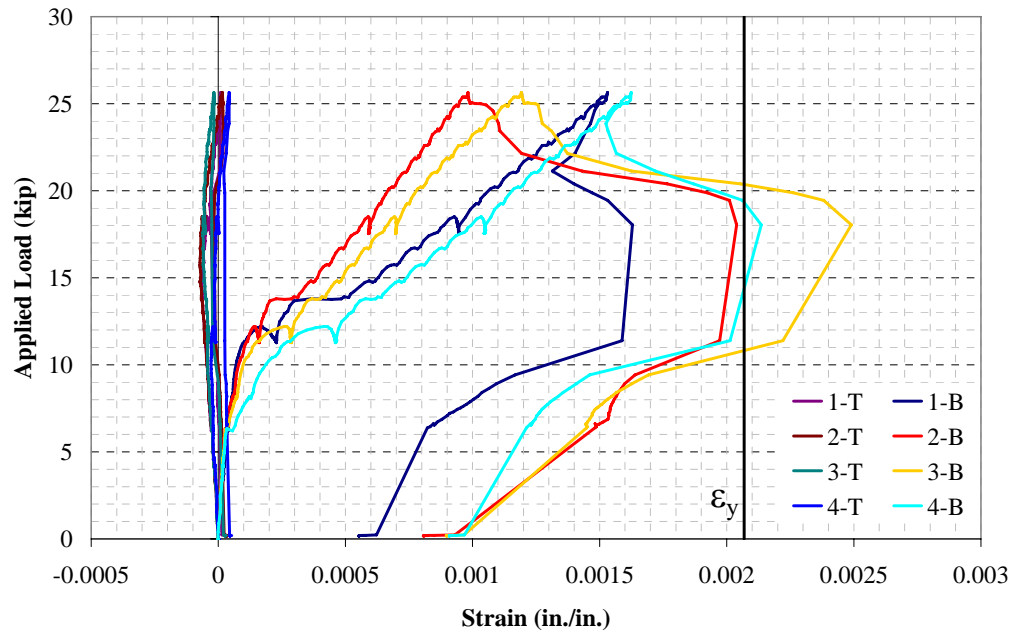


Figure 4.16: Specimen 0-3a – Quarter-span reinforcing steel load versus strain

4.6 SLAB DEFLECTION

The slab deflection data confirm that very little plastic deformation of the deck slab occurred during any of the tests. The deck slab cracked for all specimens and reached the yield load for some specimens, but the concrete breakout failure typically occurred before the reinforcement reached strains that were much larger than the yield strain. Figure 4.17 shows a typical plot of the applied load versus the top of slab mid-span deflection. This figure shows that, after the breakout failure, the deck slab was left with approximately 0.08 in. of permanent deflection. A mid-span deflection of 0.08 in. corresponds to a deflection equal to $L/975$ for these test specimens, which is a very small deflection. This plot represents a specimen with a 3-in. haunch, but it is indicative of the behavior of all the specimens both with the haunch and without the haunch.

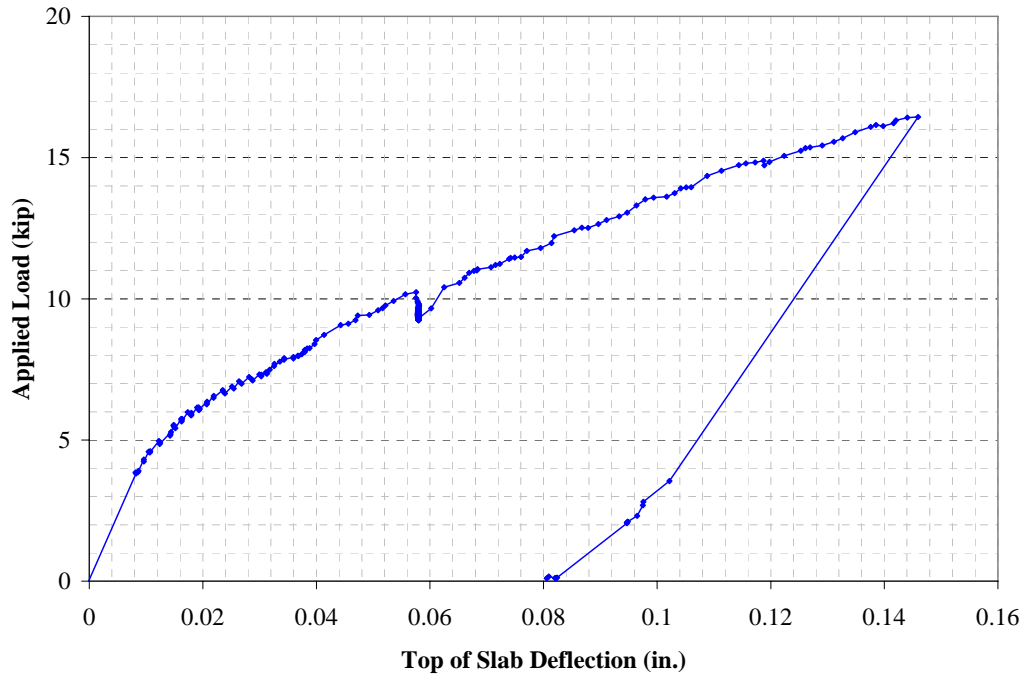


Figure 4.17: Specimen 3-3a – Typical load versus top of slab deflection plot

Figure 4.17 shows that the specimen is initially very stiff, but then it becomes much less stiff at about 5 or 6 kips. This point represents the cracking load, which was predicted in Section 4.5.1 to be approximately 8-9 kips. Prior to cracking, the section behaves with gross section properties, making the moment of inertia much greater and the slab much stiffer than a cracked slab. After the section cracks, the cracked section properties dictate the behavior and so the specimen is less stiff.

Another interesting point shown in this plot is the V-notch seen at about 10 kips. This is a point at which the loading was paused to map cracks and inspect the specimen. The deflection is held constant by the ram, and the load drops off slightly. The loading rate during a test is considered to be an intermediate loading rate, which is between a static and dynamic loading rate. The V-notch point represents a static value on the load versus deflection plot. These V-notches can also be seen in previous sections on the

applied load versus calculated stud force plots and the load versus strain plots for the deck slab reinforcing steel.

4.7 CONCRETE CYLINDER TESTS

As mentioned in Chapter 3, concrete cylinders were cast to verify the strength of the concrete at various points throughout the testing period. The cylinders were cast in 6-in. diameter by 12-in. molds. Compression tests were performed on the day testing began, after all of the A-specimens were tested (half-way), and the day that all testing was completed. These test dates corresponded to 38, 49, and 59 days after casting, respectively. The results of the cylinder compression tests are shown in Table 4.5.

Table 4.5: Concrete cylinder compression tests

Days after Casting	Average Compressive Strength (psi)	Standard Deviation (psi)
38	5,600	80
49	6,010	170
59	6,130	80

This table shows that the compressive strength of the concrete is significantly higher than the Class “S” concrete required minimum value of 4,000 psi. The compressive strength is also higher than the strength seen in the FSEL test bridge, which was approximately 4,900 psi after 28 days and 5,400 psi after 70 days. The concrete in the FSEL test bridge is also Class “S” concrete, but it was supplied by a different ready-mix concrete supplier.

CHAPTER 5

Analysis and Discussion of Test Results

5.1 PREDICTED CAPACITIES VERSUS TEST RESULTS

Using the equations found in Appendix D of the ACI 318 code, a predicted tensile capacity for each of the six unique specimens was calculated. In calculating the predicted values, the governing failure mode for all specimens was concrete breakout. The predicted values are based on a concrete compressive strength of 6,000 psi. This concrete strength was chosen because it corresponds to the strength of the concrete cylinders at the midway point of the testing program. Strength reduction factors (ϕ) were not applied to the predicted values. The detailed calculations of the predicted capacity of each specimen are given in Appendix E.

As described in detail in Chapter 2, the equations used to calculate the concrete breakout strength are as follows:

$$N_b = k_c \sqrt{f'_c} h_{ef}^{1.5} \quad \text{Equation 5.1 (ACI 318-05)}$$

$$N_{cbg} = \frac{A_{Nc}}{A_{Nco}} \psi_{ec,N} \psi_{ed,N} \psi_{c,N} N_b \quad \text{Equation 5.2 (ACI 318-05)}$$

where:

- N_b = concrete breakout strength of a single anchor in cracked concrete with no edge or group effects (lb)
- k_c = 24 for cast-in anchors
- f'_c = specified compressive strength of concrete (psi)
- h_{ef} = effective anchor embedment depth (in.)
- N_{cbg} = concrete breakout strength of an anchor or group of anchors (lb)

A_{Nc} = projected concrete failure area of an anchor or group of anchors (in.²)

A_{Nco} = projected concrete failure area of one anchor when not limited by edge distance or spacing ($= 9h_{ef}^2$) (in.²)

$\psi_{ec,N}$ = modification factor for eccentric loading

$\psi_{ed,N}$ = modification factor to account for edge distances less than $1.5h_{ef}$

$\psi_{c,N}$ = modification factor to account for cracking

The eccentric loading modification factor, $\psi_{ec,N}$, was taken as 1.0 because there was no eccentric loading of the studs. The modification factor for cracking, $\psi_{c,N}$, was taken as 1.0 because it was assumed that flexural cracking would take place prior to the breakout failure. This factor can be taken as 1.25 if no cracking occurs at service load levels. The modification factor for edge effects, $\psi_{ed,N}$, was taken as 1.0 for the specimens with no haunch, and less than 1.0 for the specimens with a 3-in. haunch. This factor is dependent on the distance to the edge as shown in Equation 5.3. It was assumed that the haunch represented an edge, and the edge effect factor was 0.96, 0.87, and 0.79 for the specimens with one, two, and three studs, respectively. The specimens with three studs have the largest reduction in capacity because the distance to the haunch is the smallest in these specimens.

$$\psi_{ed,N} = 0.7 + 0.3 \frac{c_{a,\min}}{1.5h_{ef}} \text{ if } c_{a,\min} < 1.5h_{ef} \quad \text{Equation 5.3 (ACI 318-05)}$$

where: $c_{a,\min}$ = smallest edge distance measured from the center of the stud shaft to the edge of concrete (in.)

The projected concrete failure area for the specimens with a 3-in. haunch was assumed to be the width of the top flange by three times the effective height of the stud.

The width of the flange was used in the deck transverse direction because the haunch creates an edge at both sides of the flange. The full breakout prism width of $3h_{ef}$ was used in the deck longitudinal direction because there is no edge. The shaded areas in Figure 5.1 represent the assumed projected concrete failure areas for the specimens with a 3-in. haunch. Notice that, due to the effect of the haunch edges, the projected concrete failure area for each specimen is the same regardless of the number of studs.

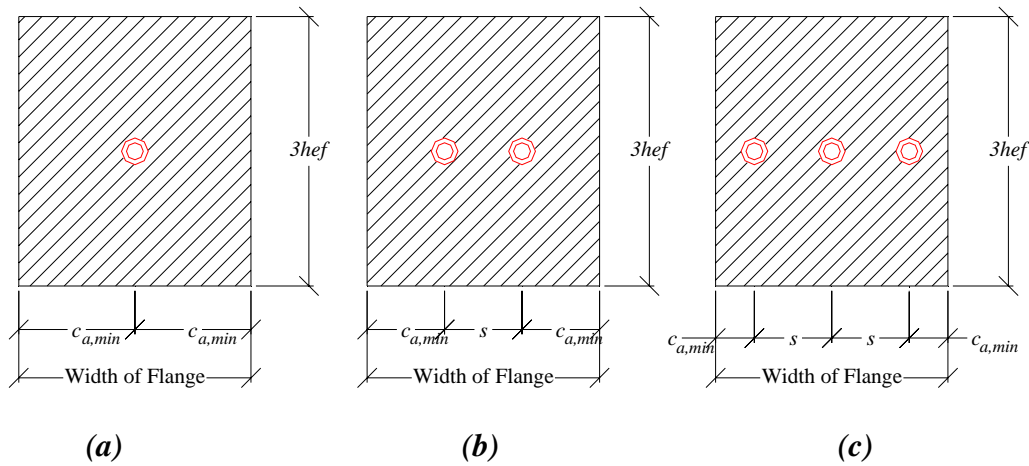


Figure 5.1: Assumed projected concrete failure area of studs for specimens with a 3-in. haunch and (a) one stud, (b) two studs, and (c) three studs

The projected failure area for the specimens with no haunch is not reduced by any edges. Therefore, the failure width in the transverse direction can be greater than the width of the flange. The projected concrete failure area was assumed to be $3h_{ef}$ in the deck longitudinal direction and $3h_{ef}$ plus the spacing between the outer studs in the deck transverse direction as shown by the shaded areas in Figure 5.2. Notice that, for the specimens without a haunch, the projected failure area increases as the number of studs is increased.

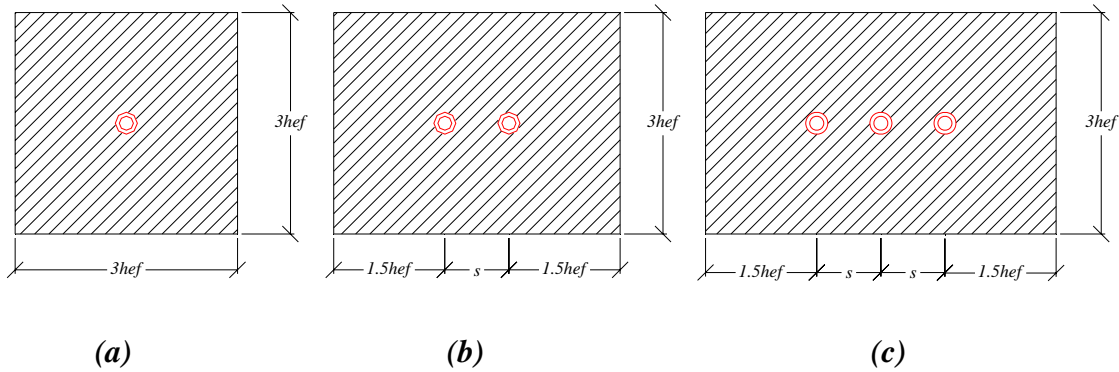


Figure 5.2: Assumed projected concrete failure area of studs for specimens with no haunch and (a) one stud, (b) two studs, and (c) three studs

The values of the important variables and the resulting predicted capacities are listed in Table 5.1. For the three specimens without a haunch, the difference in the predicted capacities comes from the difference in the A_{Nc}/A_{Nco} ratio. Adding studs increases this ratio, and thus increases the capacity. For the three specimens with a 3-in. haunch, the A_{Nc}/A_{Nco} ratio stays constant due to the effect of the haunch. The difference in the predicted capacities comes from the modification factor for edge effects, $\psi_{ed,N}$. As more studs are grouped across the flange width, the edge distance decreases. This decreases the modification factor for edge effects, and therefore the capacity decreases as the number of studs increases.

Table 5.1: Calculation of predicted capacities ($f_c' = 6,000$ psi)

Specimen		h_{ef} (in.)	$c_{a,min}$ (in.)	s (in.)	A_{Nc} (in. ²)	A_{Nco} (in. ²)	$\psi_{ec,N}$	$\psi_{ed,N}$	$\psi_{c,N}$	N_b (kip)	N_{cbg} (kip)
No Haunch	1 stud	4.625	-	-	192.5	192.5	1.0	1.0	1.0	18.5	18.5
	2 studs	4.625	-	4.0	248.0	192.5	1.0	1.0	1.0	18.5	23.8
	3 studs	4.625	-	4.0	303.5	192.5	1.0	1.0	1.0	18.5	29.2
3" Haunch	1 stud	4.625	6.0	-	166.5	192.5	1.0	0.96	1.0	18.5	15.3
	2 studs	4.625	4.0	4.0	166.5	192.5	1.0	0.87	1.0	18.5	14.0
	3 studs	4.625	2.0	4.0	166.5	192.5	1.0	0.79	1.0	18.5	12.6

The calculated values using the ACI equations are compared to the experimental test results as shown in Table 5.2.

Table 5.2: Experimental results versus nominal capacity from ACI design equations

Specimen		ACI 318-05 (kip)	Experimental Average (kip)	% Difference
No Haunch	1 stud	18.5	20.9	12.7
	2 studs	23.8	24.6	3.2
	3 studs	29.2	25.9	-11.3
3" Haunch	1 stud	15.3	22.3	45.8
	2 studs	14.0	19.2	37.1
	3 studs	12.6	17.3	37.3

The table shows that the ACI equations worked well for the specimens with no haunch. This is expected because the concrete breakout failures seen in the experimental tests were consistent with the assumed breakout failures. For the specimens with one and two studs, the equations are slightly conservative. For the specimen with three studs the equation is unconservative. However, if the strength reduction factor had been applied, the design capacity would be conservative. In the case of the specimens with no haunch, the strength reduction factor would be equal to 0.75 because steel reinforcement intersects the failure surfaces.

The ACI equations prove to be very conservative for the specimens with a 3-in. haunch. As mentioned in Chapter 2, cracking in the region of the stud connection can reduce the concrete breakout strength by as much as 25%. The predicted values for the specimens with a haunch assumed that cracking would occur ($\psi_{c,N} = 1.0$). However, while the slab cracked at the haunch edges, there were no flexural cracks in the haunch region as shown in Figure 5.3.

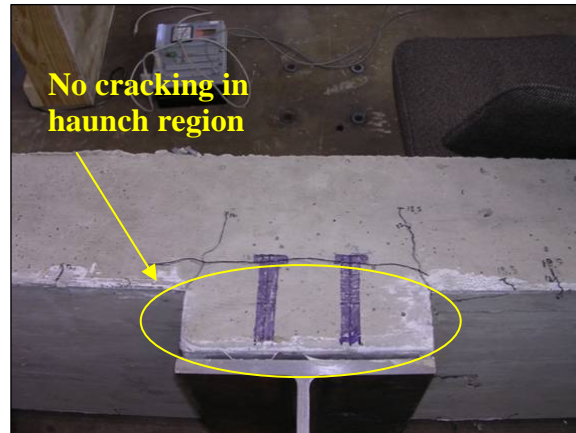


Figure 5.3: Specimen with 3-in. haunch – no flexural cracking in haunch

If the modification factor for cracking, $\psi_{c,N}$, had been taken as 1.25 rather than 1.0 for the specimens with a 3-in. haunch, then the predicted values would be much closer to the experimental values. The adjusted predicted values assuming no cracking in the specimens with a 3-in. haunch and the adjusted percent difference for each specimen are shown in Table 5.3. This table shows that the ACI equations are still slightly conservative but that the accuracy is much greater when the equations are adjusted to account for the fact that there is no cracking in the haunch.

Table 5.3: Percent difference assuming no cracking in specimens with a 3-in. haunch

Specimen		Predicted - No cracking (kip)	Experimental Average (kip)	% Difference
3" Haunch	1 stud	19.1	22.3	16.6
	2 studs	17.5	19.2	9.7
	3 studs	15.8	17.3	9.8

Another potential reason for the difference between the predicted and experimental results for the specimens with a 3-in. haunch is that the actual observed breakout failures were considerably different than the assumed breakout failure conditions. It was assumed that the haunch was an edge as shown in Figure 5.4 (a), but

in reality the haunch edge is only 3 in. Above the haunch there is additional concrete beyond the assumed edge distance as shown in Figure 5.4 (b).

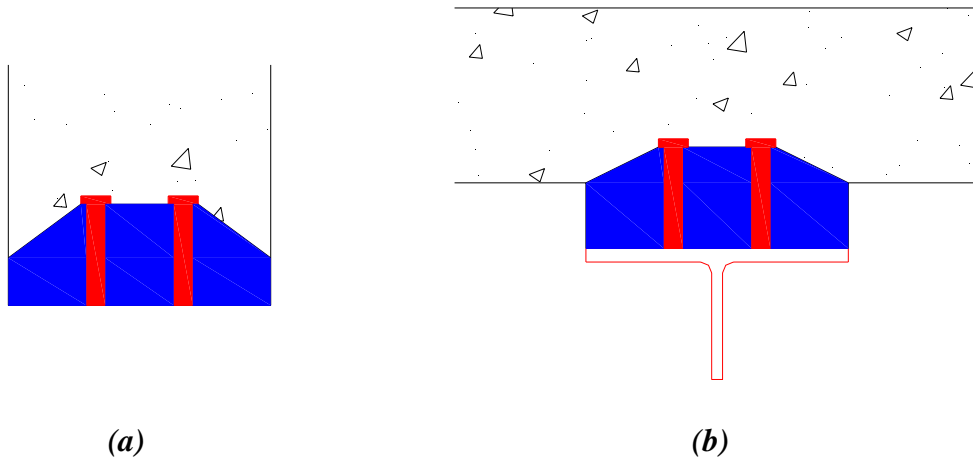


Figure 5.4: Deck transverse direction – (a) assumed breakout failure; (b) actual breakout failure

In the deck longitudinal direction, the breakout prism was assumed to have no edge effect and to extend $1.5h_{ef}$ in both directions as shown in Figure 5.5 (a). However, the failure plane ran along the whole length of the haunch as shown in Figure 5.5 (b). The result was that the entire rectangular block of concrete that was the haunch was separated from the deck slab.

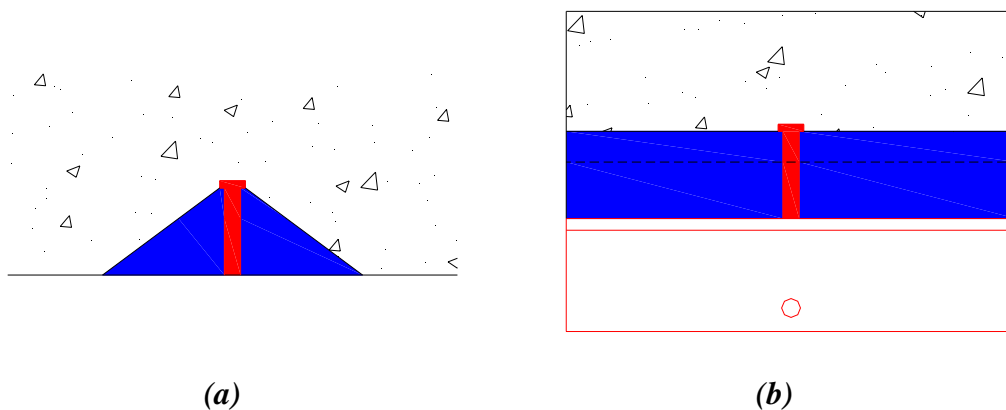


Figure 5.5: Deck longitudinal direction – (a) assumed breakout failure; (b) actual breakout failure

The assumed projected concrete failure area versus the actual concrete failure area is shown in Figure 5.6. The result of the differences between the assumed and actual concrete breakout failures was that the area of the failure plane was much larger. A larger failure plane would increase the breakout load. This may explain why the predicted capacities are still conservative even after modifying the equations to account for no cracking in the haunch region.

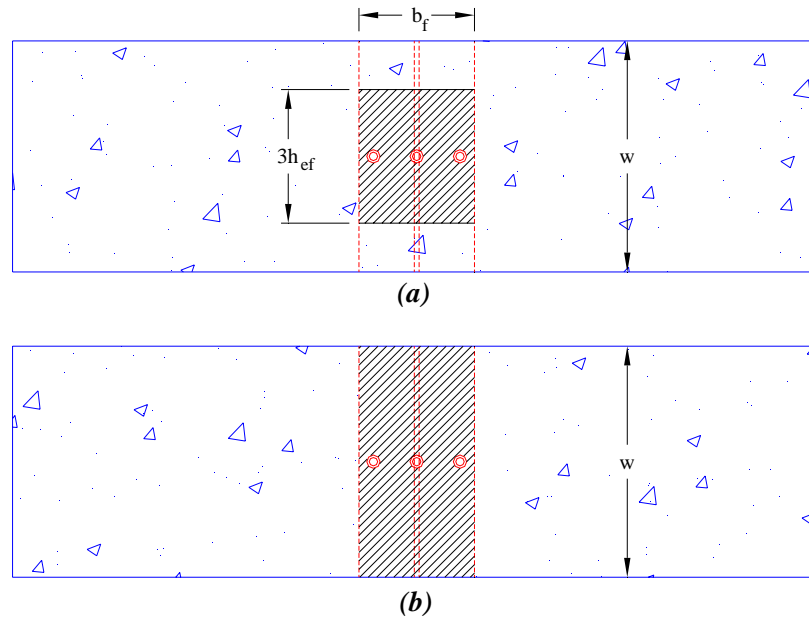


Figure 5.6: (a) Assumed projected failure area; (b) actual failure area

A designer may also consider simply multiplying the tensile capacity of concrete by the area of the failure plane as a way to quickly estimate an upper bounded capacity. In the case of the specimens with a haunch, the failure plane is simply the width of the flange multiplied by the width of the specimen ($b_f \times w$). However, this approach should not be used as it produces extremely unconservative results. The predicted capacity obtained using this methodology over-estimates the capacity by a factor of approximately 10. This method also does not take into account the reduction in strength associated with the edge effects.

5.2 EVALUATION OF CURRENT SHEAR CONNECTOR DETAIL

5.2.1 Introduction

The purpose of this experimental program was to determine the effect that a bridge haunch has on the tensile capacity of a row of shear studs and to use that information to determine if the current detail will allow for the transfer and redistribution of the required tensile force during a fracture event. Much has been learned about both the strength and behavior of the shear studs in specimens with and without a haunch. The results of this testing program not only demonstrate the effect of the haunch, but they also can be used to examine the effectiveness of the current standard shear stud bridge detail.

5.2.2 Capacity

The test results clearly show that the bridge haunch reduces the tensile capacity of the shear studs. The tensile capacity of a row of three studs without a haunch is reduced by 33% when a 3-in. haunch is in place, and the tensile capacity of a row of two studs without a haunch is reduced by 22% when a 3-in. haunch is in place.

5.2.3 Ductility

More significant than the decrease in capacity, the tests have also demonstrated that the specimens with a 3-in. haunch exhibit no ductility at failure. This lack of ductility is due to the fact that the haunch is not reinforced and that the studs do not penetrate far enough into the deck to engage the steel reinforcement. The breakout failure is a tension failure of the concrete, and therefore is a brittle failure. This is a major problem because it may make the distribution of the tensile force along the length of the girder impossible during a fracture event. In order to redistribute forces, a system must have ductility, and this current detail offers no ductility. Figure 5.7 shows the total separation of the studs and the haunch concrete from the deck. Notice in Figure 5.7 (b)

that the reinforcement steel is even with, but not intersecting, the failure plane and thus cannot provide any ductility when the breakout failure occurs.



Figure 5.7: Complete haunch separation as seen from (a) the side view and (b) underneath the specimen

For the specimens with a haunch, once the breakout capacity was reached, the horizontal cracking that separated the haunch from the deck slab formed very suddenly and propagated along the entire width of the specimen. In a wider specimen with only one row of studs in the center of the width, it is likely that the entire haunch would separate from the slab at approximately the same load. This is due to the fact that, once the breakout capacity is reached, the horizontal cracking that separates the haunch concrete from the deck slab is unstable and propagates along the entire width (longitudinal direction) of the specimen. In the case of the FSEL test bridge, where the longitudinal length is much greater (118 ft) and the studs are spaced at approximately 2 ft, it is difficult to predict how the additional rows of studs will influence this failure behavior. The other rows should prevent the haunch from completely separating from the deck slab along the entire length of the girder, but if the failure plane forms even with the top of the studs, it is possible that the other rows may not give much help.

The specimens without a haunch exhibited some ductility at failure only because the breakout failure prism was intersected by the two middle transverse deck reinforcement bars as shown in Figure 5.8. The longitudinal deck reinforcement bars are spaced too far away to intersect the breakout prism even in the specimens with no haunch and three studs.

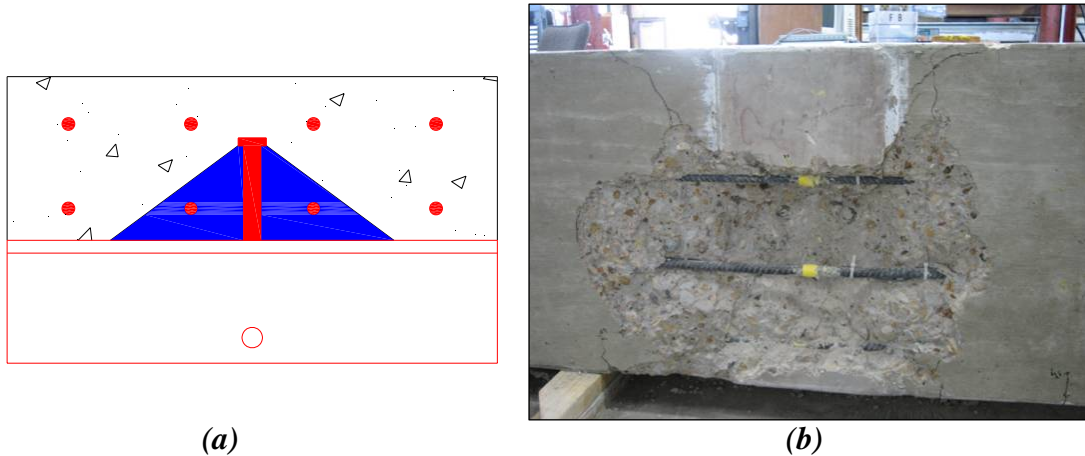


Figure 5.8: (a) Drawing and (b) photograph showing the center transverse bars running through the concrete failure prism for a specimen with no haunch

Although the specimens with no haunch exhibited some ductility as the studs pulled out of the slab, the failure is still governed by the tensile strength of the concrete and is quite brittle. At failure, the load is not held constant during a long period of deformation, but rather the load slowly decreases as the deformation increases until the studs completely breakout and the load goes to zero.

5.2.4 Efficiency

Analysis of the test results show that the shear connector detail used in the FSEL test bridge is a very inefficient use of materials. Using three studs in a row across the top flange yields a capacity less than the capacity of a single stud when there is a haunch.

Even if there were no haunch, three studs spaced very close together across the top flange only increases the capacity by approximately 25% when compared to a single stud.

The data from the strain gage data also show that the center stud resists the majority of the tensile force and that each of the outer studs resists only about 25% of the total load. Furthermore, in the case with a 3-in. haunch and a row of three studs, at failure the largest stress in the center stud was approximately 25% of the yield stress, and the largest stress in the outer studs was approximately 14% of the yield stress. In the specimens with only one stud and a 3-in. haunch, the single stud experienced a stress approximately 72% of the yield stress at failure. These results show that grouping the studs is not an efficient use of materials.

If the studs must be grouped into rows, using two studs in a row is more efficient than using three studs in a row. When two studs are used in a specimen with a haunch, the reduction in capacity is not as great as when three studs are used. In addition the force is evenly distributed between the two studs, and the stress in the studs is higher at the time of the concrete breakout failure.

5.2.5 Summary

The current detail of using a bridge haunch and grouping the studs in rows of two or three does not perform well under tensile loading. The haunch greatly reduces the capacity when multiple studs are used in a row and also prevents the connection from failing in a ductile manner. Following the current AASHTO and TxDOT standards, which require the studs to penetrate a minimum of 2 in. into the deck slab, does not allow the breakout failure prism to engage the deck reinforcement. This creates an extremely brittle failure and may prevent the redistribution of the tensile forces along the length of the girder during a fracture event.

5.3 POSSIBLE TECHNIQUES TO IMPROVE SHEAR CONNECTOR DETAIL

5.3.1 General Comments

The suggestions in the following sections are possible methods that can be used to improve the tensile behavior of the current shear stud detail. These suggestions are based on the assumption that the haunch is a necessary part of bridge construction, which cannot be eliminated despite the negative effects it has on the tensile behavior of the studs.

The AASHTO Specifications require that a designer calculate the shear capacity of a single stud and provide enough studs to resist the required design shear force. Therefore, as long as the following suggestions do not reduce the number of studs on a girder or reduce the shear capacity of a single stud then the shear resistance should not change.

5.3.2 Haunch Reinforcement

A simple way to improve the current detail without changing the spacing or grouping of the studs is simply to include reinforcement in the haunch area near each row of studs. Figure 5.9 demonstrates a potential detail for reinforcing the haunch region. The bar shown in green would be placed on each side of a row of studs. The bar would need to be spaced close enough to the studs so that it would intersect the breakout failure plane. The central transverse deck reinforcement bars, which intersected the failure prism in the specimens with no haunch, were offset from the row of studs by 3 in. Therefore, this would be an acceptable spacing to offset the proposed haunch reinforcement bars. The bar would also need to be long enough to develop both ends in the deck slab. The longitudinal deck reinforcing bars are not shown in this figure.

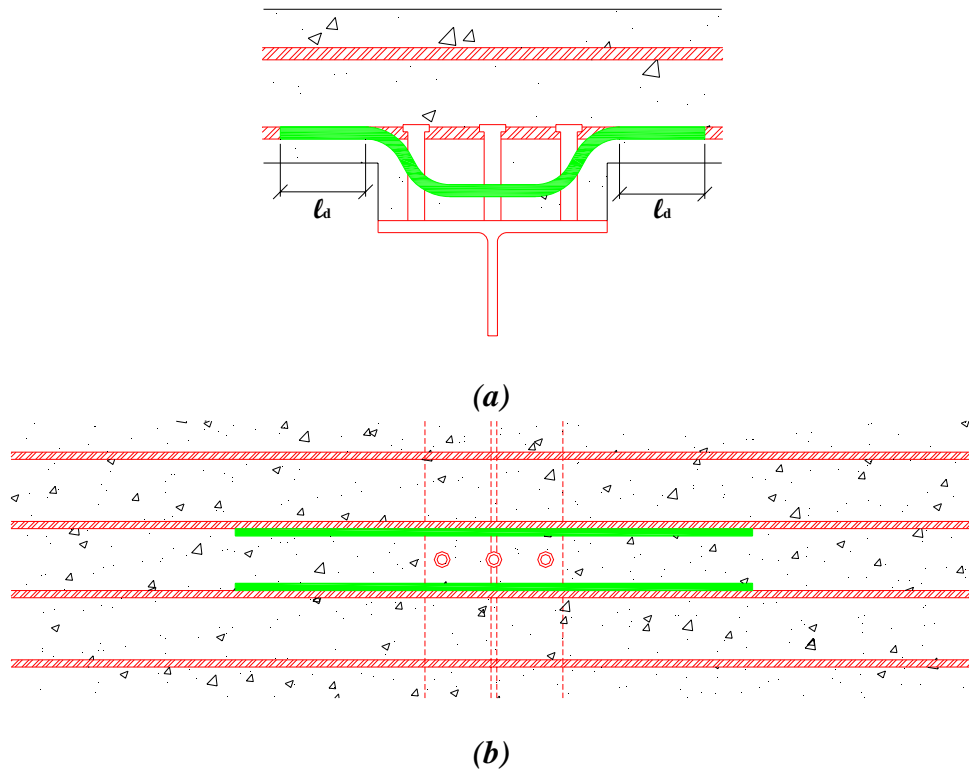


Figure 5.9: Haunch reinforcement to improve ductility (a) cross-section (b) plan view

Adding haunch reinforcement would probably not increase the capacity of the row of studs, but it would add ductility. Rather than reaching a maximum load and failing very suddenly, the behavior at failure would be similar to the behavior of the specimens with no haunch. The load would slowly drop off while the studs pull out of the slab. Figure 5.10 (a) shows the load versus pullout deflection of the current detail, and Figure 5.10 (b) shows the load versus pullout deflection curve that can be expected if haunch reinforcement is used around the studs. These plots are generated from the test data for specimens with and without a haunch, respectively. The ductility that the haunch reinforcement can add to the current detail may make the redistribution of the tension forces possible during a fracture event.

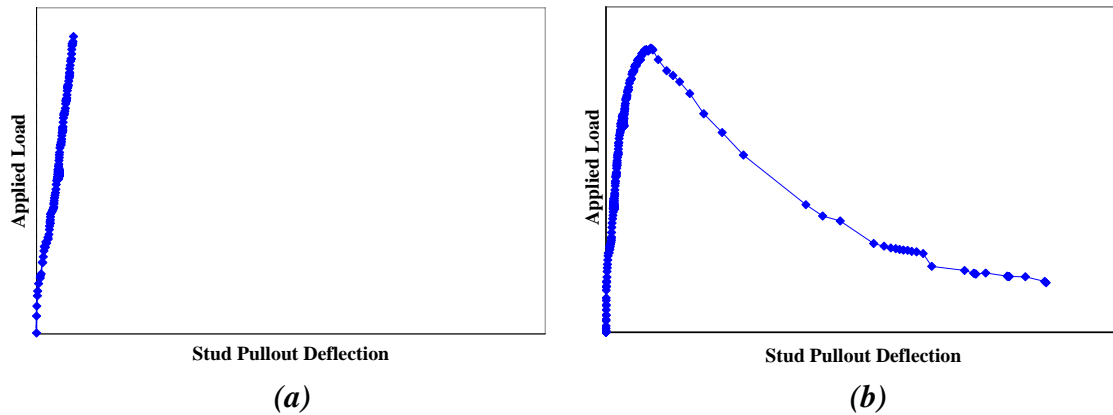


Figure 5.10: Load versus stud pullout for (a) current detail and (b) reinforced haunch detail

5.3.3 Longitudinal Spacing of Studs

The test results have shown that the current detail is an inefficient use of the shear studs. When using a haunch, a single stud reaches a much higher capacity than a group of two or three studs. Even without a haunch, using two or three studs provide less than a 25% increase in capacity. Therefore, in order to maximize the tensile force that can be resisted, it would be better to use a single stud and to space the studs longitudinally along the length of the girder as shown in Figure 5.11. Based on the test results for the specimens with a haunch, three single studs behaving independently will resist almost four times as much tensile force than three studs grouped across the flange width.

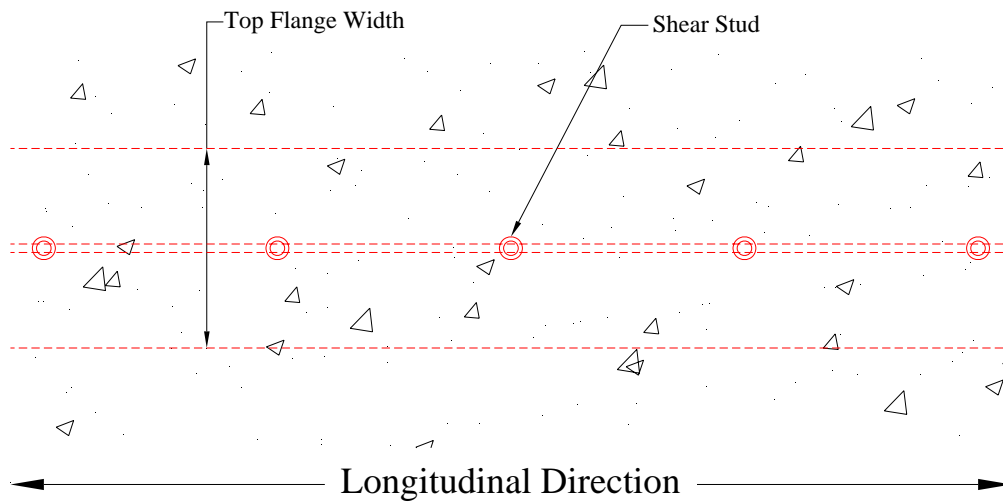


Figure 5.11: Longitudinal spacing of shear studs

Based on the breakout prism assumed by the ACI equations, the longitudinal spacing needs to be at least three times the effective height of the stud for the studs to behave independently. For a 5-in. long stud, this spacing corresponds to approximately 14 in. In the case of the 120-ft span FSEL test bridge, the studs are grouped in rows of three spaced at approximately 22 in. This corresponds to roughly 200 studs on one top flange of the box girder. If a single stud was to be spaced longitudinally at 14 in., the number of studs on one flange of a box girder from the FSEL test bridge would be just over 100. This is unacceptable because the shear resistance would become inadequate. In order to maintain the same number of studs on the FSEL test bridge, the single studs would need to be spaced longitudinally at 7 in.

Therefore, the studs will not be acting completely independently of each other if they are spaced longitudinally at this spacing. Theoretically, the group effect would include every stud along the length of the girder. However, unless there was a uniform tensile load applied to the entire girder, then the group effect would not include all of the

studs. During a fracture event the tensile force will initially be applied in the local area where the crack occurs. Therefore, the group effect will most likely only include the studs in the vicinity of the fracture.

Even with this group effect, the tensile capacity of three studs spaced longitudinally will still be much greater than the row of three studs spaced transversely across the flange width. Three studs grouped transversely across the width of the top flange experience a very large reduction in capacity because the distance between the outer studs and the haunch edge is very small. While the single studs spaced longitudinally may experience a group effect, the edge effect is kept to a minimum because the stud is in the center of the flange width.

5.3.4 Longer Studs

Another method to improve the current detail is to increase the length of the shear studs. An increase in the stud length could potentially increase both the tensile capacity and the ductility of a row of studs. As shown in Equations 5.1 and 5.2, the concrete breakout load is a function of the effective height raised to the three-halves power. Thus, for a single stud with no edge or group effects, increasing the length of the stud will increase the capacity. Using the ACI equations, for a single 7/8-in. diameter stud with no edge or group effects in Class “S” (4,000 psi) concrete, an increase in the length of the stud from 5 in. to 7 in. will increase the concrete breakout capacity from 15 kips to 26 kips.

Increasing the stud length will increase the penetration of the studs into the deck reinforcement mat. Using an 8-in. long stud with a 3-in. haunch would create the same penetration into the deck reinforcement as the test specimens with 5-in. long studs and no haunch as shown in Figure 5.12. If the studs extend far enough into the reinforcement mat, then the breakout failure prism will intersect the deck reinforcement steel. This

would then produce a ductile failure similar to the failures exhibited by the test specimens with no haunch.

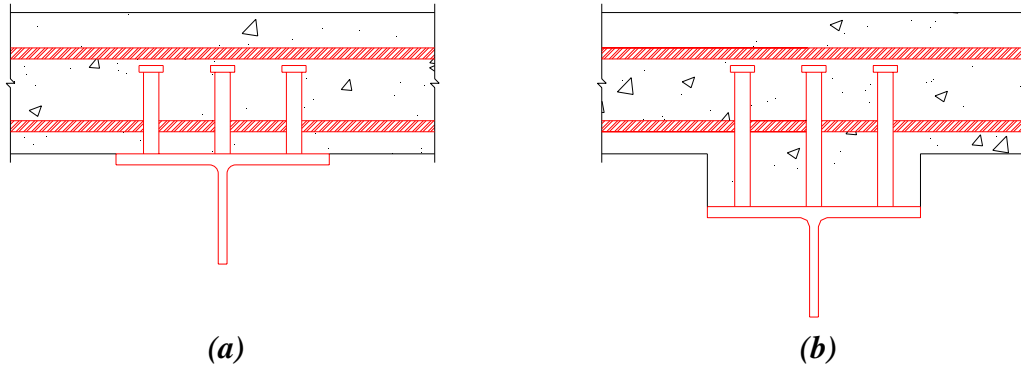


Figure 5.12: (a) 5-in. long studs with no haunch; (b) 8-in. long studs with 3-in. haunch

If the studs penetrate far enough above the top of the haunch, it is also possible that the haunch will not have as great of an effect on the tensile capacity. The concrete breakout failure prism could develop as shown in Figure 5.13. If the failure prism developed in this manner, the behavior and capacity would be similar to that of the specimens with 5-in. long studs and no haunch. This would nullify the negative effect of the bridge haunch and increase both the capacity and ductility.

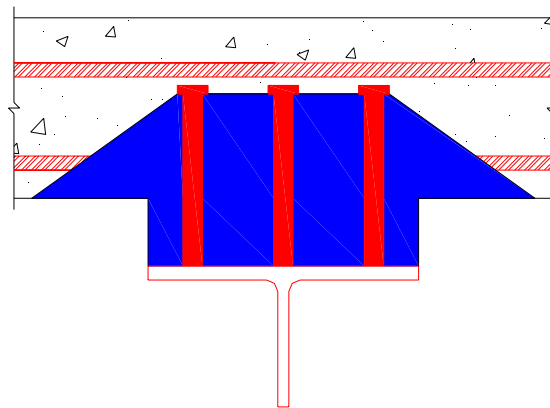


Figure 5.13: Potential concrete breakout failure prism for longer studs

Even if the failure plane forms directly at the intersection of the haunch edge and bottom of the deck slab, the failure plane will still be intersected by the transverse reinforcement steel. Thus, while the increase in capacity may not be very large, the ductility during the breakout failure would still be present. Therefore, using longer studs will improve the ductility and may also create a significant increase in capacity.

AASHTO and TxDOT specifications require that the clear cover between the top of a stud and the top of the concrete deck be at least 2 in. Therefore, in bridges with a variable haunch height the use of longer studs may require varying the stud length along the girder to match the changes in the haunch height.

5.3.5 Combination of Longer Studs and Longitudinal Spacing

Spacing single studs longitudinally along the length of the girder will increase the capacity, but if the stud only penetrates 2 in. above the haunch, then the failure will still be brittle. However, if longer studs are used in combination with the longitudinal spacing of single studs, then the capacity and the ductility can be improved. Longer studs will force the failure plane to intersect the reinforcement steel, which will create ductility. Spacing single, longer studs longitudinally will also increase the number of transverse bars that intersect the failure prism during a fracture event. This will further increase the ductility and the ability of the studs to redistribute force along the length of the girder.

When using a single stud in a row, it is possible that the governing failure mode could switch from concrete breakout to stud pullout. Figure 5.14 shows a plot of the tensile capacity versus the effective height for a single 7/8-in. diameter stud with no edge or group effects embedded in 4,000 psi cracked concrete. This plot is generated using the ACI equations for stud pullout failure and concrete breakout failure. The stud pullout capacity is constant because the equation for stud pullout is based only on the concrete strength and the bearing area under the stud head, which is constant for all length 7/8-in.

studs. The concrete breakout strength increases rapidly as the effective height increases because the equation includes a $h_{ef}^{1.5}$ term.

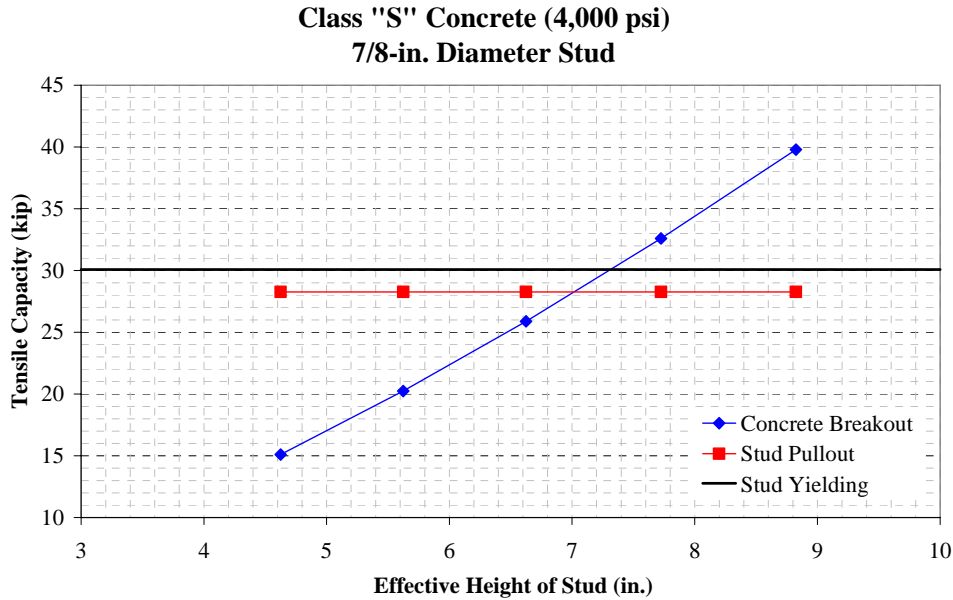


Figure 5.14: Tensile capacity versus effective height for a single 7/8-in. diameter stud embedded in 4,000 psi concrete

This figure shows that the balanced point or cross-over point occurs when the effective height is approximately 7 in. For studs with an effective height less than 7 in., concrete breakout is the governing failure. For studs with an effective height greater than 7 in., which would correspond to 8-in. long studs and above, the failure is governed by stud pullout. Therefore, if longer studs are used and spaced longitudinally along the girder, it is possible that the failure mode could switch to stud pullout. If this were to happen, the capacity would be greater, but the ductility would not increase. In a stud pullout failure, the stud pulls out with only the concrete directly under the stud head. Therefore, the failure will not engage the reinforcing steel even though the stud penetrates into the reinforcement mat.

This figure also shows that stud yielding cannot govern for a 7/8-in. stud embedded in 4,000 psi cracked concrete. However, the pullout strength and the yield strength are very close. If the concrete strength is increased, then yielding can occur before a pullout failure. If this is the case, then as long as the effective height is greater than the balanced effective height, yielding of the stud will occur before a concrete failure. The cross-over point for a single 7/8-in. diameter stud with no edge or group effects in various concrete compressive strengths is shown in Table 5.4. This table shows that yielding will occur before pullout for concrete strengths greater than or equal to 4,500 psi. Thus, for a single 7/8-in. diameter stud with no edge or group effects, yielding will govern when the effective height is greater than or equal to the balanced effective height and the concrete strength is greater than or equal to 4,500 psi. (All values in Table 5.4 assume that the concrete is cracked.)

Table 5.4: Cross-over point for a single 7/8-in. diameter stud with no edge or group effects in various concrete compressive strengths

f_c' (psi)	$h_{ef,bal}$ (in.)	N_p (kip)	N_{yield} (kip)
4000	7.02	28.3	30.1
4500	7.30	31.8	30.1
5000	7.57	35.3	30.1
5500	7.81	38.9	30.1
6000	8.04	42.4	30.1
6500	8.26	45.9	30.1
7000	8.47	49.5	30.1

5.3.6 Reduction of Stud Diameter

The methods mentioned in the previous sections are all governed by the tensile strength of the concrete deck slab, which is inherently a brittle failure. This failure becomes only slightly ductile when reinforcement bars intersect the failure surfaces. In order to guarantee that the shear stud connection will be truly ductile, the failure should

be governed by yielding of the stud rather than a brittle failure of the concrete. If yielding of the stud is the governing failure mode, there will be a yield plateau in which the load is held constant during plastic deformation. This behavior is far superior to the ductility offered by reinforcement intersecting the breakout failure prism in which the load slowly decreases with increasing deformation. Yielding of the studs would be the ideal situation for redistributing the tensile forces along the length of the girder during a fracture event.

In order to assure that yielding of the studs is the governing failure mode, the concrete breakout capacity and the stud pullout capacity must be maximized. In order to do this, it may be necessary to space the studs longitudinally along the girder. If three studs are grouped transversely across the width of the flange, the yield load of the group becomes three times the yield load of a single stud. The experimental tests have shown that the concrete breakout strength is significantly reduced when three studs are grouped in this way, and thus the breakout failure would govern over the yielding of the studs. Additionally, for a single 7/8-in. stud with no edge or group effects in Class “S” concrete (4,000 psi), either a concrete breakout failure or a stud pullout failure will occur prior to yielding regardless of the effective height of the stud. Therefore, in order to reduce the yield load of the stud and assure that yielding occurs before a concrete failure, the diameter of the stud must be reduced. Reducing the diameter of the stud, while keeping the diameter of the stud head the same, will also increase the stud pullout capacity.

However, the shear capacity of a single stud is based on the cross-sectional area of the stud as seen in the following equation from the AASHTO LRFD Bridge Specification:

$$Q_n = 0.5A_{sc}\sqrt{f'_c E_c} \leq A_{sc} F_u \quad \text{Equation 5.4}$$

where: Q_n = nominal resistance of a single stud (kip)

- A_{sc} = cross-sectional area of stud (in.²)
- f'_c = specified 28-day compressive strength of concrete (ksi)
- E_c = modulus of elasticity of concrete (ksi)
- F_u = specified minimum tensile strength of stud (ksi)

Reducing the diameter of the stud would reduce the shear capacity and increase the total number of studs required for each girder. A reduction of the stud diameter to 1/2 in. reduces the cross-sectional area to approximately one-third the area of a 7/8-in. diameter stud. This means that the shear capacity of a single stud would be one-third of the previous capacity and that the required number of studs would triple. Clearly, this is not an efficient or economical solution.

In order to hold the total number of studs constant, the diameter of the stud would have to remain constant for the calculation of the shear capacity. If the transfer of the shear force is assumed to take place at the base of the stud, the diameter of the stud could remain constant at the base in order to resist the shear force. However, the stud could then be tapered to a reduced diameter for the rest of the stud length in order to induce yielding of the stud under a tension load. Figure 5.15 shows an example of a reduced diameter shear stud. The 7/8-in. diameter at the base can be used to calculate the shear resistance, but the reduced 1/2-in. diameter would be used to calculate the yield load for the tensile loading. The 1/2-in. reduced diameter was selected because it is the largest diameter that will allow yielding to occur prior to concrete breakout for a 5-in. long single stud in 4,000 psi concrete. For a longer stud, the additional length could be added to the 7/8-in. diameter portion of the stud. Thus, the extra length can be utilized for shear resistance and the length of the reduced diameter portion of the stud remains constant.

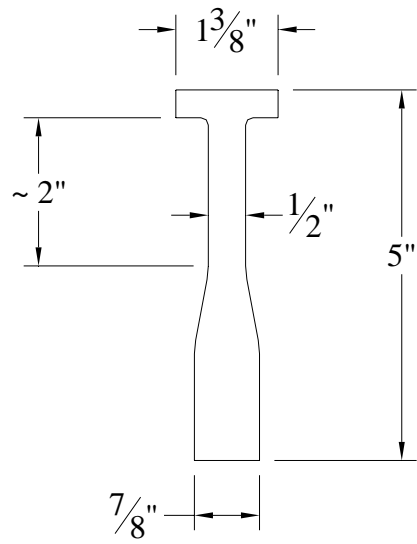


Figure 5.15: Reduced diameter shear stud

The question then arises as to where the shear transfer actually occurs when there is a haunch. It may not be correct to assume that the shear transfer takes place in the haunch region where the diameter of the stud would be kept at 7/8 in. The shear transfer may occur at the bottom of the slab, rather than the bottom of the haunch as shown in Figure 5.16. If this is the case, then the stud is actually in both shear and bending, and it may not be safe to assume that the 7/8-in. diameter can be used in the shear calculations.

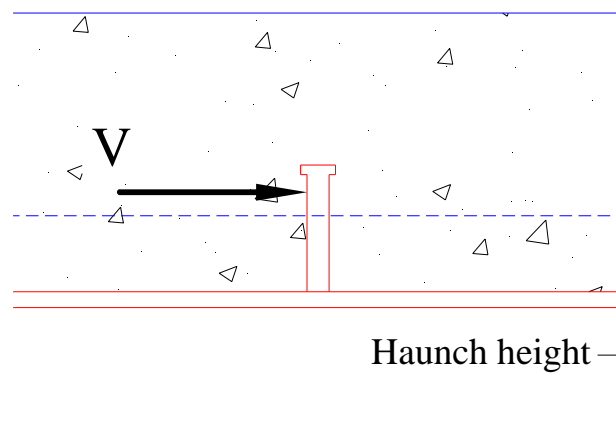


Figure 5.16: Stud under shear and bending

Forcing the tensile failure mode to be yielding of the shear stud provides the greatest ductility of this connection. The logical way to induce a yielding failure is to reduce the diameter of the studs so that the yield load is much less than the concrete failure loads, but it is unclear as to how this might affect the shear capacity of the studs. However, the potential benefits that this detail might have in terms of behavior during a fracture event warrant further investigation into this solution.

5.3.7 Summary

The laboratory tests have shown that the current shear stud detail does not perform well under tensile loading. The haunch greatly reduces the capacity of a row of studs grouped transversely across the flange width and prevents the connection from failing in a ductile manner.

The tensile behavior of the shear studs can be improved by any one or combination of the above modifications to the current detail. Adding haunch reinforcement will allow the connection to have some ductility. Spacing single studs longitudinally should increase the capacity, but not the ductility. Using longer studs should increase both ductility and capacity. Spacing single, longer studs longitudinally should increase both the capacity and ductility. However, it is possible that in single, longer studs the governing failure method will be stud pullout. This would increase the capacity, but not ductility. The best solution for ductility and the ability to redistribute load during a fracture event is to make stud yielding the governing failure. However, it is difficult to do this without affecting the shear capacity.

CHAPTER 6

Conclusions and Recommendations

6.1 SUMMARY OF OBJECTIVES

In order for a simply supported twin box girder steel bridge to be considered non-fracture critical, the bridge system must have the ability to transfer the load that was resisted by the fractured girder over to the other girder. As the fractured girder drops down, the shear studs will be loaded in tension. If the studs can transfer the tensile force to the slab, then the slab must have the ability to transfer the force to the other girder. Finally, the non-fractured girder must have enough reserve capacity to support the entire bridge dead and live load. An important assumption involved in this load transfer is that the studs and the slab behave in a ductile manner so that the load can be distributed along the length of the girder.

When analyzing the tensile capacity of the shear studs, it was determined that the bridge haunch would likely have a detrimental effect on the tensile capacity of a row of studs. In order to determine the effect of the haunch, a series of laboratory tests were performed on bridge deck sections with both no haunch and a 3-in. haunch. The results of these tests were used to evaluate the current haunch detail and to determine if the studs could transfer the required tensile force during a fracture event. The results were also used to develop possible techniques that can be used to improve the detail so that the studs might perform better during a fracture event.

6.2 CONCLUSIONS

The following conclusions were drawn from the results of the tests performed on the 12 bridge deck segments:

- 1) The haunch clearly has a detrimental effect on the tensile capacity of the shear studs. Specimens with multiple studs across the flange width and a 3-in. haunch failed at significantly lower loads than the corresponding specimens with no haunch. In specimens with a 3-in. haunch, adding studs to the row decreases the distance to the haunch edge and thus decreases the capacity.
- 2) Following the minimum design provisions, which require the stud to penetrate 2 in. into the deck slab, will create a brittle failure when the studs are loaded in tension because this depth of embedment does not create an adequate penetration above the bottom layer of the reinforcement steel. The specimens with a 3-in. haunch experienced no ductility at failure because the deck reinforcement steel did not intersect the concrete failure plane. Conversely, the specimens without a haunch experienced some ductility at failure – the load dropped off slowly as the deformations increased – because the deck reinforcement intersected the failure plane.
- 3) Due to the lack of ductility seen in the specimens with a 3-in. haunch, it may not be possible for the studs to distribute the required tensile force along the length of the girder during a fracture event. If this cannot happen, the studs will not be able to transfer the load into the slab and to the non-fractured girder.
- 4) Grouping studs transversely across the top flange width is an inefficient way to distribute the studs along the girder. In specimens with a 3-in. haunch, this arrangement creates a tensile capacity that is lower than the capacity of a single stud. Even in specimens with no

haunch, the capacity of three studs in a row is only slightly higher than the capacity of a single stud. The shear stud gage data also show that studs grouped transversely do not experience large stresses prior to a concrete breakout failure and that the force is not distributed evenly among the studs. In specimens with three studs, the center stud resists approximately half of the total force, while each of the outer studs resist about one-quarter of the total force.

- 5) During a fracture event the slab will likely experience significant cracking. The experimental tests were successful in duplicating this behavior as all of the deck segments cracked prior to the concrete breakout failure. While specimens with a 3-in. haunch had flexural cracks at the haunch edges, the increased depth in the haunch area prevented flexural cracking from occurring in that area. Flexural cracking did occur at the mid-span location for all of the specimens without a haunch.
- 6) The strain gages on the reinforcement steel show that no yielding of the deck reinforcement took place in any of the specimens with a 3-in. haunch. Yielding took place in the specimens without a haunch, but the deck segments experienced very little plastic deformation. The load versus slab deflection data also confirms that the deck segments did not experience much plastic deformation prior to the tensile failure of the shear stud connection. Typically, for the specimens without a haunch, the mid-span strain in the bottom bars was just slightly above the yield strain at maximum load. However, in some of the specimens,

strains significantly above the yield strain were measured as the breakout prism developed and the studs pulled out of the deck.

6.3 RECOMMENDATIONS AND FUTURE WORK

Based on the results of the tests performed on the 12 bridge deck segments, the following recommendations are suggested to improve the tensile behavior of the shear stud connection. These suggestions have not yet been tested in the laboratory; therefore, it is recommended that future laboratory tests are performed to determine the effect of each method and to optimize the detail accordingly.

- 1) Without changing the practice of grouping the studs transversely across the top flange, the simplest way to improve the behavior of the studs is to add haunch reinforcement around each row of studs. This will improve the ductility of the studs and help with the redistribution of force along the length of the girder during a fracture event.
- 2) Rather than grouping studs transversely in rows spaced far apart, use one stud in the center of the flange and space these single studs longitudinally at a distance that will allow for the same shear resistance. This will increase the tensile capacity so that less of the total span length would be required to resist the tension force during a fracture event.
- 3) Another method to improve the shear stud detail is to increase the length of the studs. Increasing the length of the shear studs, while keeping the haunch height constant, will increase the penetration of the studs into the deck reinforcement mat. This will force the breakout failure plane to cross the reinforcement, which will increase the ductility. Increasing the ductility will help with the redistribution of

force along the length of the girder during a fracture event. It is possible that using longer studs will also reduce the effect that the haunch has on the capacity.

- 4) If longer studs are used in combination with the longitudinal spacing of single studs, then the capacity and the ductility can be improved. Future tests need to be done to verify that stud pullout will not govern over concrete breakout. A stud pullout failure would increase the capacity of the current detail, but it would not improve ductility.
- 5) The best way to improve the tensile behavior of the shear stud detail is to guarantee that yielding of the shear studs is the governing failure mode. This will allow for the greatest ductility and redistribution of load. A possible technique to ensure yielding of the stud is to reduce the diameter of the stud in order for yielding of the reduced section to control the tensile capacity, but to keep the base diameter constant for shear resistance. Future work is needed to develop a detail that will allow for yielding of the stud to govern in tension, but that will not reduce the shear capacity of the studs.

APPENDIX A

Analysis of Bridge Components

Calculation of Tensile Force Needed to Be Transferred at Fracture

It was assumed that half of the entire weight of the bridge and half of the live load on the bridge would need to be resisted at fracture. These loads are calculated below:

Dead Load – Steel Box Girders

$$w_{girders} = 2 \times (109 \text{ in.}^2)(1 \text{ ft}^2/144 \text{ in.}^2)(0.490 \text{ kip/ft}^3)(1.15) = 0.853 \text{ kip/ft}$$

Notes: Multiplied by 2 to account for two girders. Cross-sectional area of one girder is 109 in.² Density of steel is 490 lb/ft³. The factor of 1.15 accounts for internal diaphragms, stiffeners, etc.

Dead Load – Deck Slab

$$w_{slab} = (280 \text{ in.})(8 \text{ in.} + 0.731 \text{ in.})(0.150 \text{ kip/ft}^3)(1 \text{ ft}^2/144 \text{ in.}^2) = 2.55 \text{ kip/ft}$$

Notes: Width of deck slab is 23 ft-4 in. = 280 in. (See Appendix B). Density of concrete is 150 lb/ft³. Slab thickness is 8 in., and 0.731 in. was added to account for extra concrete in the ribs of the permanent metal decking.

Dead Load – T501 Rails

$$w_{rails} = 2 \times (312 \text{ in.}^2)(1 \text{ ft}^2/144 \text{ in.}^2)(0.150 \text{ kip/ft}^3) = 0.65 \text{ kip/ft}$$

Notes: Multiplied by 2 to account for two rails. Cross-sectional area of one rail was calculated to be approximately 312 in.²

Live Load – Simulated Truck

Total truck load = 76 kips

Required Tensile Force

$$T = (w_{girders} + w_{slab} + w_{rails}) * L/2 + 76 \text{ kips}/2$$

$$T = (0.853 \text{ kip/ft} + 2.55 \text{ kip/ft} + 0.65 \text{ kip/ft})(118 \text{ ft} / 2) + 38 \text{ kip} = 277 \text{ kips}$$

$$T_{req'd} = 277 \text{ kips} \times 2.0 = 554 \text{ kips}$$

Notes: Half of the total dead load is equal to $wL/2$ and half of the truck is 38 kips.

The 277-kip force is multiplied by 2.0 for the dynamic effect. The span length of the FSEL test bridge is approximately 118 ft.

Calculation of Maximum Moment on the Bridge at Fracture

Dead Load – Mid-span Moment

$$M_{dead} = (w_{girders} + w_{slab} + w_{rails}) * L^2 / 8 = (0.853 \text{ kip/ft} + 2.55 \text{ kip/ft} + 0.65 \text{ kip/ft})(118 \text{ ft})^2 / 8$$

$$M_{dead} = 7048 \text{ kip-ft}$$

Live Load – Moment due to Truck

The distribution of the 76-kip truck load, the shear diagram and the moment diagram are shown in the figure below:

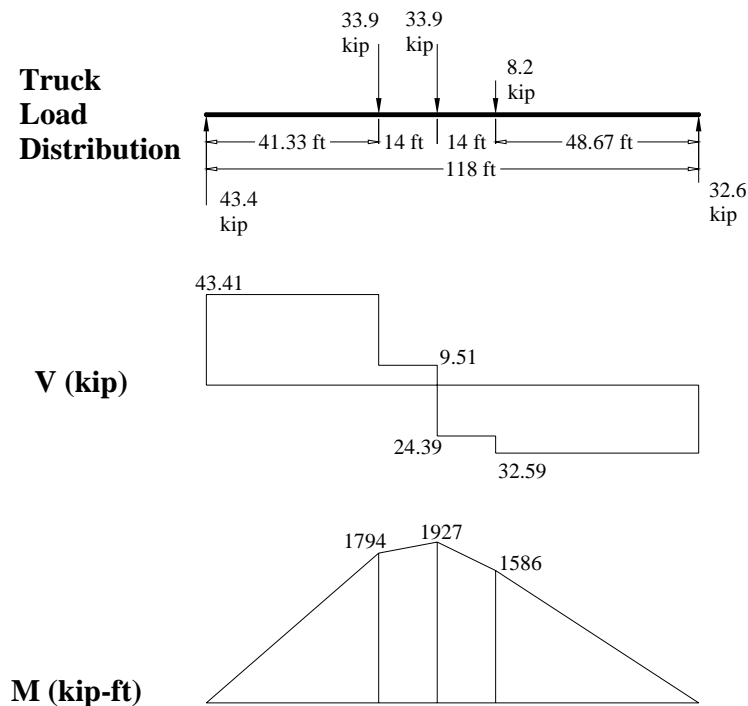


Figure A.1: Truck load distribution, shear diagram, and moment diagram

Check the total moment at the mid-span and the total moment at the point of maximum live load moment ($x = 55.33$ ft) to see which governs as maximum moment.

Mid-span Moment

$$M_{mid} = M_{DL} + M_{LL} = 7048 \text{ kip-ft} + 1838 \text{ kip-ft} = \mathbf{8886 \text{ kip-ft}}$$

Moment at $x = 55.33$ ft

$$w = w_{girders} + w_{slab} + w_{rails} = 0.853 \text{ kip/ft} + 2.55 \text{ kip/ft} + 0.65 \text{ kip/ft} = 4.05 \text{ kip/ft}$$

$$M_{DL, x=55.33 \text{ ft}} = wLx/2 - wx^2/2 = (4.05 \text{ kip/ft} * 118 \text{ ft} * 55.33 \text{ ft}/2) - (4.05 \text{ kip/ft} * (55.33 \text{ ft})^2/2)$$

$$M_{DL, x=55.33 \text{ ft}} = 7021 \text{ kip-ft}$$

$$M_{x=55.33 \text{ ft}} = M_{DL, x=55.33 \text{ ft}} + M_{LL} = 7021 \text{ kip-ft} + 1927 \text{ kip-ft} = \mathbf{8948 \text{ kip-ft (GOVERNS)}}$$

$$M_{max} = \mathbf{8948 \text{ kip-ft @ } x = 55.33 \text{ ft}}$$

$$M_{req'd} = 2.0 \times M_{max} = 2.0 \times 8948 \text{ kip-ft} = \mathbf{17,896 \text{ kip-ft}}$$

Analysis of Shear Studs

Analysis of the shear studs, calculation of the tensile capacity of a row of studs on the FSEL test bridge, and the required span length needed to resist the 554-kip force are covered in Chapter 2.

Analysis of Deck Slab

The deck slab was checked for bending capacity and shear capacity. These capacities were based on a 1-ft wide transverse deck section as shown in the figure below:

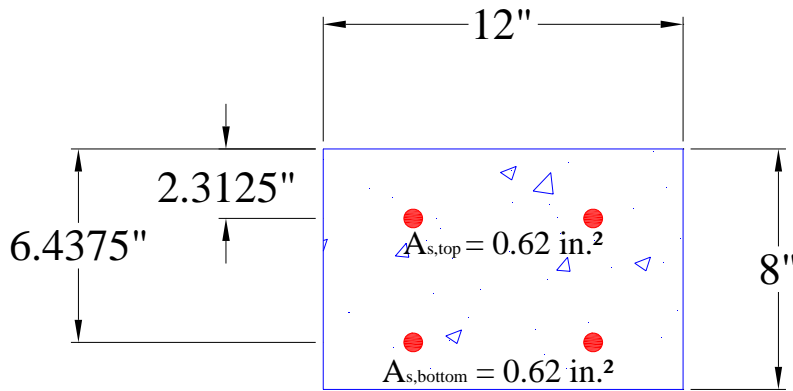


Figure A.2: Deck slab – 1-ft wide section

Positive Bending Capacity

The assumed strain and stress failure profile are shown in the figure below:

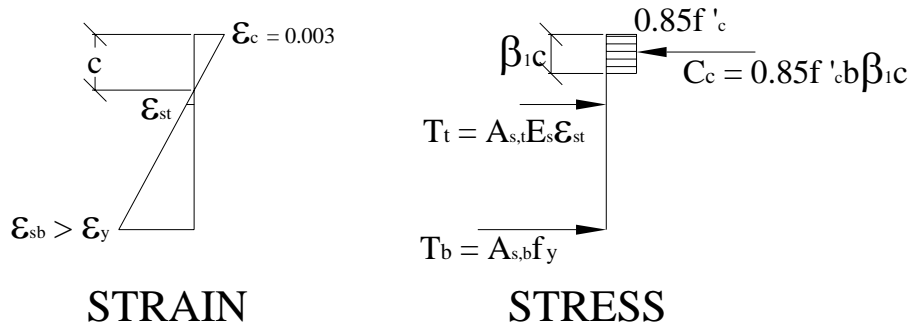


Figure A.3: Strain and stress profiles at positive moment capacity

Assumptions: Ultimate strain of concrete is 0.003 in./in. (ACI 318-05). Bottom steel reinforcement has yielded prior to failure. Top reinforcement is in tension. Concrete strength is 4 ksi (corresponds to minimum required strength for TxDOT Class S).

Let $C = T$

$$C = 0.85f'_c \beta_1 cb = 0.85*(4 \text{ ksi})*(0.85)*(12 \text{ in.})c = (34.68 \text{ kip/in.})*c$$

Note: $\beta_1 = 0.85$ for 4 ksi concrete.

$$\epsilon_{s,bottom} = (0.003 \text{ in./in.})*(6.4375 \text{ in.} - c)/c$$

$$\epsilon_{s,top} = (0.003 \text{ in./in.}) * (2.3125 \text{ in.} - c) / c$$

$$T_{bottom} = A_{s,bottom} f_y = (0.62 \text{ in.}^2)(60 \text{ ksi}) = 37.2 \text{ kips}$$

$$T_{top} = A_{s,top} \epsilon_{s,top} E_s = (0.62 \text{ in.}^2)(29,0000 \text{ ksi}) * \epsilon_{s,top} = (17,980 \text{ kips}) * \epsilon_{s,top}$$

$$(34.68 \text{ kip/in.}) * c = 37.2 \text{ kip} + (17,980 \text{ kips}) * \epsilon_{s,top}$$

$$(34.68 \text{ kip/in.}) * c = 37.2 \text{ kip} + (17,980 \text{ kips}) * (0.003 \text{ in./in.}) * (2.3125 \text{ in.} - c) / c$$

Iterate until the neutral axis depth is found.

Solving: $c = 1.67 \text{ in.}$

$$\epsilon_{s,bottom} = 0.00856 > \text{Yield strain} (= 0.00207 \text{ for } 60 \text{ ksi})$$

$$\epsilon_{s,top} = 0.00115 < \text{Yield strain}$$

$$C = 57.9 \text{ kips}$$

$$T_{top} = 20.7 \text{ kips}$$

Take moments about centroid to solve for nominal moment capacity

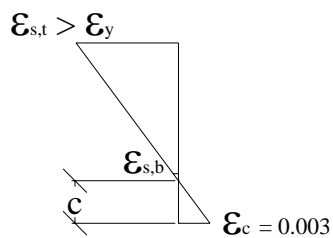
$$M_n^+ = C * (4 \text{ in.} - \beta_1 c / 2) - T_{top} * (4 \text{ in.} - 2.3125 \text{ in.}) + T_{bottom} * (6.4375 \text{ in.} - 4 \text{ in.})$$

$$M_n^+ = (57.9 \text{ kip}) * (4 \text{ in.} - 0.85 * 1.67 \text{ in.} / 2) - 20.7 \text{ kip} * (1.6875 \text{ in.}) + 37.2 \text{ kip} * (2.4375 \text{ in.})$$

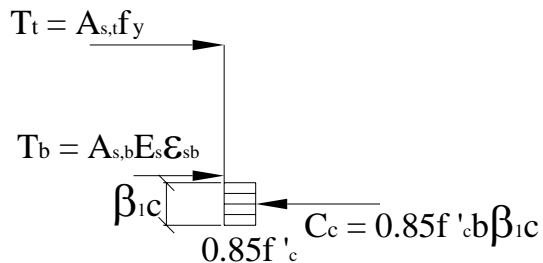
$$M_n^+ = 246 \text{ kip-in.} = \mathbf{20.5 \text{ kip-ft}}$$

Negative Bending Capacity

The assumed strain and stress failure profile are shown in the figure below:



STRAIN



STRESS

Figure A.4: Strain and stress profiles at negative moment capacity

Assumptions: Ultimate strain of concrete is 0.003 in./in. (ACI 318-05). Top steel reinforcement has yielded prior to failure. Bottom reinforcement is in tension. Concrete strength is 4 ksi (corresponds to minimum required strength for TxDOT Class S).

Let $C = T$

$$C = 0.85f_c' \beta_1 cb = 0.85*(4 \text{ ksi})(0.85)(12 \text{ in.})c = (34.68 \text{ kip/in.}) * c$$

Note: $\beta_1 = 0.85$ for 4 ksi concrete.

$$\epsilon_{s,bottom} = (0.003 \text{ in./in.}) * (1.5625 \text{ in.} - c) / c$$

$$\epsilon_{s,top} = (0.003 \text{ in./in.}) * (5.6875 \text{ in.} - c) / c$$

$$T_{bottom} = A_{s,bottom} \epsilon_{s,bottom} E_s = (0.62 \text{ in.}^2)(29,0000 \text{ ksi}) * \epsilon_{s,bottom} = (17,980 \text{ kips}) * \epsilon_{s,bottom}$$

$$T_{top} = A_{s,top} f_y = (0.62 \text{ in.}^2)(60 \text{ ksi}) = 37.2 \text{ kips}$$

$$(34.68 \text{ kip/in.}) * c = (17,980 \text{ kips}) * \epsilon_{s,bottom} + 37.2 \text{ kips}$$

$$(34.68 \text{ kip/in.}) * c = (17,980 \text{ kips}) * (0.003 \text{ in./in.}) * (1.5625 \text{ in.} - c) / c + 37.2 \text{ kips}$$

Iterate until the neutral axis depth is found.

Solving: $c = 1.34 \text{ in.}$

$$\epsilon_{s,bottom} = 0.00051 < \text{Yield strain}$$

$$\epsilon_{s,top} = 0.00977 > \text{Yield strain (= 0.00207 for 60 ksi)}$$

$$C = 46.3 \text{ kips}$$

$$T_{bottom} = 9.1 \text{ kips}$$

Take moments about centroid to solve for nominal moment capacity

$$M_n^- = C*(4 \text{ in.} - \beta_1 c / 2) + T_{top}*(4 \text{ in.} - 2.3125 \text{ in.}) - T_{bottom}*(6.4375 \text{ in.} - 4 \text{ in.})$$

$$M_n^- = (46.3 \text{ kip}) * (4 \text{ in.} - 0.85 * 1.34 \text{ in.} / 2) + 37.2 \text{ kip} * (1.6875 \text{ in.}) - 9.1 \text{ kip} * (2.4375 \text{ in.})$$

$$M_n^- = 199 \text{ kip-in.} = \mathbf{16.6 \text{ kip-ft}}$$

Bending Capacity – Shear across Deck Slab

The assumed deck slab deflected shape and bending moment diagram at fracture is shown in the figure below:

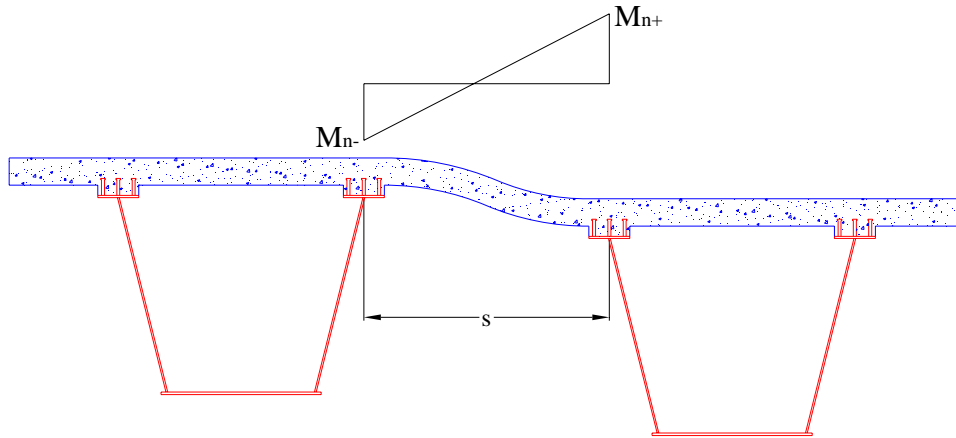


Figure A.5: Assumed bending moment in deck slab at ultimate state

$$V = (M_n^+ + M_n^-) / s = (20.5 \text{ kip-ft} + 16.6 \text{ kip-ft}) / 6 \text{ ft} = \mathbf{6.2 \text{ kips}}$$

Note: The spacing, s , is equal to 6 ft.

Thus, at the flexural capacity the deck slab can transfer 6.2 kips across a 1-ft wide section of the slab. Therefore, the total length required to transfer the 554-kip force is:

$$L = 554 \text{ kips} * (1 \text{ ft} / 6.2 \text{ kips}) = 89.4 \text{ ft}$$

$$89.4 \text{ ft} / 118 \text{ ft} = \mathbf{75.7 \% \text{ of the span length}}$$

Shear Capacity

The shear capacity was calculated using the ACI equation for shear shown below. The capacity was again based on a 1-ft wide transverse deck section. The depth used in this equation is the depth to the centroid of the tension reinforcement (= 4.375 in.).

$$V_c = 2 * (f_c')^{0.5} * b * d = 2 * (4000 \text{ psi})^{0.5} * (12 \text{ in.}) * (4.375 \text{ in.})$$

$$V_c = \mathbf{6.64 \text{ kips}}$$

Thus, at the shear capacity the deck slab can transfer 6.64 kips across a 1-ft wide section of the slab. The total length required to transfer the 554-kip force is:

$$L = 554 \text{ kips} * (1 \text{ ft} / 6.64 \text{ kips}) = 83.4 \text{ ft}$$

$$83.4 \text{ ft} / 118 \text{ ft} = \mathbf{70.7 \% \text{ of the span length}}$$

Therefore, the deck slab capacity is governed by the flexural behavior of the slab. Approximately 76% of the span length is required to transfer the 554-kip force.

Analysis of Composite Section

Calculate the plastic moment capacity of the remaining box girder. The composite section of the remaining girder is shown below:

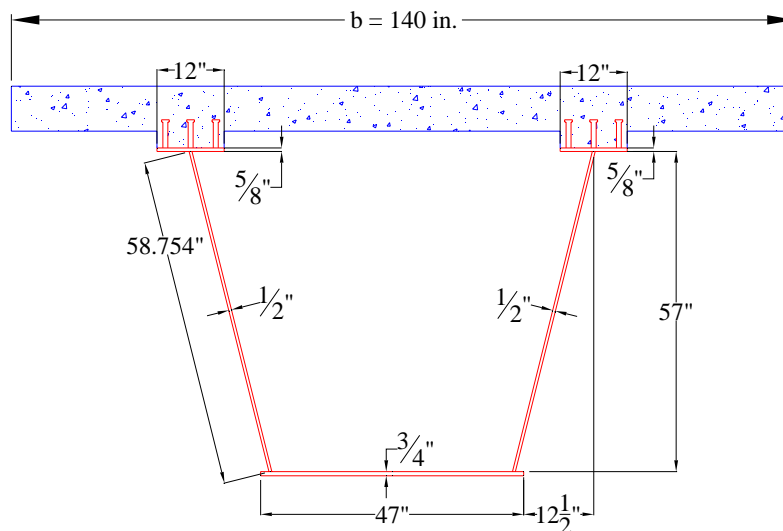


Figure A.6: Composite section

Find the plastic neutral axis by setting $T = C$:

$$T = A_s F_y = (109 \text{ in.}^2)(50 \text{ ksi}) = 5450 \text{ kips}$$

$$C = 0.85 f_c' t_s b_{eff} = 0.85 * (4 \text{ ksi})(8 \text{ in.})(140 \text{ in.}) = 3808 \text{ kips}$$

$T > C$... Therefore, plastic neutral axis is in the girder.

$$C_{steel} = (A_s F_y - C_{conc}) / 2 = (5450 \text{ kip} - 3808 \text{ kip}) / 2 = 821 \text{ kips}$$

Note: This equation determines the compressive force needed to be developed in the steel section in order to achieve equilibrium ($C = T$).

$$C_{steel, \text{ top flanges}} = 2 \times t_f b_f F_y = 2 \times (0.625 \text{ in.})(12 \text{ in.})(50 \text{ ksi}) = 750 \text{ kips}$$

Note: This calculation shows that the top flanges can resist 750 kips in compression. This is less than the required 821 kips, thus the PNA is in the web.

Let x = the location of the neutral axis below the top flange as shown in the figure below:

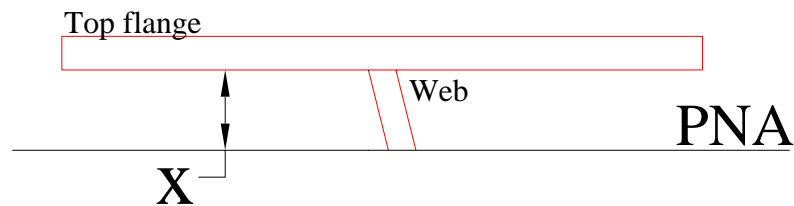


Figure A.7: Plastic neutral axis location

$$x = (821 \text{ kips} - 750 \text{ kips}) / [2 \times (0.5 \text{ in.})(17/16)^{1/2}(50 \text{ ksi})] = 1.38 \text{ in.}$$

Notes: This equation is determining the depth of the neutral axis in the webs. The factor of 2 accounts for the two webs. The $(17/16)^{1/2}$ factor is based on the geometry of the web.

Therefore:

$$C_{concrete} = 3808 \text{ kips}$$

$$C_{steel, \text{ top flanges}} = 750 \text{ kips}$$

$$C_{steel, \text{ web}} = 71 \text{ kips}$$

$$T_{web} = A_{web, \text{ tension}} F_y = 2 \times (0.5 \text{ in.})[58.754 \text{ in.} - (17/16)^{1/2}(1.38 \text{ in.})](50 \text{ ksi}) = 2866.5 \text{ kips}$$

$$T_{bottom \text{ flange}} = A_{bottom \text{ flange}} F_y = (47 \text{ in.})(0.75 \text{ in.})(50 \text{ ksi}) = 1762.5 \text{ kips}$$

Take moments about the PNA to get the nominal plastic moment capacity:

$$M_{bot \text{ flange}} = T_{bot \text{ flange}} \times (3/8 \text{ in.} + 57 \text{ in.} - 1.38 \text{ in.}) = 98,695 \text{ kip-in.}$$

$$M_{web, \text{ tens}} = T_{web} \times [(57 \text{ in.} - 1.38 \text{ in.}) / 2] = 79,721 \text{ kip-in.}$$

$$M_{web,comp} = C_{steel,web} \times (1.38 \text{ in.} / 2) = 49 \text{ kip-in.}$$

$$M_{top\ flange} = C_{steel, top\ flanges} \times (5/16 \text{ in.} + 1.38 \text{ in.}) = 1,268 \text{ kip-in.}$$

$$M_{concrete} = C_{conc} \times (4 \text{ in.} + 3 \text{ in.} + 5/8 \text{ in.} + 1.38 \text{ in.}) = 34,282 \text{ kip-in.}$$

Note: The 3-in. term added in the moment arm accounts for the haunch which puts the deck slab 3 in. above the top of the steel girder.

Thus, $M_p = 98,695 \text{ kip-in.} + 79,721 \text{ kip-in.} + 49 \text{ kip-in.} + 1,268 \text{ kip-in.} + 34,282 \text{ kip-in.}$

$$M_p = 214,015 \text{ kip-in.} = \mathbf{17,835 \text{ kip-ft}}$$

Recall that $M_{max} = 17,896 \text{ kip-ft}$ (with the amplification factor of 2.0 for dynamic effect). The plastic moment capacity appears to have just enough capacity to resist the required moment at fracture.

APPENDIX B

FSEL Bridge Deck Details and TxDOT Stud Detail

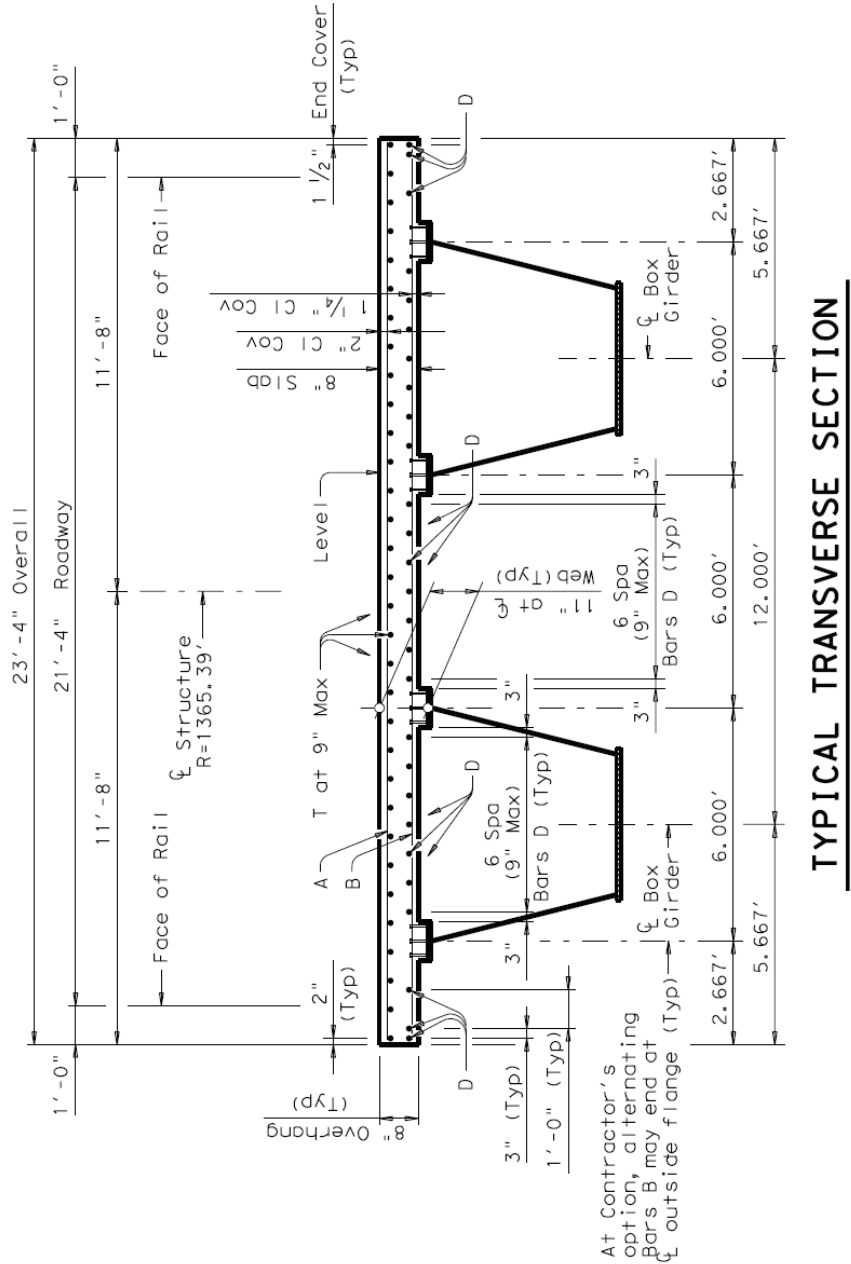


Figure B.1: FSEL bridge deck – typical transverse section

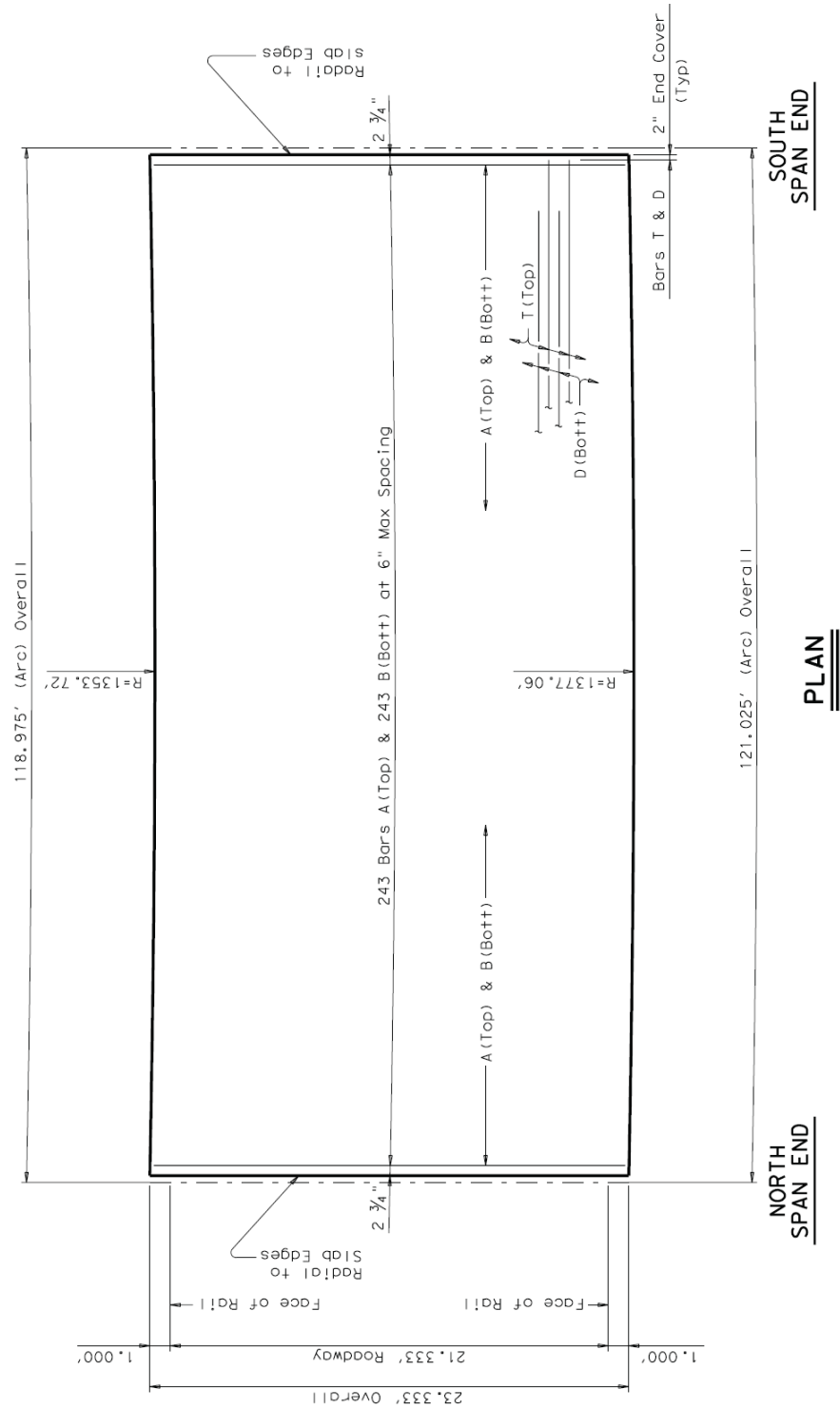


Figure B.2: FSEL bridge deck – plan view

BAR TABLE	
BAR	SIZE
A	#5
B	#5
D	#5
T	#4

FOR CONTRACTOR'S INFORMATION ONLY ESTIMATED QUANTITIES	
Class "S" Concrete	73.6 CY
Reinforcing Steel	17,837 Lb
Rail (T501)	240.00 LF

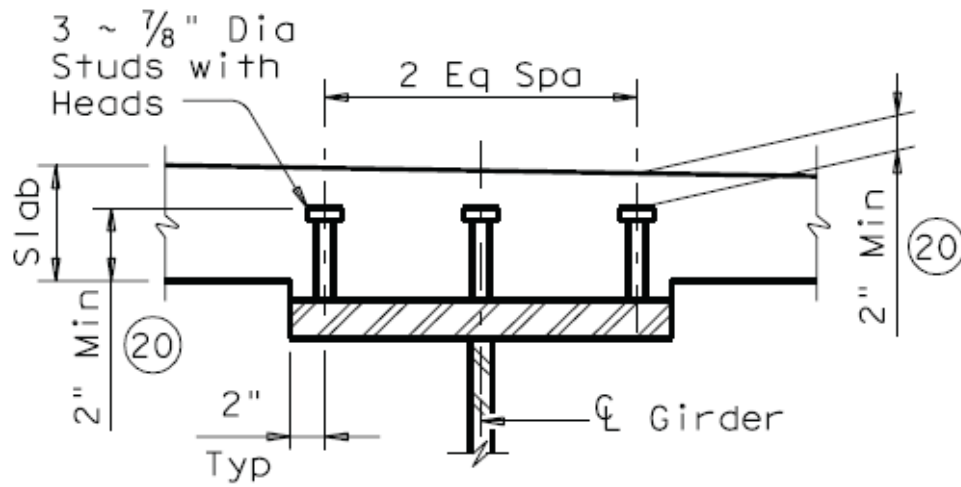
Min lap length when
required are:

#4 ~ 1'-5"
#5 ~ 1'-9"

GENERAL NOTES:

Construct slab in accordance with 2004 TxDOT Standard Specifications unless noted otherwise.
Use Class "S" Concrete for slab (f'c= 4,000 psi Min, 4,500 psi Max).
Use Grade 60 reinforcement.
Slab Thickness tolerance is + 1/2", -0".
Form deck with permanent metal deck forms. See TxDOT standard PMDF for details.
See TxDOT standard T501 for rail details.
Provide a broom finish for slab (saw-cut grooves are not required).

Figure B.3: Notes for FSEL bridge deck drawings (Fig. B.1-B.2)



STUD CONNECTOR DETAILS (21)

Weld studs to the flange in accordance with AWS D1.5.

Figure B.4: TxDOT typical stud connector detail for three studs (TxDOT Bridge Standard Drawings: Miscellaneous Details (Steel Girders and Beams), 2006)

APPENDIX C

Complete Test Specimen Details

One Stud - No Haunch

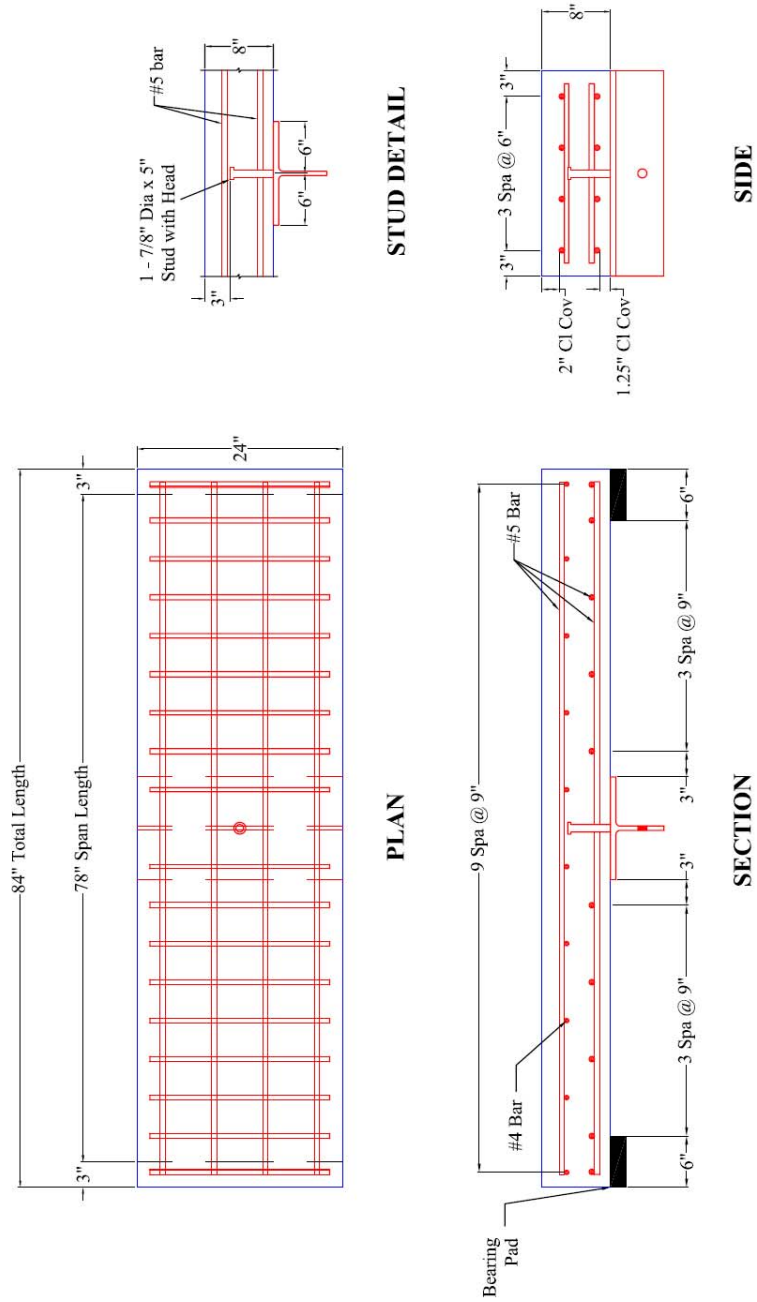


Figure C.1: Specimen 0-1 (a,b)

Two Studs - No Haunch

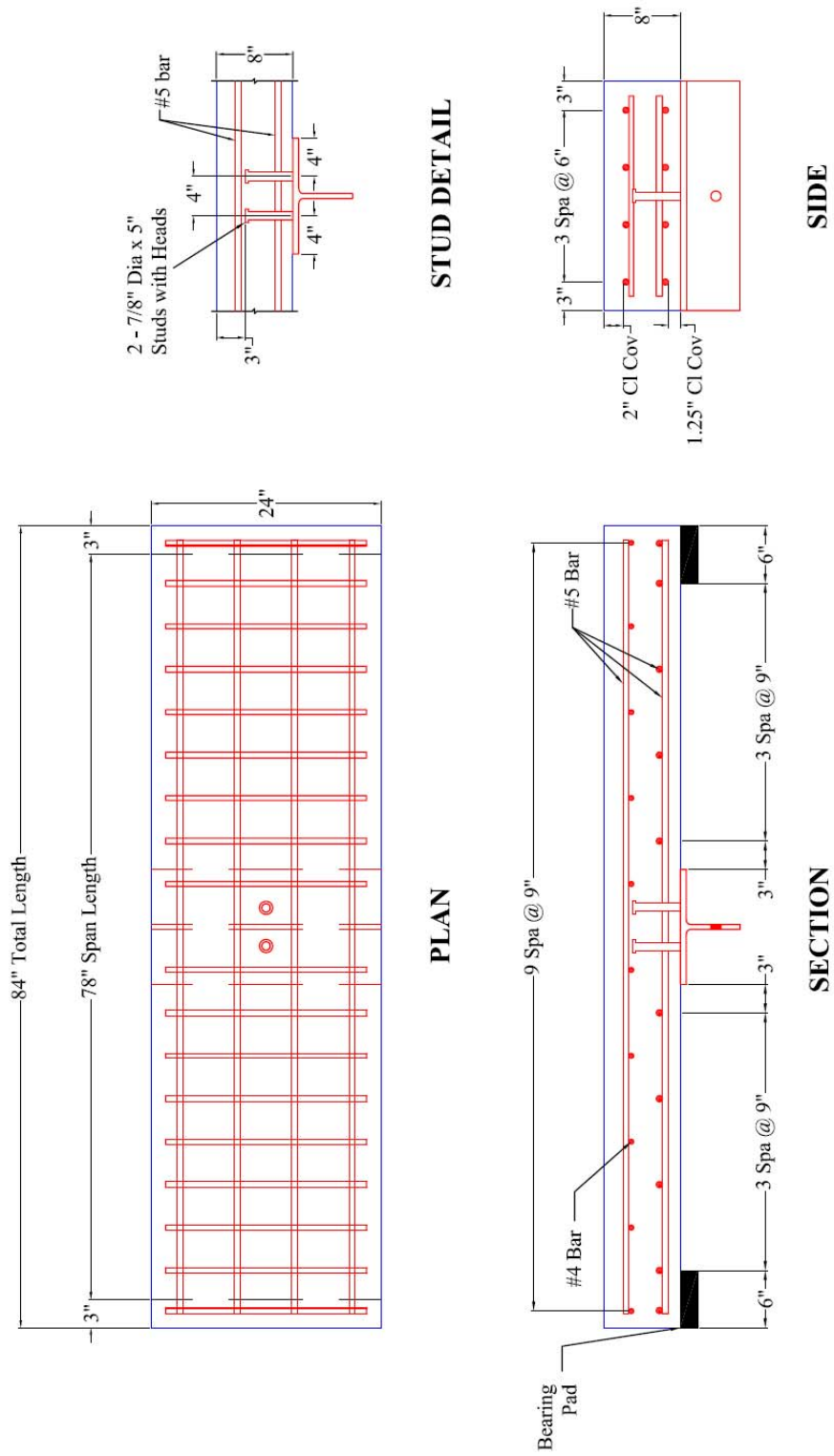


Figure C.2: Specimen 0-2 (a,b)

Three Studs - No Haunch

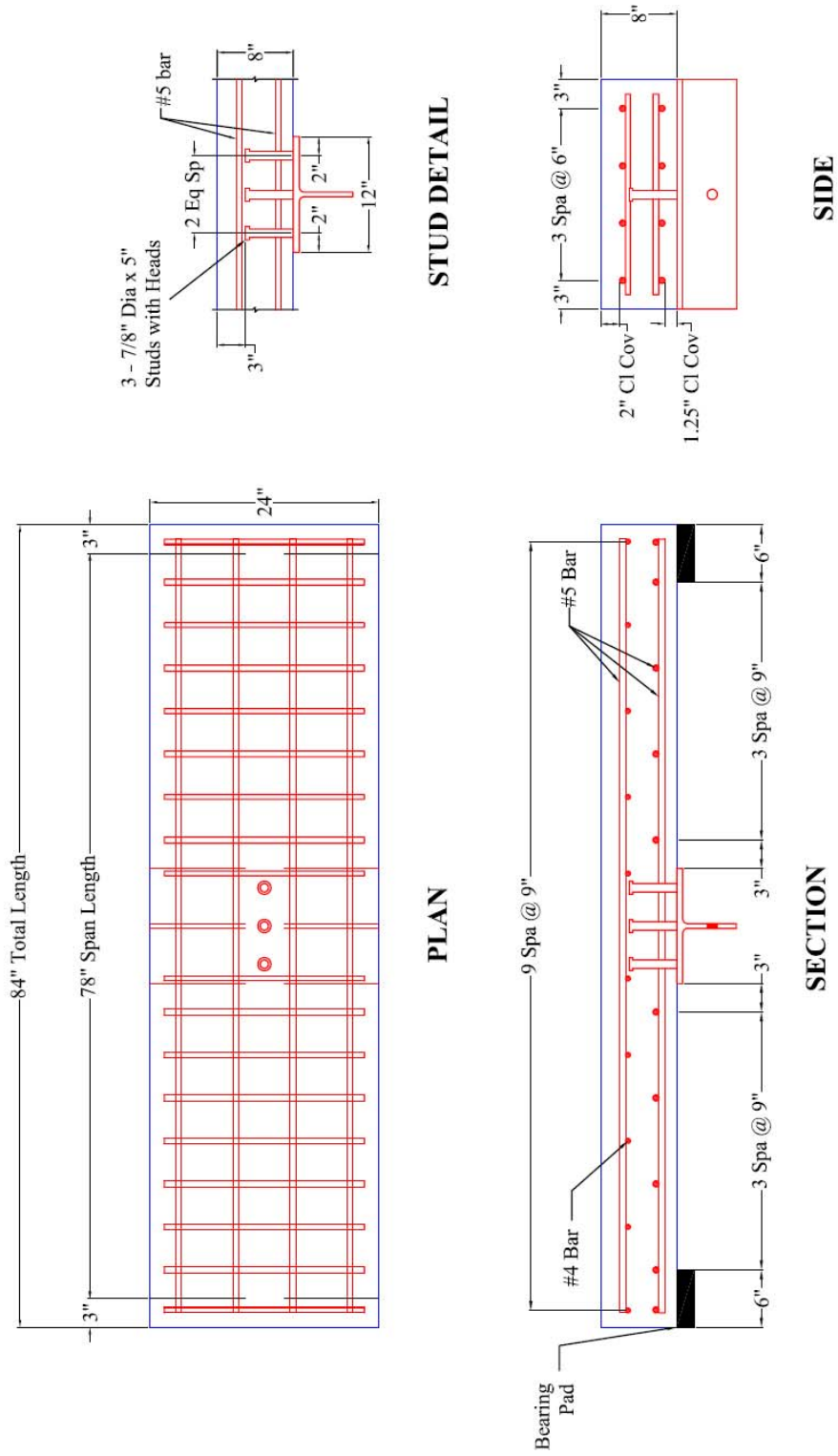


Figure C.3: Specimen 0-3 (a,b)

One Stud - 3" Haunch

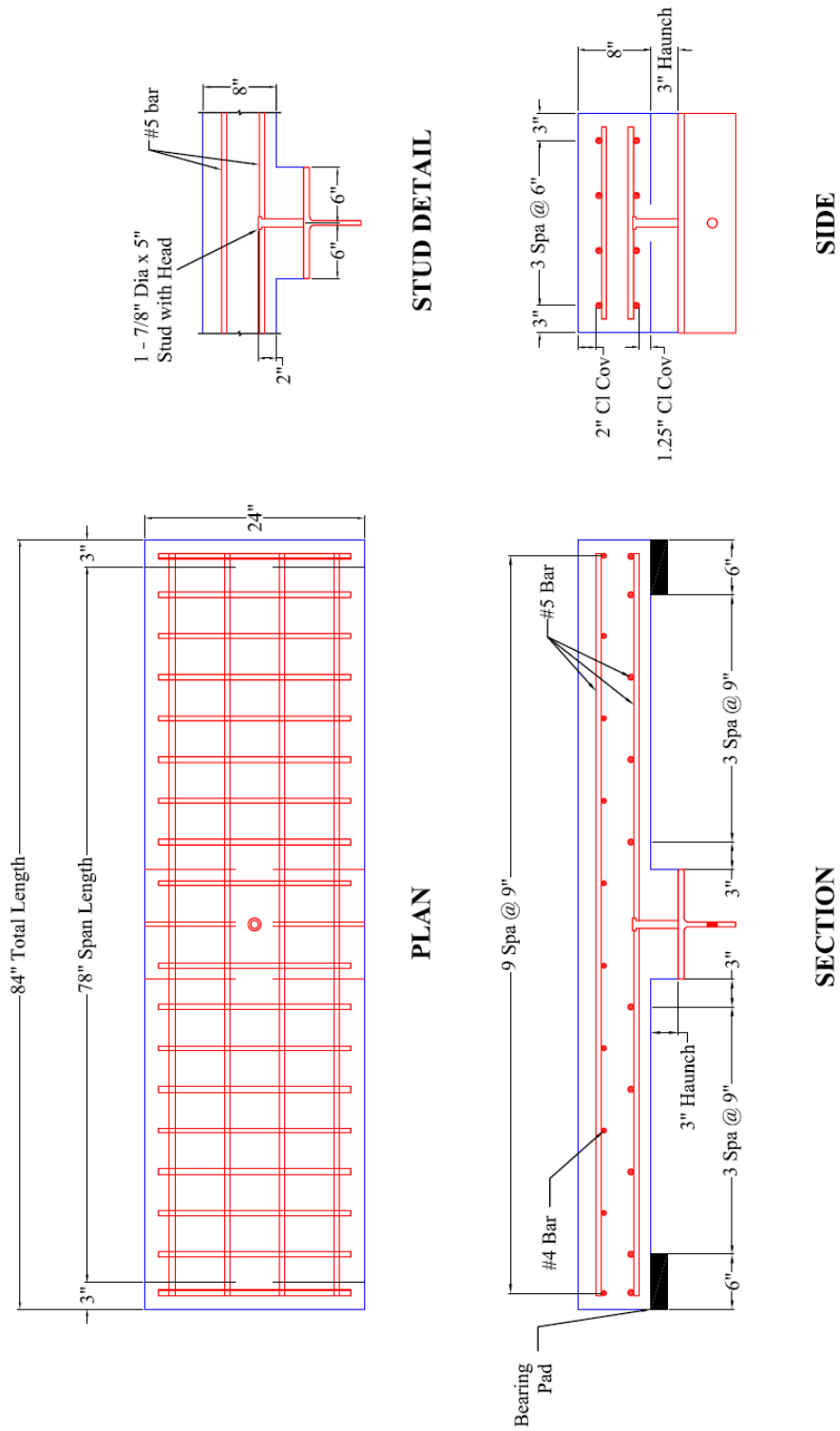


Figure C.4: Specimen 3-1 (a,b)

Two Studs - 3" Haunch

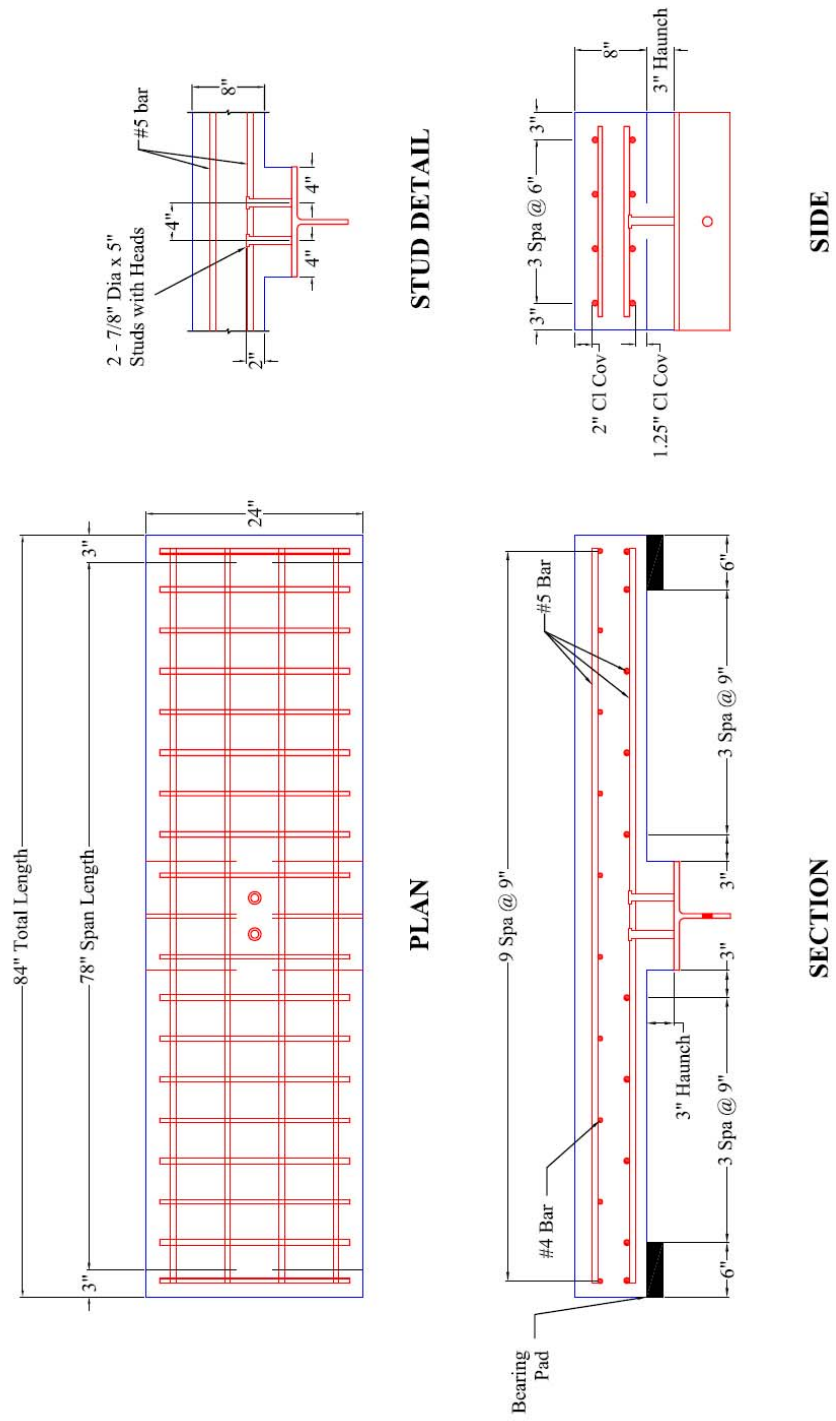


Figure C.5: Specimen 3-2 (a,b)

APPENDIX D

Test Specimens – Cracking, Yield and Ultimate Load

Slab Details

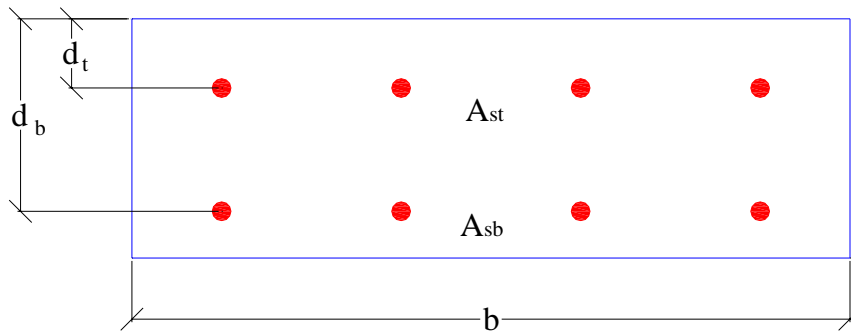


Figure D.1: Test specimen – slab cross section

Where:

b	= 24 in.
h	= 8 in.
d_t	= 2.3125 in.
d_b	= 6.4375 in.
A_{st}	= 1.23 in. ²
A_{sb}	= 1.23 in. ²
f_c'	= 6,000 psi (from cylinder tests)
f_y	= 60,000 psi

Calculation of Cracking Load

$$M_{cr} = \frac{\sigma_{cr} I}{c} = \frac{7.5 \sqrt{f_c'} I}{c}$$

$$I = 1/12 * (24 \text{ in.}) (8 \text{ in.})^3 = 1024 \text{ in.}^4$$

$$c = 4 \text{ in.}$$

$$\sigma_{cr} = 7.5(6000 \text{ psi})^{1/2} = 581 \text{ psi}$$

$$M_{cr} = (581 \text{ psi})(1024 \text{ in.}^4) / (4 \text{ in.}) = 148,723 \text{ lb-in.} = \mathbf{12.4 \text{ kip-ft}}$$

For specimens with no haunch, cracking will occur at mid-span. However, for specimens with a haunch, cracking will not occur at the mid-span due to the increased depth of the slab at this point. Rather cracking will occur first at the edges of the haunch where the depth returns to 8 in. (Note: Span length is 6.5 ft)

No haunch

$$M_{mid} = PL/4$$

$$P_{cr, \text{ no haunch}} = (M_{cr} \times 4) / L = (12.4 \text{ kip-ft} \times 4) / (6.5 \text{ ft}) = \mathbf{7.63 \text{ kips}}$$

3 in. Haunch

Cracking occurs where depth returns to 8 in. This is a distance of 33 in. from the support reaction. (Note: Mid-span is 39 in. from support reaction)

$$M_x = (P / 2)(x)$$

$$P_{cr, 3'' \text{ haunch}} = (2M_{cr}) / x = (2)(12.4 \text{ kip-ft}) / (33/12 \text{ ft}) = \mathbf{9.02 \text{ kips}}$$

Calculation of Yield Load

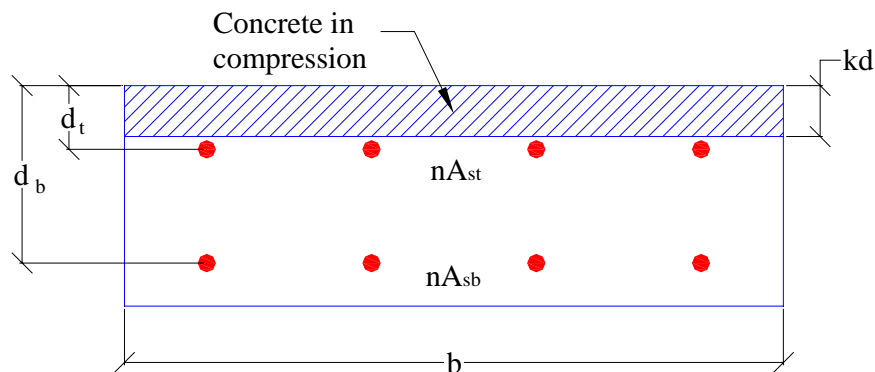


Figure D.2: Assumed location of neutral axis at yield load

By setting the first moment of area of the concrete compression block and the first moment of area of the steel reinforcement equal to each other, the depth of the neutral axis, kd , is determined:

$$b(kd)\left(\frac{kd}{2}\right) = nA_{sb}(d_b - kd) + nA_{st}(d_t - kd)$$

$$n = E_s / E_c = E_s / 57,000(f_c')^{1/2} = (29,000,000 \text{ psi}) / [57,000 \times (6000 \text{ psi})^{1/2}] = 6.57$$

$$(24 \text{ in.})(kd)^2 / 2 = (6.57)(1.23 \text{ in.}^2)(6.4375 \text{ in.} - kd) + (6.57)(1.23 \text{ in.}^2)(2.3125 \text{ in.} - kd)$$

Solving... **$kd = 1.85 \text{ in.}$**

The assumed strain and stress profiles are shown below. This concrete stress distribution is acceptable as long as $f_c < 0.7f_c'$.

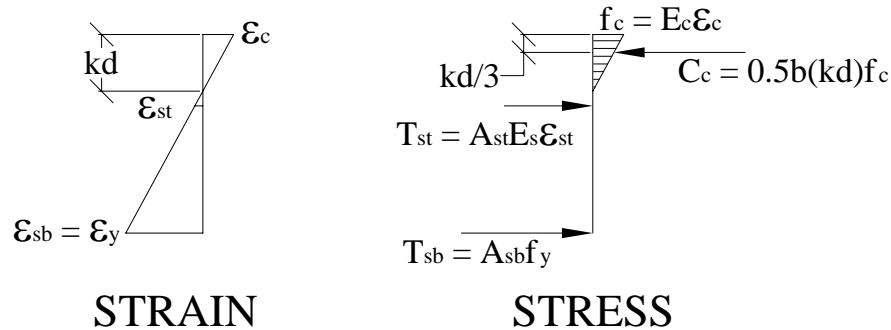


Figure D.3: Assumed strain and stress profile at yielding

$$\epsilon_c = (kd)\epsilon_y / (d_b - kd) = (1.85 \text{ in.})(0.00207) / (6.4375 \text{ in.} - 1.85 \text{ in.}) = 0.000832 \text{ in./in.}$$

$$f_c = E_c \epsilon_c = 57(6000 \text{ psi})^{1/2}(0.000832 \text{ in./in.}) = 3.67 \text{ ksi} < 0.7f_c' (= 4.2 \text{ ksi})$$

$$\epsilon_{s,top} = \epsilon_c(d_t - kd) / kd = (0.000832)(2.3125 \text{ in.} - 1.85 \text{ in.}) / (1.85 \text{ in.}) = 0.00021 \text{ in./in.}$$

$$C_c = (1/2)f_c b(kd) = 0.5(3.67 \text{ ksi})(24 \text{ in.})(1.85 \text{ in.}) = 81.3 \text{ kips}$$

$$T_{s,top} = A_{s,top} \epsilon_{s,top} E_s = (1.23 \text{ in.}^2)(0.00021)(29,000 \text{ ksi}) = 7.5 \text{ kips}$$

$$T_{s,bottom} = A_{s,bottom} f_y = (1.23 \text{ in.}^2)(60 \text{ ksi}) = 73.8 \text{ kips}$$

Take moments about centroid to solve for yield moment:

$$M_y = C_c*(4 \text{ in.} - kd/3) - T_{top}*(4 \text{ in.} - 2.3125 \text{ in.}) + T_{bottom}*(6.4375 \text{ in.} - 4 \text{ in.})$$

$$M_y = (81.3 \text{ kips}) \cdot (4 \text{ in.} - 1.85 \text{ in.}/3) - 7.5 \text{ kips} \cdot (1.6875 \text{ in.}) + 73.8 \text{ kips} \cdot (2.4375 \text{ in.})$$

$$M_y = 442 \text{ kip-in.} = \mathbf{36.9 \text{ kip-ft}}$$

$$P_y = (M_y \times 4) / L = (36.9 \text{ kip-ft} \times 4) / (6.5 \text{ ft}) = \mathbf{22.7 \text{ kips}}$$

Calculation of Ultimate Load

The assumed strain and stress failure profile are shown in the figure below:

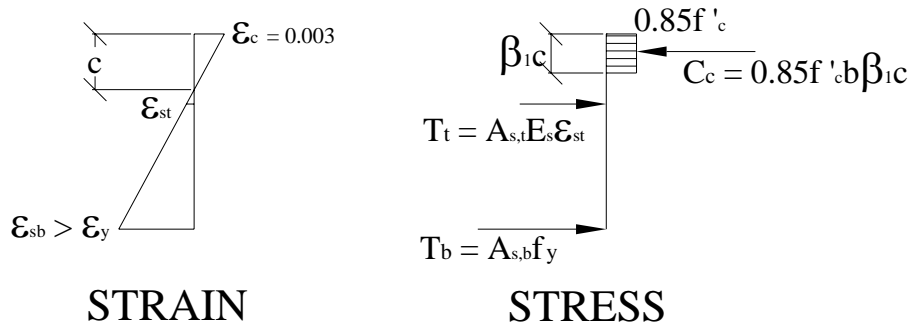


Figure D.4: Assumed strain and stress profiles at ultimate moment capacity

Assumptions: Ultimate strain of concrete is 0.003 in./in. Bottom steel reinforcement has yielded prior to failure. Top reinforcement is in tension. Concrete strength is 6 ksi (corresponds to cylinder strength at halfway point in testing program).

Let $C = T$

$$C = 0.85f'_c \beta_1 c b = 0.85 \cdot (6 \text{ ksi}) \cdot (0.75) \cdot (24 \text{ in.}) \cdot c = (91.8 \text{ kip/in.}) \cdot c$$

Note: $\beta_1 = 0.75$ for 6 ksi concrete.

$$\epsilon_{s,bottom} = (0.003 \text{ in./in.}) \cdot (6.4375 \text{ in.} - c) / c$$

$$\epsilon_{s,top} = (0.003 \text{ in./in.}) \cdot (2.3125 \text{ in.} - c) / c$$

$$T_{bottom} = A_{s,bottom} f_y = (1.23 \text{ in.}^2) \cdot (60 \text{ ksi}) = 73.8 \text{ kips}$$

$$T_{top} = A_{s,top} \epsilon_{s,top} E_s = (1.23 \text{ in.}^2) \cdot (29,000 \text{ ksi}) \cdot \epsilon_{s,top} = (35,670 \text{ kips}) \cdot \epsilon_{s,top}$$

$$(91.8 \text{ kip/in.}) \cdot c = 73.8 \text{ kips} + (35,670 \text{ kips}) \cdot \epsilon_{s,top}$$

$$(91.8 \text{ kip/in.}) * c = 73.8 \text{ kips} + (35,670 \text{ kips}) * (0.003 \text{ in./in.}) * (2.3125 \text{ in.} - c) / c$$

Iterate until the neutral axis depth is found.

$$\text{Solving: } c = 1.47 \text{ in.}$$

$$\epsilon_{s,bottom} = 0.0101 > \text{Yield strain (} = 0.00207 \text{ for 60 ksi)}$$

$$\epsilon_{s,top} = 0.0017 < \text{Yield strain}$$

$$C = 135.0 \text{ kips}$$

$$T_{top} = 61.2 \text{ kips}$$

Take moments about centroid to solve for nominal moment capacity.

$$M_n = C * (4 \text{ in.} - \beta_1 c / 2) - T_{top} * (4 \text{ in.} - 2.3125 \text{ in.}) + T_{bottom} * (6.4375 \text{ in.} - 4 \text{ in.})$$

$$M_n = (135 \text{ kip}) * (4 \text{ in.} - 0.75 * 1.47 \text{ in.} / 2) - 61.2 \text{ kip} * (1.6875 \text{ in.}) + 73.8 \text{ kip} * (2.4375 \text{ in.})$$

$$M_n = 542 \text{ kip-in.} = \mathbf{45.2 \text{ kip-ft}}$$

$$P_n = (M_n \times 4) / L = (45.2 \text{ kip-ft} \times 4) / (6.5 \text{ ft}) = \mathbf{27.8 \text{ kips}}$$

APPENDIX E

Predicted Tensile Capacity of Test Specimens

The predicted capacities were calculated using Appendix D of the ACI 318 Building Code. The following failure methods must be checked for each of the six unique test specimens: steel fracture, concrete breakout, and stud pullout.

Stud Details

$$h = 5 \text{ in.}$$

$$t_{head} = 0.375 \text{ in.}$$

$$h_{ef} = 4.625 \text{ in.}$$

$$d_{shaft} = 0.875 \text{ in.}$$

$$d_{head} = 1.375 \text{ in.}$$

$$f_y = 51 \text{ ksi (from mill test reports – See Appendix F)}$$

$$f_u = 66 \text{ ksi (from mill test reports – See Appendix F)}$$

Specimens with No Haunch

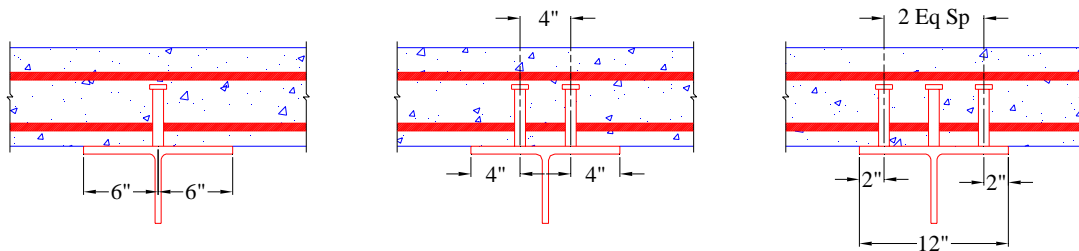


Figure E.1: Stud details for specimens with no haunch

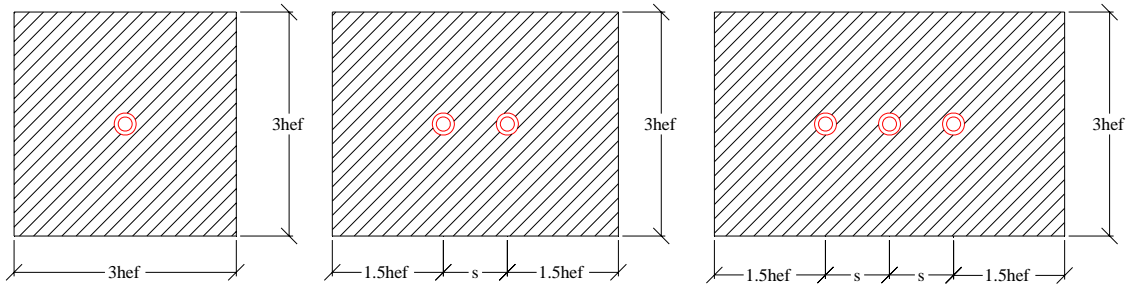


Figure E.2: Concrete breakout – projected failure areas for specimens with no haunch (A_{Nc})

No Haunch – One Stud

Steel Strength:

$$N_{sa} = nA_{se}f_{uta} = (1)(\pi/4)(0.875 \text{ in.})^2(66 \text{ ksi}) = \mathbf{39.7 \text{ kips}}$$

Note: f_{uta} = tensile strength of the stud; A_{se} = cross-sectional area of stud shaft

Concrete Breakout:

$$N_{cb} = [A_{Nc} / A_{Nco}] \psi_{ed,N} \psi_{c,N} N_b$$

Note: N_{cb} is the concrete breakout strength

$$A_{Nc} = 9h_{ef}^2 = 9(4.625 \text{ in.})^2 = 192.5 \text{ in.}^2$$

Note: A_{Nc} is the projected failure area of the stud

$$A_{Nco} = 9h_{ef}^2 = 9(4.625 \text{ in.})^2 = 192.5 \text{ in.}^2$$

Note: A_{Nco} is the projected failure area of one stud with no edge or group effects

$$\psi_{ed,N} = 1.0 \text{ (No edge effects)}$$

Note: $\psi_{ed,N}$ is a modification factor for edge effects (applied when $c_{a,min} < 1.5h_{ef}$)

$$\psi_{c,N} = 1.0 \text{ (Cracking assumed to occur)}$$

Note: $\psi_{c,N}$ is a modification factor for cracking (= 1.25 when analysis indicates no cracking; otherwise = 1.0)

$$N_b = k_c(f_c')^{1/2} h_{ef}^{1.5} = (24)(6,000 \text{ psi})^{1/2}(4.625 \text{ in.})^{1.5}(1 \text{ kip} / 1000 \text{ lb}) = 18.5 \text{ kips}$$

Note: $f_c' = 6000$ psi based on cylinder tests at midpoint of testing program

$k_c = 24$ for all cast-in headed anchors

$$N_{cb} = [192.5 \text{ in.}^2 / 192.5 \text{ in.}^2](1.0)(1.0)(18.5 \text{ kip}) = \mathbf{18.5 \text{ kips}}$$

Pullout:

$$N_{pn} = \psi_{c,P} 8 A_{brg} f_c' = (1.0)(8)(0.884 \text{ in.}^2)(6 \text{ ksi}) = \mathbf{42.4 \text{ kips}}$$

Note: A_{brg} is the bearing area of the stud head. It is equal to the area of the stud head minus the area of the stud shaft ($= \pi/4 * [(1.375 \text{ in.})^2 - (0.875 \text{ in.})^2] = 0.884 \text{ in.}^2$). $\psi_{c,P}$ is a modification factor for cracking ($= 1.4$ if no cracking; otherwise $= 1.0$)

Therefore, concrete breakout failure governs with $N_{cb} = 18.5 \text{ kips}$

No Haunch – Two Studs

Steel Strength:

$$N_{sa} = n A_{sef} f_{uta} = (2)(\pi/4)(0.875 \text{ in.})^2(66 \text{ ksi}) = \mathbf{79.4 \text{ kips}}$$

Concrete Breakout:

$$N_{cbg} = [A_{Nc} / A_{Nco}] \psi_{ec,N} \psi_{ed,N} \psi_{c,N} N_b$$

$$A_{Nc} = 3h_{ef} \times (1.5h_{ef} + s + 1.5h_{ef}) = 3(4.625 \text{ in.}) \times [3(4.625 \text{ in.}) + 4 \text{ in.}] = 248.0 \text{ in.}^2$$

$$A_{Nco} = 9h_{ef}^2 = 9(4.625 \text{ in.})^2 = 192.5 \text{ in.}^2$$

$$\psi_{ec,N} = 1.0 \text{ (No eccentric loading)}$$

Note: $\psi_{ec,N}$ is a modification factor to account for eccentric loading of a group of studs. It is less than 1.0 for groups with eccentric loading.

$$\psi_{ed,N} = 1.0 \text{ (No edge effects)}$$

$$\psi_{c,N} = 1.0 \text{ (Cracking assumed to occur)}$$

$$N_b = k_c (f_c')^{1/2} h_{ef}^{1.5} = (24)(6,000 \text{ psi})^{1/2} (4.625 \text{ in.})^{1.5} (1 \text{ kip} / 1000 \text{ lb}) = 18.5 \text{ kips}$$

$$N_{cbg} = [248.0 \text{ in.}^2 / 192.5 \text{ in.}^2](1.0)(1.0)(1.0)(18.5 \text{ kip}) = \mathbf{23.8 \text{ kips}}$$

Pullout:

$$N_{pn} = 2 \times \psi_{c,p} \delta A_{brg} f_c' = 2 \times (1.0)(8)(0.884 \text{ in.}^2)(6 \text{ ksi}) = \mathbf{84.8 \text{ kips}}$$

Therefore, concrete breakout failure governs with $N_{cbg} = \mathbf{23.8 \text{ kips}}$

No Haunch – Three Studs

Steel Strength:

$$N_{sa} = n A_{sef} f_{uta} = (3)(\pi/4)(0.875 \text{ in.})^2(66 \text{ ksi}) = \mathbf{119.1 \text{ kips}}$$

Concrete Breakout:

$$N_{cbg} = [A_{Nc} / A_{Nco}] \psi_{ec,N} \psi_{ed,N} \psi_{c,N} N_b$$

$$A_{Nc} = 3h_{ef} \times (1.5h_{ef} + s + s + 1.5h_{ef}) = 3(4.625 \text{ in.}) \times [3(4.625 \text{ in.}) + 2(4 \text{ in.})] = 303.5 \text{ in.}^2$$

$$A_{Nco} = 9h_{ef}^2 = 9(4.625 \text{ in.})^2 = 192.5 \text{ in.}^2$$

$$\psi_{ec,N} = 1.0 \text{ (No eccentric loading)}$$

$$\psi_{ed,N} = 1.0 \text{ (No edge effects)}$$

$$\psi_{c,N} = 1.0 \text{ (Cracking assumed to occur)}$$

$$N_b = k_c (f_c')^{1/2} h_{ef}^{1.5} = (24)(6,000 \text{ psi})^{1/2} (4.625 \text{ in.})^{1.5} (1 \text{ kip} / 1000 \text{ lb}) = 18.5 \text{ kips}$$

$$N_{cbg} = [303.5 \text{ in.}^2 / 192.5 \text{ in.}^2](1.0)(1.0)(1.0)(18.5 \text{ kip}) = \mathbf{29.2 \text{ kips}}$$

Pullout:

$$N_{pn} = 3 \times \psi_{c,p} \delta A_{brg} f_c' = 3 \times (1.0)(8)(0.884 \text{ in.}^2)(6 \text{ ksi}) = \mathbf{127.2 \text{ kips}}$$

Therefore, concrete breakout failure governs with $N_{cbg} = \mathbf{29.2 \text{ kips}}$

Specimens with a 3 in. Haunch

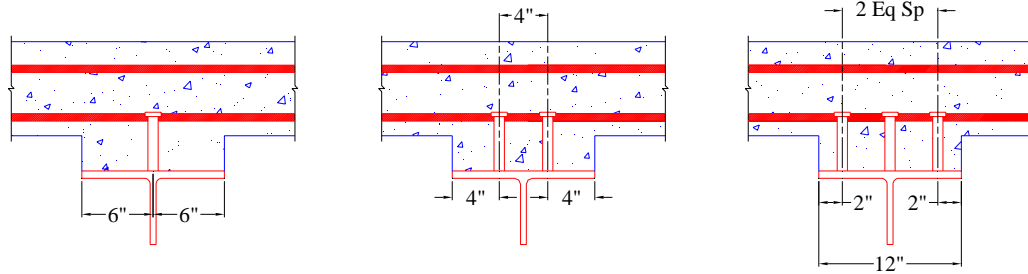


Figure E.3: Stud details for specimens with a 3 in. haunch

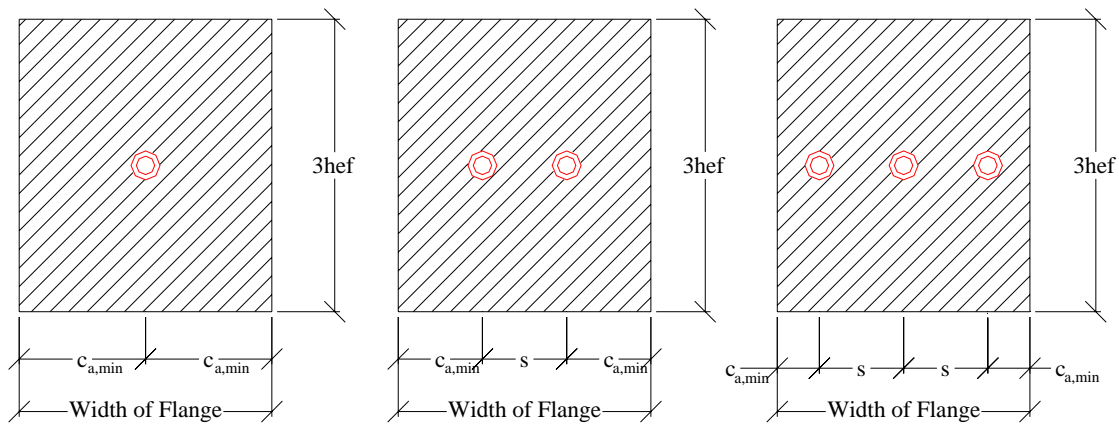


Figure E.4: Concrete breakout – projected failure areas for specimens with a 3 in. haunch (A_{Nc})

3 in. Haunch – One Stud

Steel Strength:

$$N_{sa} = nA_{sef_{uta}} = (1)(\pi/4)(0.875 \text{ in.})^2(66 \text{ ksi}) = \mathbf{39.7 \text{ kips}}$$

Concrete Breakout:

$$N_{cb} = [A_{Nc} / A_{Nco}] \psi_{ed,N} \psi_{c,N} N_b$$

$$A_{Nc} = (c_a + c_a) \times 3h_{ef} = (6 \text{ in.} + 6 \text{ in.}) \times 3(4.625 \text{ in.}) = 166.5 \text{ in.}^2$$

$$A_{Nco} = 9h_{ef}^2 = 9(4.625 \text{ in.})^2 = 192.5 \text{ in.}^2$$

$$\psi_{ed,N} = 0.7 + 0.3 \times [c_{a,min} / (1.5h_{ef})] = 0.7 + 0.3 \times [4 \text{ in.} / (1.5(4.625 \text{ in.}))] = 0.959$$

$$\psi_{c,N} = 1.0 \text{ (Cracking assumed to occur)}$$

$$N_b = k_c(f_c')^{1/2}h_{ef}^{1.5} = (24)(6,000 \text{ psi})^{1/2}(4.625 \text{ in.})^{1.5}(1 \text{ kip} / 1000 \text{ lb}) = 18.5 \text{ kips}$$

$$N_{cb} = [166.5 \text{ in.}^2 / 192.5 \text{ in.}^2](0.959)(1.0)(18.5 \text{ kip}) = \mathbf{15.3 \text{ kips}}$$

Pullout:

$$N_{pn} = \psi_{c,p}8A_{brg}f_c' = (1.0)(8)(0.884 \text{ in.}^2)(6 \text{ ksi}) = \mathbf{42.4 \text{ kips}}$$

Therefore, concrete breakout failure governs with $N_{cb} = \mathbf{15.3 \text{ kips}}$

3 in. Haunch – Two Studs

Steel Strength:

$$N_{sa} = nA_{sef}f_{uta} = (2)(\pi/4)(0.875 \text{ in.})^2(66 \text{ ksi}) = \mathbf{79.4 \text{ kips}}$$

Concrete Breakout:

$$N_{cb} = [A_{Nc} / A_{Nco}]\psi_{ed,N}\psi_{c,N}N_b$$

$$A_{Nc} = (c_a + s + c_a) \times 3h_{ef} = (4 \text{ in.} + 4 \text{ in.} + 4 \text{ in.}) \times 3(4.625 \text{ in.}) = 166.5 \text{ in.}^2$$

$$A_{Nco} = 9h_{ef}^2 = 9(4.625 \text{ in.})^2 = 192.5 \text{ in.}^2$$

$$\psi_{ed,N} = 0.7 + 0.3 \times [c_{a,min} / (1.5h_{ef})] = 0.7 + 0.3 \times [4 \text{ in.} / (1.5(4.625 \text{ in.}))] = 0.873$$

$$\psi_{c,N} = 1.0 \text{ (Cracking assumed to occur)}$$

$$N_b = k_c(f_c')^{1/2}h_{ef}^{1.5} = (24)(6,000 \text{ psi})^{1/2}(4.625 \text{ in.})^{1.5}(1 \text{ kip} / 1000 \text{ lb}) = 18.5 \text{ kips}$$

$$N_{cb} = [166.5 \text{ in.}^2 / 192.5 \text{ in.}^2](0.873)(1.0)(18.5 \text{ kip}) = \mathbf{14.0 \text{ kips}}$$

Pullout:

$$N_{pn} = 2 \times \psi_{c,p}8A_{brg}f_c' = 2 \times (1.0)(8)(0.884 \text{ in.}^2)(6 \text{ ksi}) = \mathbf{84.8 \text{ kips}}$$

Therefore, concrete breakout failure governs with $N_{cbg} = \mathbf{14.0 \text{ kips}}$

3 in. Haunch – Three Studs

Steel Strength:

$$N_{sa} = nA_{sef}f_{uta} = (3)(\pi/4)(0.875 \text{ in.})^2(66 \text{ ksi}) = \mathbf{119.1 \text{ kips}}$$

Concrete Breakout:

$$N_{cb} = [A_{Nc} / A_{Nco}] \psi_{ed,N} \psi_{c,N} N_b$$

$$A_{Nc} = (c_a + s + s + c_a) \times 3h_{ef} = (2 \text{ in.} + 4 \text{ in.} + 4 \text{ in.} + 2 \text{ in.}) \times 3(4.625 \text{ in.}) = 166.5 \text{ in.}^2$$

$$A_{Nco} = 9h_{ef}^2 = 9(4.625 \text{ in.})^2 = 192.5 \text{ in.}^2$$

$$\psi_{ed,N} = 0.7 + 0.3 \times [c_{a,min} / (1.5h_{ef})] = 0.7 + 0.3 \times [2 \text{ in.} / (1.5(4.625 \text{ in.}))] = 0.786$$

$$\psi_{c,N} = 1.0 \text{ (Cracking assumed to occur)}$$

$$N_b = k_c (f_c')^{1/2} h_{ef}^{1.5} = (24)(6,000 \text{ psi})^{1/2} (4.625 \text{ in.})^{1.5} (1 \text{ kip} / 1000 \text{ lb}) = 18.5 \text{ kips}$$

$$N_{cb} = [166.5 \text{ in.}^2 / 192.5 \text{ in.}^2] (0.786)(1.0)(18.5 \text{ kip}) = \mathbf{12.6 \text{ kips}}$$

Pullout:

$$N_{pn} = 3 \times \psi_{c,p} \delta A_{brg} f_c' = 2 \times (1.0)(8)(0.884 \text{ in.}^2)(6 \text{ ksi}) = \mathbf{127.2 \text{ kips}}$$

Therefore, concrete breakout failure governs with $N_{cbg} = \mathbf{12.6 \text{ kips}}$

REFERENCES

- ACI Committee 318. (2005). *Building Code Requirements for Structural Concrete (ACI 318-05) and Commentary (ACI 318R-05)*. American Concrete Institute, Farmington Hills, MI.
- American Association of State Highway Transportation Officials. (2004). *AASHTO LRFD Bridge Design Specifications*. Washington, D.C.
- American Association of State Highway Transportation Officials/American Welding Society. (2002). *AASHTO/AWS D1.5M/D1.5:2002 Bridge Welding Code*. AASHTO/AWS, Washington D.C./Miami, FL.
- Connor, Robert J., Dexter, Robert, and Mahmoud, Hussam. (2005). "Inspection and Management of Bridges with Fracture-Critical Details." *National Cooperative Highway Research Program Synthesis 354*. Transportation Research Board, National Academy Press, Washington, D.C.
- Daniels, J. H., Kim, W., and Wilson, J. L. (1989). "Recommended Guidelines for Redundancy Design and Rating of Two-Girder Steel Bridges." *National Cooperative Highway Research Program Report 319*. Transportation Research Board, National Academy Press, Washington, D.C.
- Eligehausen, Rolf and Balogh, Tamas. (1995). "Behavior of Fasteners Loaded in Tension in Cracked Reinforced Concrete." *ACI Structural Journal*, vol. 92, no. 3, pp. 365-379.
- Fuchs, Werner, Eligehausen, Rolf, and Breen, John E. (1995). "Concrete Capacity Design (CCD) Approach for Fastening to Concrete." *ACI Structural Journal*, vol. 92, no. 1, pp. 73-94.
- Ghosn, M. and Moses, F. (1998). "Redundancy in Highway Bridge Superstructures." *National Cooperative Highway Research Program Report 406*. Transportation Research Board, National Academy Press, Washington, D.C.
- Texas Department of Transportation. (2001). *Bridge Design Manual*.
- Texas Department of Transportation. (2001). *Bridge Detailing Manual*.
- Texas Department of Transportation. (2006). *Bridge Standard Drawings*.
- Shirvani, Mansour, Klingner, Richard E., and Graves III, Herman L. (2004). "Breakout Capacity of Anchors in Concrete – Part 1: Tension." *ACI Structural Journal*, vol. 101, no. 6, pp. 812-820.

VITA

James Patrick Sutton was born in West Islip, New York on July 4, 1983, the son of James Christopher and Mary Katherine Sutton. He is the brother of Erin, Patrick and Mary Beth Sutton. He attended Regis High School in New York, New York where he graduated in June 2001. He obtained his Bachelor of Science in Civil Engineering from Villanova University in May 2005 and entered the Graduate School at the University of Texas in August 2005 to pursue a Master of Science in Engineering degree. While at the University of Texas, he worked as a Graduate Research Assistant at the Phil M. Ferguson Structural Engineering Laboratory. He completed his M.S.E. in May 2007.

Permanent address: 15 Creek Court
Easton, Pennsylvania 18040

This thesis was typed by the author.